

# Shannon-Kotel'nikov Mappings for Analog Point-to-Point Communications

Pål Anders Floor, Tor A. Ramstad,

## Abstract

In this paper an approach to joint source-channel coding (JSCC) named Shannon-Kotel'nikov mappings (S-K mappings) is presented. S-K mappings are continuous, or piecewise continuous direct source-to-channel mappings operating directly on amplitude continuous and discrete time signals. Such mappings include several existing JSCC schemes as special cases. Many existing approaches to analog- or hybrid discrete analog JSCC provide both excellent performance as well as robustness to variations in noise level. This at low delay and relatively low complexity. However, a theory explaining their performance and behaviour on a general basis, as well as guidelines on how to construct close to optimal mappings in general, does not currently exist. Therefore, such mappings are often found based on educated guesses inspired of configurations that are known in advance to produce good solutions, combination of already existing mappings, numerical optimization or machine learning methods.

The objective of this paper is to introduce a theoretical framework for analysis of analog- or hybrid discrete analog S-K mappings. This framework will enable calculation of distortion when applying such schemes on point-to-point links, reveal more about their fundamental nature, and provide guidelines on how they should be constructed in order to perform well at both low and arbitrary complexity and delay. Such guidelines will likely help constrain solutions to numerical approaches and help explain why machine learning approaches finds the solutions they do. This task is difficult and we do not provide a complete framework at this stage: We focus on high SNR and memoryless sources with an arbitrary continuous unimodal density function and memoryless Gaussian channels. We also provide example of mappings based on surfaces which are chosen based on the provided theory.

## Index Terms

P. A. Floor is with the Colour Laboratory, Department of Computer Science, Norwegian University of Science and Technology (NTNU), Gjøvik, Norway (e-mail: paal.anders.floor@ntnu.no)

T. A. Ramstad is with the Department of Electronic Systems, Norwegian University of Science and Technology (NTNU), Trondheim, Norway (e-mail: tor.ramstad@ntnu.no).

This work was supported by NTNU via the project CUBAN and the Research Council of Norway (NFR) via the project MELODY nr. 187857/S10.

Joint source channel coding, analog mappings, distortion analysis, geometry, OPTA.

# Shannon-Kotel'nikov Mappings for Analog Point-to-Point Communications

## I. INTRODUCTION

Over the last two decades more and more attention has been directed towards miniature devices, for example in-body sensors and miniature electronic modules replacing certain neural network function in the brain. For this reason (and several others), it has again become important to study communication systems with low complexity and delay. In that respect it is crucial to construct communication schemes with the highest possible performance with respect to (w.r.t.) delay and complexity constraints. Further, it is crucial to derive what performance such schemes will have w.r.t. what is ultimately possible.

This paper deals with noise reduction through *dimension expansion* as well as compression through *dimension reduction* of *analog information sources* using a set of joint source-channel codes (JSCC) named *Shannon-Kotel'nikov mappings* (S-K mappings). Carefully constructed S-K mappings are known to perform well at low complexity and delay [1], [2], [3], [4], [5], [6].

Shannons' *Separation Theorem* or *Information Transmission Theorem* (see e.g. [7, pp. 224-227]) for communication of a single source over a point-to-point link states that source coding and channel coding can be performed separately, without any loss compared to a joint technique. To prove that separation is optimal, arbitrary complexity and delay is assumed. With a constraint on complexity and delay, separate source and channel coding (SSCC) does not necessarily result in the best possible performance, which some well known examples illustrate: It was shown in [8], [9] that for an independent and identically distributed (i.i.d.) source and an additive white Gaussian noise (AWGN) channel, both of the same bandwidth, the information theoretical bound<sup>1</sup> is achieved by a simple linear source-channel mapping operating on a symbol-by-symbol basis. This result was generalized in [9], [10] to special combinations of correlated sources and channels with memory. Furthermore, it was shown in [11], that with an ideal feedback channel, the information theoretical bounds are achieved when the channel-source bandwidth ratio is

<sup>1</sup>By *information theoretical bound* we refer to a bound derived with no restriction on complexity and delay.

an integer. With limited (or no) feedback, the asymptotic bounds cannot be obtained at finite complexity and delay when source and channel are of different bandwidth or dimension, or in general, when the source and channel are not *probabilistically matched* [12]. An open question is therefore what the best possible performance is in the case of finite complexity and delay. Some efforts have dealt with this issue [13], [14].

Several analog and semi-analog JSCC schemes for the bandwidth mismatch case, operating at low and arbitrary complexity and delay, have been suggested in the literature: The *Analog Matching* scheme in [15] is a structured semi-analog approach built on *lattices* that achieves the information theoretical bounds in the limit of infinite complexity and delay for any colored Gaussian source transmitted on any colored Gaussian channel. The performance of analog matching scheme in the finite complexity and delay regime is, to our knowledge, unknown at present. Schemes that are known to perform well with low complexity and delay are the *hybrid digital-analog* (HDA) schemes in [16], [17], [18], [1], [19], [20], certain analog mappings like the *Archimedes Spiral* [21], [22], [23] and mappings found by machine learning [6].

In this paper we investigate a general set of analog JSCC schemes named Shannon-Kotel'nikov mappings (S-K mappings). The S-K mapping approach is inspired by many earlier works: First of all, Shannon suggested the use of continuous (analog) mappings through space curves as a way of getting close to the information theoretical bounds [24]. Simultaneously, Kotel'nikov developed a theory for analyzing distortion of certain amplitude continuous and time discrete systems realized as parametric curves in  $N$  dimensions<sup>2</sup> in [25]. Vaishampayan's efforts [26], [27] are pioneering works on this subject in more recent times. The effort by Gastpar et. al. [12] is another important contribution and Merhav's efforts [28], [29] provides insight into the underlying workings of such scheme through analysis based on Statistical Mechanics. Other important works includes the development of *power constrained channel optimized vector quantizers* (PCCOVQ) [26], [30], [31], the HDA schemes in [16], [17], [18], [1], the linear *Block pulse amplitude modulation* (BPAM) scheme in [32], [26] and the use of parametric curves for both bandwidth expansion [27] and compression [21], [22]. Other recent efforts dedicated to analog or semi-analog mappings are found in [2], [33], [34], [35], [15], [36], [5], [37]. Lately Deep Learning was applied to find the optimal structure of such mappings [6]. These efforts conclude that such schemes perform

<sup>2</sup>These are basically bandwidth (or dimension) expanding systems with *pulse position modulation* as a special case.

well at low complexity and delay, some providing excellent performance not matched by any other known scheme.

Besides Goblík's [38], Gastpar's [12] and Merhav's approaches [28], [29], there are, as far as we know, no theory providing means to analyze such mappings as well as guideline their construction on a general basis. The objective of this paper is therefore to introduce a theoretical framework based on *differential geometry*, that includes many analog and hybrid discrete-analog schemes. This approach seek to complement that of Merhav and Gastpar. We study the case of memoryless and independent analog sources drawn from an arbitrary unimodal density function. The sources are transmitted on memoryless and independent Gaussian point-to-point channels, possibly with limited feed back providing channel state information. S-K mappings apply when the channel-source bandwidth (or dimension) ratio is a positive rational number. Most of the results in this paper are proved under the assumption of *high* signal-to-noise ratio (SNR). We focus on low complexity and delay but also consider how these mappings potentially perform by letting their *dimensionality* increase. That is, what gains may be obtained if we increase the mappings dimensions in order to code blocks of data samples. Future research can extend the concepts of this paper to more general cases. Note that [15] treats a more general setting than this paper; colored sources and channels. The framework developed in this paper treats a broader set of mappings however<sup>3</sup>.

The proposed theoretical framework facilitate calculation and analysis of the overall distortion in order to reveal the fundamental nature of S-K mappings, as well as guideline their construction. Treating nonlinear mappings on a general basis is a difficult problem, and we do not present a complete theory at this point, rather introduce a set of tools that provide certain guidelines on construction of such mappings. The main reason for developing a theory is to gain knowledge on how to optimally construct such mappings in general, not having to rely on educated guesses, numerical optimization sensitive to initial conditions, or deep learning approaches in which little is known about why a certain result is produced.

The paper is organized as follows: In Section II the problem is formulated, the information theoretical limit *OPTA* is introduced, S-K mappings are defined and important concepts from

<sup>3</sup>Note that we have made efforts to consider correlated sources for S-K mappings for both dimension expansion [39] and dimension reduction [40]. However, this is a more heuristic approach than what is presented in this paper.

differential geometry are presented. In Section III a distortion framework for S-K mappings based on concepts from differential geometry is developed and guidelines for their construction are given. In Section IV asymptotic analysis is considered and it is shown under which conditions S-K mappings may achieve optimality for Gaussian sources. Section V provides examples on construction of S-K mappings using surfaces (3:2 and 2:3 mappings) to illustrate the theory developed in proceeding sections. In Section VI a final discussion is given and extensions of the theory are briefly discussed.

## II. PROBLEM FORMULATION AND PRELIMINARIES

Assume a source  $\mathbf{x} \in \mathbb{R}^M$ , drawn from a continuous unimodal multivariable probability density function (pdf)  $f_{\mathbf{x}}(\mathbf{x})$ , with i.i.d. components  $x_i$ .  $\mathbf{x}$  is mapped through an S-K mapping (defined in Section II-B) to a vector  $\mathbf{z} \in \mathbb{R}^N$  which is transmitted over a memoryless channel with average power  $P$  so that  $1/N \sum_{i=1}^N E\{z_i^2\} \leq P$ , and additive Gaussian noise  $\mathbf{n} \in \mathbb{R}^N$  with joint pdf  $f_{\mathbf{n}}(\mathbf{n})$  with  $n_i \sim \mathcal{N}(0, \sigma_n^2)$  i.i.d. The channel output  $\hat{\mathbf{z}}$  is mapped through an S-K mapping at the receiver to reconstruct the source.

As a measure of performance, the end-to-end mean squared error per source sample between the input- and reconstructed vector,  $D_t = (1/M)E\{\|\mathbf{x} - \hat{\mathbf{x}}\|^2\}$ , is considered and compared to the *optimal performance theoretically attainable* (OPTA) [9].

### A. OPTA

OPTA in the i.i.d. case is obtained by equating the rate-distortion function for the relevant source with the relevant channel capacity. The equation is solved with respect to the signal-to-distortion ratio (SDR), which becomes a function of the channel signal-to-noise ratio (SNR) [9]. For the case of Gaussian sources and channels, OPTA is explicitly given by

$$\frac{\sigma_x^2}{D_t} = \left(1 + \frac{P}{\sigma_n^2}\right)^{f_c/f_s} = \left(1 + \frac{P}{\sigma_n^2}\right)^{N/M}, \quad (1)$$

where  $\sigma_x^2$  is the source variance,  $\sigma_x^2/D_t$  is the SDR and  $P/\sigma_n^2$  is the channel SNR. Assuming Nyquist sampling and an ideal Nyquist channel, the ratio between channel signalling rate  $f_c$ , and source sampling rate  $f_s$ , can be obtained by combining  $M$  source samples with  $N$  channel samples. That is,  $f_c/f_s \approx N/M = r$ , where  $r$  is a positive rational number ( $r \in \mathbb{Q}_+$ ), named *dimension change factor*. If  $r > 1$ , the channels dimension is higher than that of the source

and this can be utilized for noise reduction. If  $r \in [0, 1)$ , the source dimension, and hence the information, have to be reduced in a lossy way before transmission. We denote the operation where a source of dimension  $M$  is mapped onto a channel of dimension  $N$  an  $M:N$  mapping.

### B. Shannon-Kotel'nikov mappings

S-K mappings operate directly on amplitude continuous, discrete time signals. Let  $\mathcal{S}$  denote a general S-K mapping and  $\mathbf{S}$  a specific realization. We have the following definition:

#### *Definition 1: Shannon-Kotel'nikov mapping*

An S-K mapping  $\mathcal{S}$  is a continuous or piecewise continuous nonlinear or linear transformation between  $\mathbb{R}^M$  (source space) and  $\mathbb{R}^N$  (channel space). There are three cases to consider:

1. Equal dimension  $M = N$ :  $\mathcal{S}$  is a bijective<sup>4</sup> mapping.
2. Dimension expansion  $M < N$ :  $\mathcal{S} \subseteq \mathbb{R}^N$  is a mapping that can be realized by a hyper surface described by the parametrization<sup>5</sup>

$$\mathbf{S}(\mathbf{x}) = [S_1(\mathbf{x}), S_2(\mathbf{x}), \dots, S_N(\mathbf{x})], \quad (2)$$

where each source vector  $\mathbf{x}$  should have a unique representation  $\mathbf{S}(\mathbf{x}) \in \mathcal{S}$ .  $\mathcal{S}$  can be seen as an  $M$  dimensional (locally Euclidean) manifold embedded in  $\mathbb{R}^N$ .

3. Dimension reduction  $M > N$ :  $\mathcal{S} \subseteq \mathbb{R}^M$  is a mapping that can be realized by a hyper surface described by the parametrization

$$\mathbf{S}(\mathbf{z}) = [S_1(\mathbf{z}), S_2(\mathbf{z}), \dots, S_M(\mathbf{z})], \quad (3)$$

where each channel vector  $\mathbf{z}$  should have a unique representation  $\mathbf{S}(\mathbf{z}) \in \mathcal{S}$ .  $\mathcal{S}$  can be seen as an  $N$  dimensional (locally Euclidean) manifold embedded in  $\mathbb{R}^M$ .  $\square$

Case 1 is trivial for Gaussian i.i.d. sources, i.e. OPTA is obtained by a linear mapping with MMSE decoding at the receiver (often referred to as uncoded transmission) [8]. This paper is concerned with the case  $M \neq N$  (case 2 and 3). However, the  $M = N$  case fall out as special cases for some of the results given. Piecewise continuity is considered in order to include hybrid

<sup>4</sup>MMSE decoding is needed at low SNR in order to obtain optimality, effectively weakening this condition.

<sup>5</sup>This is not a restriction, i.e. the mapping does not need to be described by a parametrization.

discrete-analog (HDA) schemes. S-K mappings therefore include most mappings except fully discrete ones, like digital source- and channel codes (although the fundamental principles are indeed related).

### C. Useful Concepts from Differential Geometry

Our analysis of S-K mappings is based on concepts from differential geometry not commonly used in Information Theory. The results presented here are taken from E. Kreyszig's book [41]. The introduction here is brief and more detail can be found in Appendix A as well as the document in [42] which is publicly available online.

Note that we use variables  $u$  (and  $u_i$ ) in this section to keep the discussion general, not referring specifically to source- or channel variables. We consider parametric curves in  $\mathbb{R}^3$  first for simplicity: Any continuous ( $C^1$ ) curve  $\mathcal{C} : \mathbf{S} \in \mathbb{R}^3$  can be represented by the parametrization  $\mathbf{S}(u) = [S_1(u), S_2(u), S_3(u)]$ ,  $u \in \mathbb{R}$ .

In the following we denote the derivatives w.r.t to a general parameter,  $u$ , as  $\mathbf{S}'$ ,  $\mathbf{S}''$  etc. In the special case of the parameter being the arch length we denote the derivatives  $\dot{\mathbf{S}}$ ,  $\ddot{\mathbf{S}}$  etc, that is, when we parameterize the curve via

$$\ell(u) = \int_{u_0}^u \sqrt{\mathbf{S}' \cdot \mathbf{S}'} du = \int_{u_0}^u \|\mathbf{S}'\| du. \quad (4)$$

Then the norm of the derivative of the curve at any point, corresponding to the length of its tangent vector at that point, is unity. I.e.,  $\|\dot{\mathbf{t}}\| = \|\dot{\mathbf{S}}\| = 1$ ,  $\forall u$  (See Appendix A-A).

There are three unit vectors connected to any curve  $\mathcal{C} : \mathbf{S} \in \mathbb{R}^3$ : The *unit tangent vector*  $\mathbf{t} = \dot{\mathbf{S}} = \mathbf{S}' / \|\mathbf{S}'\|$ , the *unit principal normal vector*  $\mathbf{p} = \dot{\mathbf{t}} / \|\dot{\mathbf{t}}\| = \ddot{\mathbf{S}} / \|\ddot{\mathbf{S}}(x_0)\|$ , and the *unit binormal vector*  $\mathbf{b} = \mathbf{t} \times \mathbf{p}$ . The vectors  $\mathbf{t}$ ,  $\mathbf{p}$  and  $\mathbf{b}$  make out a vector space of mutually orthogonal vectors named *moving trihedron* which is so defined at each point along the curve  $\mathcal{C}$ . This is nicely illustrated in [41, pp. 36-37]. These three vectors further define three mutually orthogonal planes: i) *Osculating Plane* spanned by  $\mathbf{t}$  and  $\mathbf{p}$ , ii) *normal plane* spanned by  $\mathbf{p}$  and  $\mathbf{b}$ , and iii) *rectifying plane* spanned by  $\mathbf{t}$  and  $\mathbf{b}$ . For a parametric curve,  $\mathbf{S}(u)$ , one can define *curvature* w.r.t. arch length as  $\kappa_0 = \|\ddot{\mathbf{S}}(u_0)\|$  [41, p. 34]. Then we also have  $\mathbf{p} = (1/\kappa)\ddot{\mathbf{S}} = \rho\ddot{\mathbf{S}}$ .

The *torsion* [41, p. 37-40] is defined as  $\tau(x) = -\mathbf{p} \cdot \dot{\mathbf{b}} = |\dot{\mathbf{S}} \ddot{\mathbf{S}} \ddot{\mathbf{S}}| / \|\ddot{\mathbf{S}}\|^2$ . When  $\tau = 0$ ,  $\forall x$ , we have a plane curve. Whenever  $\tau \neq 0$ , the curve will “twist” up into  $\mathbb{R}^3$  (or  $\mathbb{R}^N$  in general).

For a general parametrization, the curvature and torsion are given by [41, pp.35,39]

$$\kappa = \frac{\sqrt{\|\mathbf{S}'\|^2 \|\mathbf{S}''\|^2 - (\mathbf{S}' \cdot \mathbf{S}'')^2}}{\|\mathbf{S}'\|^{\frac{3}{2}}}, \quad \tau = \frac{|\mathbf{S}' \cdot \mathbf{S}'' \cdot \mathbf{S}'''|}{\|\mathbf{S}'\|^2 \|\mathbf{S}''\|^2 - (\mathbf{S}' \cdot \mathbf{S}'')^2}. \quad (5)$$

Consider arc length parametrization with an amplification  $\alpha$ , which we name *scaled arc length parametrization*. Then we have  $\|\mathbf{S}'(u_0)\| = \alpha \|\dot{\mathbf{S}}(u_0)\| = \alpha$ ,  $\forall u_0$ , and so  $\kappa$  in (5) reduces to  $\kappa(u_0) = \|\mathbf{S}_0''(u_0)\| / \|\mathbf{S}_0'\|^2$  (since  $\mathbf{S}_0' \perp \mathbf{S}_0''$ , still).

The curvature can locally be interpreted as a circle of radius  $\rho = 1/\kappa$ , named *radius of curvature*, lying in the osculating plane of  $\mathbf{s}$ . The corresponding circle is named *osculating circle*.

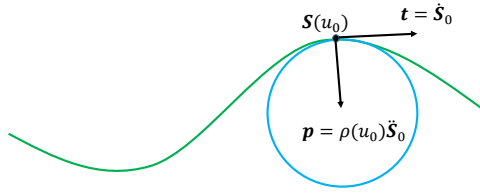


Fig. 1. Curvature concept illustrated in  $\mathbb{R}^2$ . For curves in  $\mathbb{R}^N$ ,  $N > 2$ , the blue (osculating) circle lies in the osculating plane.

*circle* and its center named *centre of curvature*. I.e., the curvature in a neighborhood of  $u_0$  is equivalent to that of a circle with radius  $\rho$ . This concept of curvature is also valid for curves in  $\mathbb{R}^M$ ,  $M \geq 3$ . Fig. 1 illustrates the curvature for a parametric curve in  $\mathbb{R}^2$ .

The generalization of curvature to surfaces is quite involved. Therefore, the main results are stated here, whilst details are provided in Appendix A-B and [42]. A surface (or manifold)  $M \in \mathbb{R}^3$  can be described by a parametrization as in (2), (3). In the following, partial derivatives of surfaces will be denoted as

$$\mathbf{S}_\alpha = \frac{\partial \mathbf{S}}{\partial u^\alpha}, \quad \mathbf{S}_{\alpha\beta} = \frac{\partial^2 \mathbf{S}}{\partial u^\alpha \partial u^\beta}. \quad (6)$$

The use of subscripts and superscripts here relates to *Einstein's Summation convention* as described in Appendix A-B.

The curvature of a surface depends on the direction along the surface one moves in, and therefore the choice of *coordinate curves* on that surface: A curve,  $\mathcal{C}$ , on a surface  $\mathcal{S} : \mathbf{S}(u^1, u^2)$  can be determined by the parametric representation  $\mathcal{C} : u^1 = u^1(t), u^2 = u^2(t)$ , of class  $r \geq 1$ , where the parameter  $t \in \mathbb{R}$ . The *coordinate curves* on  $\mathcal{S}$ ,  $u^1 = \text{constant}$  and  $u^2 = \text{constant}$ , corresponds to parallel curves in the  $u^1, u^2$ -plane.

At any point of a curve  $\mathcal{C} \in \mathcal{S}$ , the corresponding unit normal to  $\mathcal{S}$ ,  $\mathbf{n} = \mathbf{S}_1 \times \mathbf{S}_2 / \|\mathbf{S}_1 \times \mathbf{S}_2\|$ , lies in the normal plane of  $\mathcal{C}$  which also contains its principal normal  $\mathbf{p}$ . The angle between  $\mathbf{n}$  and  $\mathbf{p}$  denoted  $\gamma$ , depends on the geometry of both  $\mathcal{C}$  and  $\mathcal{S}$  in a neighborhood of the point  $P$  under consideration. We have two extremes: 1)  $\gamma = \pi/2$ ,  $\forall u_0 \in \mathcal{C}$ , implying that  $\mathbf{p} \perp \mathbf{n}$ , and  $\mathcal{C}$  is a plane curve, and so  $\mathcal{S}$  is a plane. 2)  $\gamma = 0$ ,  $\forall u_0 \in \mathcal{C}$ , implying that  $\mathbf{p} \parallel \mathbf{n}$ . Then  $\mathcal{C}$  is a *geodesic* on  $\mathcal{S}$ . That is the arc with the shortest possible length between two points on  $\mathcal{S}$  [41, pp.160-162]. Geodesics are straight lines in a plane and great circles on a sphere, and is generally the path that minimizes *energy*<sup>6</sup>

Consider now the intersection between  $\mathcal{S}$  and a plane containing both the tangent to  $\mathcal{C}$  at  $P$  and the normal to  $\mathcal{S}$  at  $P$ . The curves of intersection are named *normal sections* of  $\mathcal{S}$ . The *normal curvature*,  $\kappa_n$ , of  $\mathcal{S}$  at  $P$  corresponds to the direction of the tangent to the normal section at  $P$ , and is given by  $\kappa_n = b_{\alpha\beta} du^\alpha du^\beta / g_{\alpha\beta} du^\alpha du^\beta$  (see Appendix A-B3, Eq. 69), where  $g_{ij} = \mathbf{S}_i \cdot \mathbf{S}_j$  are the components of the *metric tensor*, or *first fundamental form* (FFF) of  $\mathcal{S}$ , and  $b_{\alpha\beta} = \mathbf{S}_{\alpha\beta} \cdot \mathbf{n}$  are components of the *second fundamental form* (SFF) of  $\mathcal{S}$  (see Appendix A-B2 for details). Furthermore,  $\kappa_n = 1/R$  where  $|R|$  is the radius of curvature of the corresponding normal section at  $P$ . Since  $\kappa = 1/\rho$  one can write  $\rho = R \cos \gamma$ .

A special case of particular interest is the extremal values of  $\kappa_n$ , named *Lines of Curvature* (LoC). How to determine LoC is shown in Appendix A-B3. If one chooses LoC as coordinate curves then the surfaces's curvature in those directions are given by  $\kappa_i = b_{ii}/g_{ii}$ ,  $\forall i$ . The normal curvature  $\kappa_n$  for any (tangent) direction can be represented in terms of  $\kappa_1$  and  $\kappa_2$  according to *Theorem of Euler* [41, p. 132] (see also [42]) as  $\kappa_n = \kappa_1 \cos^2 \alpha + \kappa_2 \sin^2 \alpha$ , with  $\alpha$  the angle between an arbitrary direction at  $P$  and the direction corresponding to  $\kappa_1$ .

### III. DISTORTION ANALYSIS FOR S-K MAPPINGS

In this section we provide results needed to quantify distortion for S-K mappings.

#### A. Dimension Expanding S-K mappings.

In this section Kotelnikov's theory from [25, pp.62-99] on 1:N mappings is generalized to include vector sources, enabling analysis of more general mappings. The results presented in this section are extensions of [44].

<sup>6</sup>This curve is the solution to the *Euler-Lagrange Equations* in Variational Calculus [43, pp.13-17].

Fig. 2 depicts the block diagram for a dimension expanding S-K communication system.

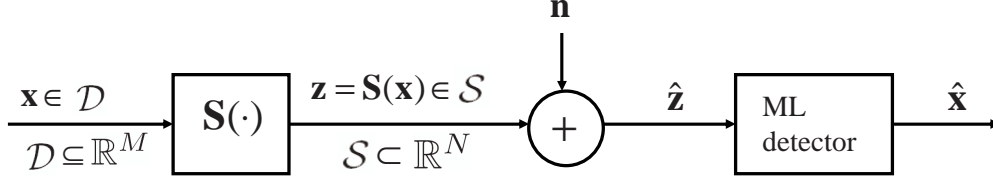


Fig. 2. Dimension expanding ( $M < N$ ) communication system for S-K mappings.

Consider the source vector  $\mathbf{x} \in \mathcal{D} \subseteq \mathbb{R}^M$ , with  $\mathcal{D}$  its domain.

The source is represented by a hyper surface in the channel space  $\mathbf{x} \mapsto \mathbf{S}(\mathbf{x}) \in \mathcal{S} \subset \mathbb{R}^N$ , a *signal hyper surface* (see Definition 9).

Applying a specific realization of  $\mathcal{S}$ ,  $\mathbf{S}$ , the likelihood function of the received signal  $\hat{\mathbf{S}} = \mathbf{S}(\mathbf{x}) + \mathbf{n}$  is

$$f_{\hat{\mathbf{S}}|\mathbf{x}}(\hat{\mathbf{S}}|\mathbf{x}) = \left( \frac{1}{2\pi\sigma_n^2} \right)^{N/2} e^{-\frac{\|\hat{\mathbf{S}} - \mathbf{S}(\mathbf{x})\|^2}{2\sigma_n^2}}, \quad (7)$$

The maximum likelihood (ML) estimate is then defined as [45]<sup>7</sup>

$$\hat{\mathbf{x}} = \max_{\mathbf{x} \in \mathbb{R}^M} f_{\hat{\mathbf{S}}|\mathbf{x}}(\hat{\mathbf{S}}|\mathbf{x}), \quad (8)$$

and is maximized by the vector  $\mathbf{x}$  that minimizes  $\|\hat{\mathbf{S}} - \mathbf{S}(\mathbf{x})\|$ . I.e., the ML estimate of  $\mathbf{x}$  corresponds to the point on  $\mathbf{S}$  closest to the received vector in Euclidean distance.

Ideally one could formulate the exact distortion for any such scheme once a specific representation  $\mathbf{S}$  is chosen. However, this is inconvenient when it comes to analysis of the behavior of such mappings as it is usually very hard, if at all possible, to find closed form solutions. For this reason we use an approach suggested by Kotel'nikov in [25, pp.62-99]. Kotel'nikov reasoned that there are two main contributions to the total distortion using such mappings: *low intensity noise* and *strong noise*. Low intensity noise is when the error in the reconstruction at the decoder varies gradually with the magnitude of the noise samples. Distortion due to low intensity noise can be analyzed without reference to a specific realization  $\mathbf{S}$  when the noise can

<sup>7</sup>Ideally MMSE estimation should be considered but is difficult to deal with analytically for such mappings. This will result in a loss at low SNR. See for example [36].

be considered *weak*. The resulting distortion is named *weak noise distortion*, denoted by  $\bar{\varepsilon}_{wn}^2$ , and defined in section III-A1). Strong noise is often known as *anomalous errors* in the literature, and results from a *threshold effect*<sup>8</sup> [24]. The resulting distortion is named *anomalous distortion* and denoted by  $\bar{\varepsilon}_{an}^2$ .

1) *Weak noise distortion*: To analyze non-linear mappings without reference to a specific structure the concepts introduced in Section II-C and the Taylor expansion applies: We begin by quantifying *weak noise distortion* for dimension expanding S-K mappings: Let  $\mathbf{S}_{lin}(\mathbf{x})$  denote 1st order Taylor approximation of  $\mathbf{S}(\mathbf{x})$  at  $\mathbf{x}_0$

$$\mathbf{S}_{lin}(\mathbf{x}) = \mathbf{S}(\mathbf{x}_0) + J(\mathbf{x}_0)(\mathbf{x} - \mathbf{x}_0), \quad (9)$$

where  $J(\mathbf{x}_0)$  denotes the *Jacobian* (see Appendix A-B) of  $\mathbf{S}$  evaluated at  $\mathbf{x}_0$ . Fig. 3(a) shows how the ML estimate is compute the approximation in (9)for the 2:3 case. We have the following proposition providing the exact distortion under linear approximation:

*Proposition 1: Minimum weak noise distortion*

For any continuous i.i.d. source  $\mathbf{x} \in \mathbb{R}^M$  with unimodal pdf  $f_{\mathbf{x}}(\mathbf{x})$  communicated on an i.i.d. Gaussian channel of dimension  $N$  using a continuous dimension expanding S-K mapping  $\mathbf{S}$  where  $S_i \in C^r(\mathbb{R}^M)$ ,  $r \geq 1$ ,  $i = 1, \dots, N$ , the minimum distortion under the linear approximation in (9) is given by

$$\bar{\varepsilon}_{wn}^2 = \frac{\sigma_n^2}{M} \iint \cdots \int_{\mathcal{D}} \sum_{i=1}^M \frac{1}{g_{ii}(\mathbf{x})} f_{\mathbf{x}}(\mathbf{x}) d\mathbf{x}, \quad (10)$$

obtained when the metric tensor (or FFF)  $G$  of  $\mathbf{S}$  (Appendix A-B) is diagonal with entries  $g_{ii} = \|\partial \mathbf{S}(\mathbf{x}) / \partial x_i\|^2$ . I.e., the squared norm of the tangent vector along the  $i$ 'th coordinate curve.

*Proof*: See Appendix B-A1. □

The name *weak noise distortion* is due to Def. 2 given later in this section. Eqn. (10) states that weak noise distortion becomes smaller by increasing the  $g_{ii}$ 's. This is equivalent to making tangent vectors at any given point of  $\mathbf{S}$  longer, and is obtained by stretching  $\mathbf{S}$  like a rubber-sheet. Simple bending (or cutting) of the signal hyper surface does not reduce weak noise distortion.

The concept is illustrated in Fig. 3(b) for the 1: $N$  case when  $\mathcal{S}$  is a curve. Stretching of the

<sup>8</sup>A thorough treatment of threshold effects, going beyond what we present here, is given in [29], [46]

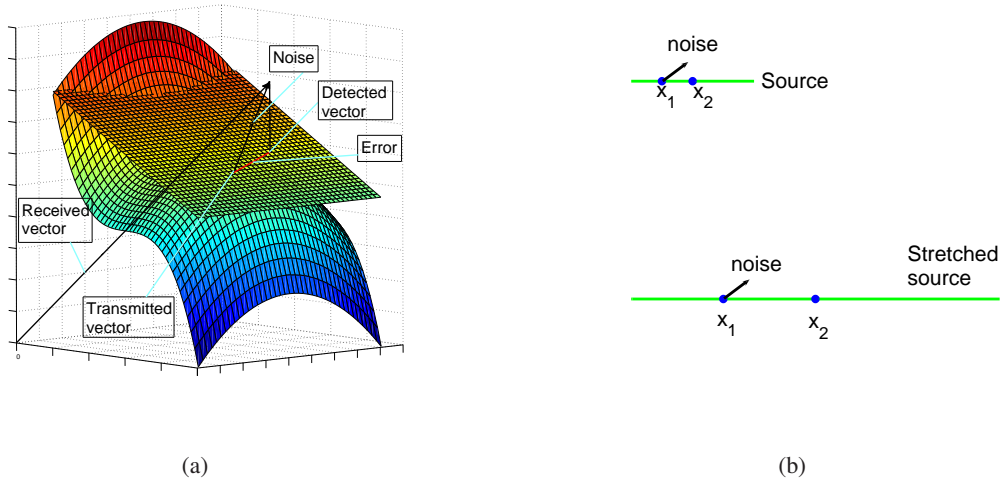


Fig. 3. Dimension expanding S-K mappings. 3(a) ML estimate approximation for a 2:3 mapping under the weak noise regime. 3(b) Kotel'nikovs concept of analog error reduction for 1: $N$  mappings.

curve makes the source appear "larger" compared to a given noise vector, or equivalently, the more the source is stretched at the transmitter trough  $\mathcal{S}$  the more the noise will be attenuated at the receiver, resulting in smaller distortion. This result by itself implies that the source space should be stretched indefinitely. However, as will be seen in Section III-A2, under a channel power constraint, this cannot be done without introducing large anomalous errors.

**Remark:** Proposition 1 is extendable to piecewise continuous mappings since one can integrate over each surface element, then sum all the contributions afterwards (see example in [16]).

The following corollary is a special case of Proposition 1:

*Corollary 1: Shape preserving mapping*

When  $\mathcal{S}$  has a diagonal metric tensor  $G$  where  $g_{ii}(\mathbf{x}) = g_{jj}(\mathbf{x}) = \alpha, \forall \mathbf{x}, i, j$ , with  $\alpha$  a constant, the weak noise distortion becomes

$$\bar{\epsilon}_{wn}^2 = \frac{\sigma_n^2}{\alpha^2}. \quad (11)$$

That is, all source vectors are equally scaled when mapped through  $\mathcal{S}$  and the noise will affect all values of  $\mathbf{x}$  equally.

*Proof:* Insert  $g_{ii}(\mathbf{x}) = g_{jj}(\mathbf{x}) = \alpha$  in (10). □

A shape preserving mapping can be seen as an amplification factor  $\alpha$  from source to channel. Although a shape preserving mapping leads to simple analysis, its not necessarily optimal in general (especially when  $M, N$  is finite). A result obtained in [47, 294-297] using variational calculus can be used for 1: $N$  mappings to find the optimal  $g_{11}(x)$  for a given source pdf.

In order to determine the error made in the distortion estimate under linear approximation, we need to consider 2nd order Taylor expansion. We have the following proposition:

*Proposition 2: Error under 2nd order Taylor approximation*

Under 2nd order Taylor approximation, the special case of 1: $N$  mappings (curves) has an error in the absence of anomalies given by

$$\varepsilon_{wn}^2 \approx \frac{\sigma_n^2}{\|\mathbf{S}'_0\|^2} \left( 1 + \frac{1}{4} \sigma_n^2 \frac{\|\mathbf{S}''_0\|^2}{\|\mathbf{S}'_0\|^4} \right) = \frac{\sigma_n^2}{\|\mathbf{S}'_0\|^2} \left( 1 + \frac{1}{4} \sigma_n^2 \kappa^2(x_0) \right), \quad (12)$$

valid for any S-K mapping  $\mathbf{S}(x) \in C^m$ ,  $n \geq 2$ . The last equality is true under scaled arc length parametrization. Further, for any dimension expanding S-K mapping as defined in Def. 9, with LoC coordinate curves, the error is given by

$$\varepsilon_{wn}^2(\mathbf{x}_0) \approx \frac{\sigma_n^2}{M} \sum_{i=1}^M \left\{ \frac{1}{g_{ii}(\mathbf{x}_0)} \left( 1 + \frac{\sigma_n^2}{4} \frac{b_{ii}^2(\mathbf{x}_0)}{g_{ii}^2(\mathbf{x}_0)} \right) \right\} = \frac{\sigma_n^2}{M} \sum_{i=1}^M \left\{ \frac{1}{g_{ii}(\mathbf{x}_0)} \left( 1 + \frac{\sigma_n^2}{4} \kappa_i^2(\mathbf{x}_0) \right) \right\}. \quad (13)$$

Here,  $\kappa_i = b_{ii}/g_{ii}$  is the curvature along coordinate curve  $i$ , with  $g_{ii}$  the diagonal components of the metric tensor (FFF) and  $b_{ii}$  the diagonal components of the *Second Fundamental Form* (SFF) as described in Appendix A-B.

*Proof:* See Appendix B-A2. □

**Remark:** We only treat 2nd order Taylor approximation here to simplify the analysis. It will be seen in Section III-B that higher order terms are even less influential as  $\sigma_n$  is to a power twice that of the order, which at high SNR ( $\sigma_n \ll 1$ ) leads to a negligible contribution.

Note that in the absence of anomalies, one can characterize distortion for S-K mappings in general without choosing a specific  $\mathcal{S}$  in advance, as it is expressed solely w.r.t. FFF and SFF components. This makes it easier to evaluate the distortion analytically for such mappings.

From (13) it is clear why a linear system is convenient at low SNR as  $\kappa_i = 0, \forall i$  and the error becomes minimal, corresponding exactly to the weak noise distortion. For higher SNR

one would therefore seek nonlinear mappings with low curvature  $\forall \mathbf{x}$ , or mappings consisting of parallel lines or planes (like HDA systems). Therefore the weak noise regime, as defined next, is a good approximation for any *reasonably* chosen mappings at high SNR.

We can now define what we mean by *weak noise* more rigorously:

*Definition 2: Weak noise regime (dimension expansion)*

Let  $\mathbf{x}_0$  denote the transmitted vector and  $\mathbf{S}(\mathbf{x}_0)$  its representation in the channel space. We say that we are in the *weak noise regime* whenever the 2nd order term in (13) (the term containing  $\kappa_i$ ), are negligible compared to the 1st order term. That is, (9) is a close approximation to  $\mathbf{S}$  and the weak noise distortion in (10) provides an accurate approximation to the actual distortion in the absence of anomalies.  $\square$

We clarify the weak noise concept through examples:

**Examples:** When is Definition 2 satisfied?

- i)  $\text{SNR} \rightarrow \infty$  (or  $\sigma_n \rightarrow 0$ ): The linear approximation in (9) is exact as  $\mathcal{S}$  is locally Euclidean.
- ii)  $\mathbf{S}$  is linear or HDA (in the absence of anomalous errors): Now  $\kappa_i = 0, \forall i$ . A linear mapping is optimal as  $\text{SNR} \rightarrow 0$  (or very low SNR) [32], [48]. More generally, HDA systems are composed of piecewise line- or surface elements.
- iii) Small maximal principal curvature  $\kappa_{\max}$ : The smaller  $\kappa_{\max}$  of  $\mathbf{S}$  is, the larger  $\sigma_n$  can be before (10) becomes inaccurate. This follows from (13). This is also inline with solution mappings resulting from numerical optimization algorithms (like PCCOVQ), which tend to bend less and less the lower the SNR is [49], [31].

2) *Anomalous distortion:* With a channel power constraint,  $\mathcal{S}$  must be constrained to line within some  $N - 1$  sphere<sup>9</sup>. In order to make weak noise distortion small, the relevant hyper surface must first be stretched, then bent and twisted to "fit" within this sphere. Fig. 4(b) illustrates how this can be done in the 1:2 case. Take a decomposition of the noise  $\mathbf{n}$  into a tangential component to the signal curve  $\mathbf{n}_{wn} = \mathbf{n}_{||}$ , and a normal component  $\mathbf{n}_{an} = \mathbf{n}_{\perp}$  as depicted in

<sup>9</sup>The definition of an  $N$ -sphere is  $\mathbb{S}^N = \{\mathbf{y} \in \mathbb{R}^{N+1} | d(\mathbf{y}, 0) = \text{constant}\}$  [50, p.7], where  $d$  is the distance from any point  $\mathbf{y}$  on  $\mathbb{S}^N$  to the origin of  $\mathbb{R}^{N+1}$ . E.g. the *sphere* embedded in  $\mathbb{R}^3$  is denoted  $\mathbb{S}^2$ , the "2-sphere".

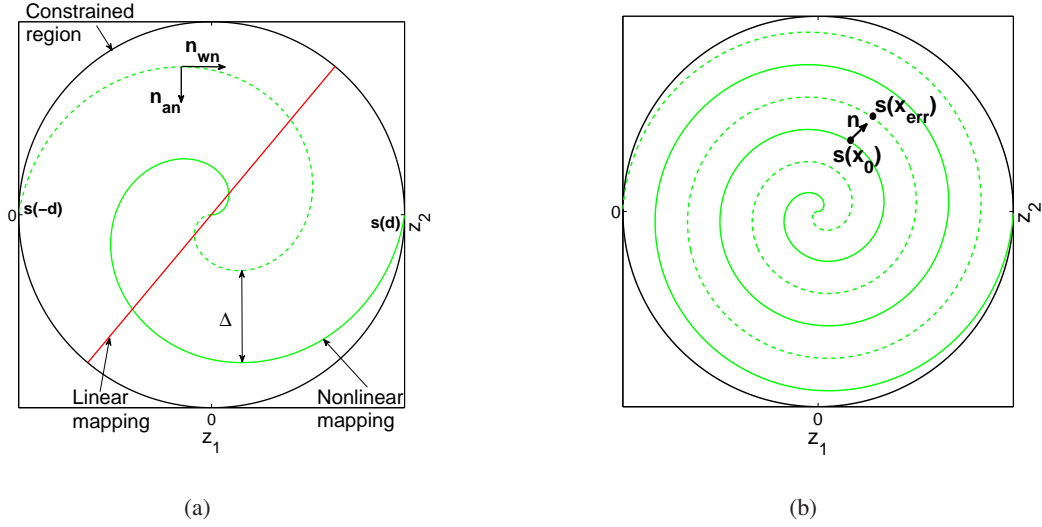


Fig. 4. Example of 1:2 S-K mappings ( $\pm d$  denote the boundary of  $\mathcal{D}$ ). 4(a) Linear and nonlinear mappings (negative source values represented by dashed curve). 4(b) As the spiral arms get close, noise may take the transmitted vector  $S(x_0)$  closer to another fold of the curve leading to large decoding errors.

Fig. 4(a).  $n_{wn}$  contributes to weak noise, whilst  $n_{an}$  contributes to *anomalous errors*, which are large errors occurring whenever  $\|n_{an}\|$  crosses a certain threshold. Then the transmitted vector  $S(x_0)$  representing  $x_0$ , will be detected as the vector  $S(x_{err})$  on another fold of the curve. This happens if the distance,  $\Delta$ , between the spiral arms is chosen too small w.r.t.  $\sigma_n$ . Although  $S(x_{err})$  is not far away from  $S(x_0)$  in the channel space, the value it represents,  $x_{err}$ , is far away from  $x_0$  in source space, leading to large reconstruction errors. The occurrence of anomalous errors depend on  $\sigma_n$ , and the minimum distance  $\Delta_{min}$  between folds of  $S$  as well as its curvature. For anomalous errors to occur with a small probability,  $\Delta_{min}$  should be chosen as large as possible. There is thus a tradeoff between reducing weak noise distortion (where  $\Delta_{min}$  should be as small as possible) and anomalous distortion. The exception is at low SNR where linear mappings may do just as well [32], [48]. In this case anomalous errors do not occur, and we will always be in the "weak noise regime" of Def. 2 as  $\kappa_i = 0, \forall i$  in (84) (see Fig. 4(a)).

To quantify anomalous distortion it is convenient to consider *Canal Surfaces* [41, pp. 266-268]. We begin with curves (1: $N$  mappings), the extension to surfaces is straight forward:

*Definition 3: Canal Surface*

A Canal Surface is the *envelope*,  $E$ , to the family,  $F$ , of congruent spheres (or  $N - 1$  hyperspheres  $\mathbb{S}^{N-1}$ ), and is the set of all *characteristics* to  $F$ , defined as the point set represented by [41, p. 263]

$$S_c(z_i, x) = 0, \quad \frac{\partial S_c(z_i, x)}{\partial x} = 0 \quad i = 1, \dots, N, \quad (14)$$

where  $S_c = 0$  defines a surface in  $\mathbb{R}^3$  (or hypersurface in  $\mathbb{R}^N$ ). The characteristic is a curve in  $\mathbb{R}^3$  (or a hypersurface of dimension  $N - 2$  in  $\mathbb{R}^N$ ). The *characteristic points* of the canal surface are the intersection of the characteristic given by [41, p. 266]

$$S_c(z_i, x) = 0, \quad \frac{\partial S_c(z_i, x)}{\partial x} = 0, \quad \frac{\partial^2 S_c(z_i, x)}{\partial x^2} = 0, \quad i = 1, \dots, N. \quad (15)$$

□

An important special case is the family,  $F$ , of spheres with constant radius  $r$  and center on a curve  $C : \mathbf{y}(x)$ , which can be represented as  $S_c(\mathbf{z}, x) = (\mathbf{z} - \mathbf{y}(x)) \cdot (\mathbf{z} - \mathbf{y}(x)) - r^2 = 0$ . In this case the characteristics of  $F$  are circles and the characteristic points are points of intersection of these circles. This concept can be directly applied to 1: $N$  S-K mappings in Gaussian noise by setting  $\mathbf{y} = \mathbf{S}(x)$ ,  $\mathbf{z}$  be the *channel coordinates* and  $x$  be the source values.

The extension to  $M:N$  mappings is straight forward: The *Canal Hypersurface* of an  $M$ -dimensional  $\mathcal{S}$  embedded in  $\mathbb{R}^N$  is the envelope of the congruent hyper-spheres  $\mathbb{S}^{N-M-1}$ . We refer to canal hypersurface simply as “canal surface” in the following.

Canal surfaces are important for S-K mappings as they under certain conditions can guarantee a low probability for anomalous errors, and in the asymptotic case one can avoid them completely as will be seen in Section IV-A:

*Lemma 1:* Consider  $M:N$  dimension expanding S-K mapping  $\mathcal{S}$ . Let  $\rho_{\min} = 1/\kappa_{\max}$ , with  $\kappa_{\max}$  the maximal principal curvature of  $\mathcal{S}$ , and  $r$  the radius of the hyper-sphere  $\mathbb{S}^{N-M-1}$ . Further, let  $\Delta_{\min}$  be the minimum distance between any fold of  $\mathcal{S}$  for any  $\mathbf{x}$ : Then the corresponding canal surface (the envelope of  $\mathbb{S}^{N-M-1}$ ) will not intersect itself at any point, that is, the canal surface will have no characteristic points  $\iff$  i)  $\Delta_{\min} > 2r$  and ii)  $\rho_{\min} > r$  for all points of  $\mathcal{S}$ .

*Proof:* See Appendix B-A3. □

**Remark I:** Note that condition ii) is incorporated into condition i). The reason we state condition ii) is to constrain the curvature of  $\mathcal{S}$  so that it can be removed from the analysis later.

**Remark II:** For 1: $N$  mappings,  $\kappa_{\max}$  is basically the curvature of the signal curve itself.

We give an example on a 1:3 mapping: Fig. 5 depicts a canal surface surrounding a curve in channel space  $\mathbb{R}^3$ . The radius of the canal surface is linked to the noise through  $\mathbf{n}_{an} = \mathbf{n}_\perp$ .

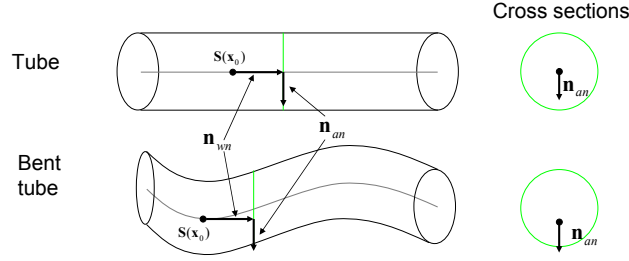


Fig. 5. Canal Surfaces: Top figure: Linear signal curve  $\mathbb{L} \times \mathbb{S}^1$ . Bottom figure: nonlinear signal curve  $\mathbf{S} \times \mathbb{S}^1$ .

Bending of the tube (nonlinear mappings) can increase the probability for anomalous errors, implying that a straight line has the lowest possible probability for such errors in any case. Therefore any non-linear mapping is potentially sub-optimal due to a less efficient suppression of anomalous errors. However, according to Lemma 1 one can avoid this problem as long as the radius of curvature of  $\mathbf{S}$  is small enough. By setting

$$\rho_s > r = \rho_n \geq \sqrt{\frac{N-1}{N}} b_n \sigma_n^2, \quad (16)$$

then no characteristic points will exist, and the canal surface will not intersect itself if condition i) above is also satisfied.

We provide a definition of anomalous distortion valid in the vicinity of the optimal operational SNR. That is, only jumps to the nearest point on another fold,  $\mathbf{S}(x_{err})$ , from a given transmitted point,  $\mathbf{S}(\mathbf{x}_0)$ , are considered (jumps across several folds may happen as  $\sigma_n$  grows, but this is far from optimal). Fig. 4 shows the terminology used in the following definition.

*Definition 4: Anomalous distortion*

Let  $\mathbf{x}_0$  denote the transmitted vector and  $\mathbf{S}(\mathbf{x}_0)$  be its representation in the channel space. Let  $\mathbf{n}_{an}$  denote the  $K(\leq N)$  dimensional component of a decomposition of the noise vector  $\mathbf{n}$

that points in the direction of the closest point  $\mathbf{S}(\mathbf{x}_{err})$  on any other fold of  $\mathbf{S}$  from  $\mathbf{S}(\mathbf{x}_0)$  (as seen in Fig. 4(a)).  $\mathbf{x}_{err}(\mathbf{x}_0)$  denotes the reconstructed vector in the case of this anomaly. Let  $\Delta_{min}(\mathbf{x}_0)$  denote the Euclidean distance between  $\mathbf{S}(\mathbf{x}_0)$  and  $\mathbf{S}(\mathbf{x}_{err})$ . Further, let  $\rho_{an} = \|\mathbf{n}_{an}\|$  with  $f_{\rho_{an}}(\rho_{an})$  its pdf. The probability that  $\mathbf{x}_0$  is detected as  $\mathbf{x}_{err}$  is then

$$P_{an}(\mathbf{x}_0) = \int_{\Delta_{min}(\mathbf{x}_0)/2}^{\infty} f_{\rho_{an}}(\rho_{an}) d\rho_{an}. \quad (17)$$

The anomalous distortion close to the optimal operational SNR is then defined as

$$\bar{\varepsilon}_{an}^2 = E_{\mathbf{x}} \{ P_{an}(\mathbf{x}) \|\mathbf{x} - \mathbf{x}_{err}(\mathbf{x})\|^2 \}. \quad (18)$$

□

Since anomalous distortion is structure dependent one cannot find a closed form expression before a specific  $\mathcal{S}$  has been chosen.

#### B. $M:N$ Dimension Reducing S-K mappings.

Results presented in this section are extensions of [51]. Fig. 6 shows a block diagram for the dimension reducing communication system under consideration. As defined in Section II-B, a

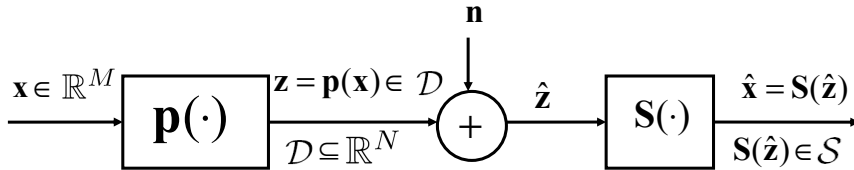


Fig. 6. Dimension reducing ( $M < N$ ) communication system for S-K mappings.

dimension reducing S-K mappings  $\mathcal{S}$  is an  $N$  dimensional subset of the source space  $\mathbb{R}^M$  that can be realized by a hyper surface  $\mathbf{S}$  as in (3), parameterized by the channel signal  $\mathbf{z}$ . In this sense, the S-K mapping is a representation of the channel in the source space.

To reduce the dimension of a source under a channel power constraint, its information content must be reduced, i.e., a lossy scheme is inevitable. This is obtained by approximating any source vector by its projection onto  $\mathcal{S}$ , an operation denoted  $\mathbf{q}(\mathbf{x}) \in \mathbf{S} \subset \mathbb{R}^M$ . The dimension

is subsequently changed from  $M$  to  $N$  by a lossless operator  $\mathbf{d}_r : \mathcal{S} \rightarrow \mathcal{D}_c \subseteq \mathbb{R}^N$ , where  $\mathcal{D}_c$  is the domain of the channel signal determined by the channel power constraint (an  $N$ -dimensional ball with radius  $\rho_N$  in the Gaussian case). The total operation is named *projection operation*, and denoted  $\mathbf{p} = \mathbf{d}_r \circ \mathbf{q} : \mathbf{x} \in \mathbb{R}^M \mapsto \mathbf{p}(\mathbf{x}) \in \mathcal{D}_c \subseteq \mathbb{R}^N$ . The vector  $\mathbf{z} = \mathbf{p}(\mathbf{x})$  is transmitted over an AWGN channel with noise  $\mathbf{n} \in \mathbb{R}^N$ . The effect of channel noise will be a displacement of the projected source vector along  $\mathcal{S}$ . With a continuous S-K mapping, the distortion due to channel noise will be gradually increasing with  $\sigma_n^2$ , i.e. no anomalous errors will occur. Anomalous errors may occur if  $\mathcal{S}$  is piecewise continuous (like HDA schemes). The reconstructed vector is  $\hat{\mathbf{x}} = \mathbf{S}(\hat{\mathbf{z}})$  (ML detection). The concept is illustrated for a 2:1 mapping in Fig. 7(b).

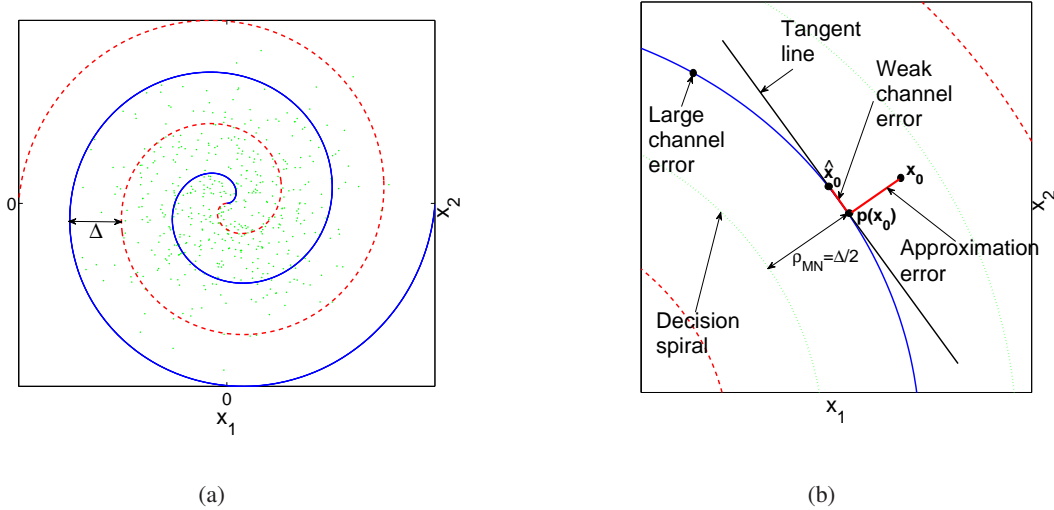


Fig. 7. Dimension reducing S-K mapping for the 2:1 case. 7(a) Covering of source space with parametric curve. The dashed lines represent negative channel values. Green dots are source vectors drawn from a 2D Gaussian distribution. 7(b) Local behavior: The spiral segments are close to Osculating circles.

There are two main contributions to the total distortion for continuous  $\mathcal{S}$ ; *approximation distortion* from the lossy projection operation, and *channel distortion* resulting from channel noise mapped through  $\mathcal{S}$  at the receiver. In addition, it is also important that the source vectors with highest probability are allocated to the channel representations with low power to minimize the channel power and reduce the effect of noise as detailed in [52, p.103].

1) *Channel distortion*: The received vector  $\hat{\mathbf{z}} = \mathbf{z} + \mathbf{n}$  must be passed through  $\mathcal{S}$  to reconstruct  $\mathbf{x}$ . When noise is sufficiently small (relative to the curvature of  $\mathcal{S}$ ), distortion can be modelled by

considering the tangent space of  $\mathcal{S}$ . That is, one can consider the linear approximation  $\mathbf{S}_{lin}(\mathbf{z}_0)$  of  $\mathbf{S}(\mathbf{z})$  at  $\mathbf{z}_0$

$$\mathbf{S}_{lin}(\mathbf{z}_0 + \mathbf{n}) = \mathbf{S}(\mathbf{z}_0) + J(\mathbf{z}_0)\mathbf{n}. \quad (19)$$

The following proposition gives the exact distortion under linear approximation:

*Proposition 3: Minimum Weak Channel Distortion*

For any continuous i.i.d. Gaussian channel of dimension  $N$  and any dimension reducing S-K mapping  $\mathbf{S}$  where  $S_i \in C^r(\mathbb{R}^M)$ ,  $r \geq 1$ ,  $i = 1, \dots, M$ , the distortion due to channel noise under the linear approximation in (19) is given by

$$\bar{\varepsilon}_{chw}^2 = \frac{\sigma_n^2}{M} \iint \cdots \int_{\mathcal{D}_c} \sum_{i=1}^N g_{ii}(\mathbf{z}) f_{\mathbf{z}}(\mathbf{z}) d\mathbf{z}, \quad (20)$$

where  $f_{\mathbf{z}}(\mathbf{z})$  is the channel pdf, and  $g_{ii}$  the diagonal components of the metric tensor of  $\mathbf{S}$ .

*Proof:* See Appendix B-B1. □

The name *weak channel distortion* is due to Def. 5 given below. Prop. 3 states that weak channel distortion increases in magnitude as  $\mathcal{S}$  is stretched since then  $g_{ii}$  increases. To keep the channel distortion small,  $\mathcal{S}$  should therefore be stretched as little as possible<sup>10</sup>.

The following corollary is a special case of Proposition 3:

*Corollary 2: Shape preserving mapping*

When  $\mathbf{S}$  has a diagonal metric tensor with  $g_{ii}(\mathbf{z}) = g_{jj}(\mathbf{z}) = \alpha, \forall z, i, j$ , and  $\alpha$  constant, the weak channel distortion becomes

$$\bar{\varepsilon}_{ch}^2 = \frac{N\sigma_n^2}{M} \alpha^2. \quad (21)$$

I.e. all channel vectors are equally scaled when mapped through  $\mathbf{S}$ , thus noise will affect all source vectors  $\mathbf{x}$  equally.

*Proof:* Insert  $g_{ii}(\mathbf{z}) = g_{jj}(\mathbf{z}) = \alpha$  in (20). □

<sup>10</sup>The opposite is sought in the dimension expansion case as an increase of  $g_{ii}$  leads to larger attenuation of noise at the receiver side, whereas in the dimension reduction case, increase of  $g_{ii}$  will amplify the noise at the receiver.

Under Corollary 2,  $\mathcal{S}$  can be seen as an amplification  $\alpha$  from channel to source at the receiver.

When channel noise becomes larger (compared to the curvature of  $\mathcal{S}$ ), its distortion will depend on the global structure of  $\mathbf{S}$  as illustrated in Fig. 7(b). In order to determine the error made in the distortion estimate under linear approximation, we consider 2nd order Taylor expansion. We have the following proposition:

*Proposition 4: Error under 2nd order Taylor approximation (dimension reduction)*

Under a 2nd order Taylor approximation and the special case of  $M:1$  mappings (curves) the error due to channel noise is given by

$$\varepsilon_{ch}^2(x_0) = \sigma_n^2 \|\mathbf{S}'_0\|^2 + \frac{3\sigma_n^4 \|\mathbf{S}''_0\|^2}{4 \|\mathbf{S}'_0\|^4} = \|\mathbf{S}'_0\|^2 \sigma_n^2 + \frac{3\sigma_n^4 \kappa^2(x_0)}{4}, \quad (22)$$

which is valid for any S-K mapping  $\mathbf{S}(x) \in C^n$ ,  $n \geq 2$ . The last equality is true under scaled arc length parametrization. Further, for any dimension reducing S-K mapping as defined in Def. 9, with LoC coordinate curves, the error is given by

$$\varepsilon_{ch}^2(\mathbf{x}_0) \approx \frac{\sigma_n^2}{M} \sum_{i=1}^N \left( g_{ii}(\mathbf{z}_0) + \frac{3\sigma_n^2}{4} \kappa_i^2(\mathbf{z}_0) \right) = \frac{\sigma_n^2}{M} \sum_{i=1}^N \left( g_{ii}(\mathbf{z}_0) + \frac{3\sigma_n^2}{4} \frac{b_{ii}^2(\mathbf{z}_0)}{g_{ii}^2(\mathbf{z}_0)} \right). \quad (23)$$

Again  $g_{ii}$  are the diagonal components of the metric tensor (or FFF) and  $b_{ii}$  the diagonal components of the SFF.

*Proof:* See Appendix B-B2. □

Note the similarity to dimension expansion in Proposition 2: The distortion is scaled by the components of the SFF (or curvature) in nearly the same manner. The scaling w.r.t.  $g_{ii}$  is opposite, which is expected.

**Remark:** In the proof of Prop. 4 one arrives at the expression (Appendix B-B2, Eq. (91))

$$\varepsilon_{ch}^2(x_0) = \sigma_n^2 \|\dot{\mathbf{S}}(x_0)\|^2 + \frac{3\sigma_n^4}{4} \|\ddot{\mathbf{S}}(x_0)\|^2 + \frac{5\sigma_n^6}{12} \|\ddot{\mathbf{S}}(x_0)\|^2 = \sigma_n^2 + \frac{3}{4} \kappa_0^2 \sigma_n^4 + \frac{5}{12} \kappa_0^2 \tau_0^2 \sigma_n^6, \quad (24)$$

for the channel error under 3rd order Taylor expansion. The last equality results from the *canonical representation* in [41, p.48], valid for any curve  $\mathbf{s} \in C^3$  (of class  $C^r$ ,  $r \geq 3$ ). This shows that higher order terms get even smaller as  $\sigma_n$  decreases, at least for curves with small curvature ( $\kappa_0$ ) and torsion ( $\tau_0$ ). Referring back to Section III-A, this is the reason why we did not consider Taylor expansion beyond 2nd order there. The error in the ML-estimate increases with

$\kappa$  and  $\tau$ . However, for continuous mappings,  $\kappa$  and  $\tau$  need to be non-zero in order to cover the sources space and thereby keep the approximation distortion low. One should therefore choose a curve that fills the source space with the smallest possible  $\kappa$  and  $\tau$ .

Consider the channel error given by the 2nd order approximation to  $\mathbf{S}$  in (23).

*Definition 5: Weak noise regime (dimension reduction)*

Let  $\mathbf{z}_0$  denote the transmitted vector and  $\mathbf{S}(\mathbf{z}_0)$  its representation in the source space. We are in the *weak noise regime* whenever the second (or higher) order term in (23), i.e., the terms containing  $\kappa_i$ , are negligible compared to the 1st order term. That is, (19) is a close approximation to  $\mathbf{S}$  and the weak channel distortion in (20) provides an accurate approximation to the actual distortion due to channel noise.  $\square$

From (23) it is clear why a linear system is convenient at low SNR, as  $\kappa_i = 0$  and the error becomes minimal, corresponding exactly to the weak channel distortion. For higher SNR one would seek nonlinear mappings with low curvature or mappings consisting of parallel lines or planes (just like HDA systems). And therefore the weak noise regime is a good approximation for any *reasonably* chosen mappings at high SNR.

2) *Approximation distortion*: Approximation distortion results from the lossy operation  $\mathbf{p}$ . Its size depends on the average distance source vectors have to  $\mathcal{S}$ . In order to make the approximation distortion as small as possible,  $\mathcal{S}$  should cover the source space so that every  $\mathbf{x}$  is as close to it as possible. Covering of the source space is obtained by stretching, bending and twisting the transformed channel space  $\mathcal{S}$  inside the subset of the source space with significant probability mass<sup>11</sup> (an example for the 2:1 case is provided in Fig. 7(a)). This is in conflict with the requirement of reducing channel distortion in which the stretching of  $\mathcal{S}$  should be minimized. There is thus a tradeoff between the two distortion contributions.

Since approximation distortion is structure dependent, one cannot find a closed form expression for it in general. However, one can find a general expression valid for certain *simple* mapping structures that becomes exact as the dimension of the mapping becomes large.

<sup>11</sup>*significant probability mass* refers to all events except those with very low probability. E.g., like the “ $4\sigma$  loading” used in [53, pp. 124-125] when constructing scalar quantizers.

*Definition 6: Uniform S-K mapping*

For an S-K mapping where at each point,  $\mathbf{S}(\mathbf{z}_0)$ ,  $\forall \mathbf{z}_0 \in \mathcal{D}_c$ , there is a fixed distance  $\Delta$  to the nearest point on another fold of  $\mathbf{S}$ , is named a *uniform S-K mapping*. The maximal approximation error from  $\mathbf{x}$  to  $\mathbf{S}$  will then be  $\Delta/2$  for any  $\mathbf{x}$  to any point of  $\mathbf{S}$ .  $\square$

**Remark:** Note that for a uniform mapping, any vector being approximated to any point of  $\mathbf{S}$  will be confined within a Canal Surface as defined in Section III-A2, Definition 3.

The 2:1 S-K mapping shown in Fig. 7(a) is a uniform mapping (except close to the origin). For uniform S-K mappings, a similar distortion lower bound as that derived for vector quantizers in [54] can be found for small  $\Delta$ , i.e., a *sphere bound* [55]. We have the following proposition:

*Proposition 5: Sphere bound for approximation distortion*

For a uniform S-K mapping with distance  $\Delta$  between its closest folds, the approximation distortion is bounded by

$$\bar{\varepsilon}_a^2 \geq \frac{M - N}{4M(M - N + 2)} \Delta^2, \quad (25)$$

As this is a sphere bound, equality is achieved in the limit when  $M, N \rightarrow \infty$  [55] with  $N/M = r$  constant when  $\Delta$  is sufficiently small (i.e., at high SNR).

*Proof:* See Appendix B-B3.  $\square$

**Remark:** Note that the bound in (25) is exact in some low-dimensional cases. For example when  $M = 2$ ,  $N = 1$  using archimedes spiral, as this case is equivalent to a scalar quantizer.

#### IV. ASYMPTOTIC ANALYSIS FOR S-K MAPPINGS

We investigate how S-K mappings behave as the *dimensionality*<sup>12</sup> (or *block-length*) of the mappings increases. That is, can S-K mappings achieve OPTA as  $M, N \rightarrow \infty$  in general?

<sup>12</sup>I.e., letting  $M, N$  increase while  $r = N/M \in \mathbb{Q}^+$  is kept constant.

### A. Asymptotic analysis for dimension expanding S-K mappings.

In this section we determine under which conditions dimension expanding S-K mappings may achieve OPTA for  $\forall r \in \mathbb{Q}[1, \infty)$  in the limit  $M, N \rightarrow \infty$ . We only treat the case of Gaussian sources and channels. The results presented are extensions of [56].

Proving existence of (hyper) surfaces mapping between  $\mathbb{R}^M$  and  $\mathbb{R}^N$  satisfying a wanted distortion criterion is very hard, if at all possible. We therefore turn to a geometrical argument considering volumes. I.e., how large volume the transformed source will occupy in the channel space. We generalize results for 1: $N$  mappings presented in [57, pp.666-674].

We start with a Proposition concerning anomalous errors in the asymptotic case  $M, N \rightarrow \infty$ :

#### *Proposition 6: Asymptotic anomalous distortion*

Let the noise be normalized with the channel dimension  $N$ ,  $\tilde{\mathbf{n}} = \mathbf{n}/\sqrt{N}$ , and let  $\Delta_{min}$  denote the smallest distance to the closest point,  $\mathbf{S}(\mathbf{x}_{err})$ , on any other fold of  $\mathbf{S}$  for any transmitted vector  $\mathbf{S}(\mathbf{x}_0)$ . Furthermore, let  $\mathbf{n}_{an}$  denote the  $K(\leq N)$  dimensional component of a decomposition of  $\mathbf{n}$  pointing in the direction of the shortest distance to  $\mathbf{S}(\mathbf{x}_{err})$  from  $\mathbf{S}(\mathbf{x}_0)$ . Then anomalous distortion  $\bar{\varepsilon}_{an}^2 \rightarrow 0$  as  $K, N \rightarrow \infty$  if  $\Delta_{min} > 2\sqrt{K/N}\sigma_n$ .

*Proof:* Consider first normalized Gaussian noise vectors  $\tilde{\mathbf{n}}$ . By definition, these vectors have a mean length  $\sigma_n$ . It is shown in [57, pp.324-325] that the variance of  $\|\tilde{\mathbf{n}}\|$  decreases as  $N$  increases and that  $\lim_{N \rightarrow \infty} \|\tilde{\mathbf{n}}\| = \sigma_n$  with probability one. For  $\mathbf{n}_{an}$ , a  $K(< N)$  dimensional subset of  $\tilde{\mathbf{n}}$ , we get  $\|\mathbf{n}_{an}\| = \sqrt{K/N}\sigma_n$  with probability one.  $\square$

**Remark:** Note that this is equivalent to the requirement of no characteristic points for canal surfaces given in Lemma 1. I.e.,  $1/\kappa_{max} \geq \rho_n \geq \sqrt{b_n\sigma_n^2(N-M)/N}$ , with  $K = N - M$  and  $b_n \rightarrow 1$  as  $M, N \rightarrow \infty$ .

Proposition 6 is the key to performance improvement from increased dimensionality. From Definition 4 in Section III-A and Proposition 6 one can do some reasoning: The distribution of  $\rho = \|\tilde{\mathbf{n}}\|$ ,  $\tilde{\mathbf{n}} \in \mathbb{R}^N$ , is for the Gaussian case given by [58, p. 237]

$$f_\rho(\rho) = \frac{2(\frac{N}{2})^{\frac{N}{2}} \rho^{N-1}}{\Gamma(\frac{N}{2})\sigma_n^N} e^{-\frac{N\rho^2}{\sigma_n^2}}, \quad N \geq 1, \quad (26)$$

where  $\Gamma(\cdot)$  is the *Gamma function* [59]. Fig. 8(a) shows (26) for selected values of  $N$ . Note that the probability mass of  $\rho$  becomes more located around  $\sigma_n$  as  $N$  increases. Considering

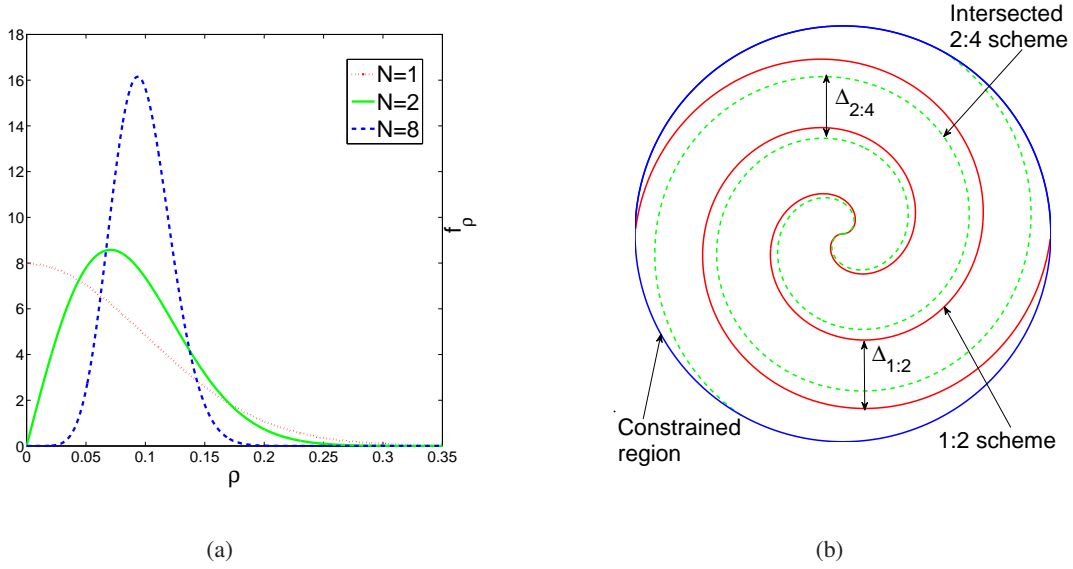


Fig. 8. 8(a) The pdf of  $\rho = \|\tilde{\mathbf{n}}\|$  when  $\sigma_n = 0.1$ . 8(b) How to close in on OPTA by increasing dimensionality. The green line illustrates an intersected surface. Since  $\Delta_{2:4} < \Delta_{1:2}$  for the same anomalous error probability, the 2:4 mapping may be stretched a bit further, thereby reducing  $\varepsilon_{wn}^2$ .

this effect w.r.t. S-K mappings, a gain can be obtained when increasing dimensionality as the minimum distance  $\Delta_{min}$  between different folds of  $\mathcal{S}$  can be reduced: Consider  $r = 2$ , which can be accomplished by both 1:2 and 2:4 mappings. Further, choose a 2:4 mapping with a diagonal  $G$  with  $g_{11} = g_{22}$ , both chosen optimally. The 2:4 mapping can then be “packed” more densely in the channel space as  $f_\rho(\rho)$  narrows, making  $\Delta_{2:4}$  smaller compared to  $\Delta_{1:2}$ . This yields additional stretching of the source space, i.e.  $g_{ii}$  can be made slightly larger, and one should therefore get closer to OPTA with the 2:4 mapping. Fig. 8(b) illustrates this concept. Note that the intersected 2:4 mapping in the figure is just an example to illustrate the concept, not an actual 2:4 mapping. We have to consider the whole 4-dimensional space for this to be true, as will be apparent from Proposition 9 in Section V.

Note that since linear mappings are shape preserving and do not introduce anomalous errors, they will enhance performance by increasing dimensionality. Therefore they are sub-optimal except when  $\text{SNR} \rightarrow -\infty$ , or  $M = N$  (for the Gaussian case).

According to Proposition 6, anomalous errors can be avoided as  $M, N \rightarrow \infty$  by making  $\Delta_{min} \geq 2\sqrt{K/N}\sigma_n$ . We want to determine the smallest obtainable weak noise distortion under

this condition without violating a channel power constraint. As will be seen in the following, for a fixed noise variance  $\sigma_n^2$ , this is the same as satisfying Lemma 1.

In order to determine the volume that  $\mathcal{S}$  occupies within a constrained region of the channel space it must be enclosed within an entity that has the same dimension as the channel space. Arguments in [57, pp. 670-672] reveal that for 1: $N$  mappings this entity should be a tube with constant radius  $\rho_{MN} \geq \|\mathbf{n}_{an}\| > \sqrt{b_{NM}^2 \sigma_n^2 (N-1)/N}$  ( $b_N \rightarrow 1$  as  $N \rightarrow \infty$ ), with the signal curve as its “center”. This is a  $N-1$  dimensional “tube” denoted by the cartesian product  $\mathbf{S} \times \mathbb{S}^{N-2}$ , with  $\mathbb{S}^{N-2}$  an  $N-2$  sphere with radius  $\rho_{MN}$ , or locally  $\mathbb{L} \times \mathbb{S}^{N-2}$ , where  $\mathbb{L}$  is a small line-segment. This is a canal surface (see Definition 3 in Section III-A2). To see why this canal surface should be chosen, consider the 1:3 mapping in Fig. 5. If the tube bends the probability for anomalous errors increase. The probability for anomalous errors is therefore minimized for  $\mathbb{L} \times \mathbb{S}^1$  (locally). Also, making the tube wider in certain places makes the signal curve occupy unnecessary space, leading to sub-optimal space utilization and a larger weak noise distortion than necessary. However, a bent canal surface will work as long as there are no characteristic points, and for the same reason as in Definition 2, we have a local  $\mathbb{L} \times \mathbb{S}^{N-2}$  structure as long as the curvature is small enough (see Definition 7). I.e., as long as Lemma 1 is satisfied.

To analyze  $M:N$  mappings,  $\mathbf{S} \times \mathbb{S}^{N-2}$  must be generalized to enclose  $M$ -dimensional hyper surfaces. Take a 2:4 mapping as an example: Locally, we now have a disc denoted by  $\mathbb{B}^2$  (corresponding to the stretched source) that must be enclosed in a 4-dimensional entity. There are now two orthogonal vectors perpendicular to  $\mathbb{B}^2$  ( $\dim(\mathbf{n}_{an}) = 2$ ) that must be shorter than a certain maximum length to make anomalous errors appear with low probability. To achieve the same symmetrical entity as for curves, these two vectors must be located within a circle with radius  $\rho_{MN}$ , where  $\rho_{MN} > \sqrt{b_N^2 \sigma_n^2 / 2 + \delta^2}$  in order to avoid anomalous errors. The entity  $\mathbf{S} \times \mathbb{S}^1$ , which locally is represented by  $\mathbb{B}^2 \times \mathbb{S}^1$ , therefore results. Continuing this argument to an  $M:N$  mapping leads to the entity  $\mathbf{S} \times \mathbb{S}^{N-M-1}$ , which locally is  $\mathbb{B}^M \times \mathbb{S}^{N-M-1}$ . Here  $\mathbb{B}^M$  is an  $M$ -dimensional *ball* with radius  $\rho_M$  i.e., a spherical region in  $\mathbb{R}^M$  connected to a certain *radius*  $\rho_M$ .  $\rho_M$  will be unbounded in lower dimensional case, whether it will become the mean of the relevant source distribution as  $M \rightarrow \infty$ .  $\mathbb{S}^{N-M-1}$  is an  $N-M-1$  sphere with radius  $\rho_{MN} \geq \sqrt{b_{NM}^2 \sigma_n^2 (N-M)/N}$ . This is the same as the canal hyper surface introduced in Section III-A2 (Definition 3). We make the following definition:

*Definition 7: Local  $\mathbb{B}^M \times \mathbb{S}^{N-M-1}$  regime*

The S-K mapping  $\mathbf{S}$  is locally at the *center* of  $\mathbb{B}^M \times \mathbb{S}^{N-M-1}$  if: i) Definition 2 is satisfied ii) The distance to the closest point on a different fold of  $\mathbf{S}$  is  $\Delta_{min} = 2\rho_{MN} \geq 2\sqrt{(N-M)/N(\sigma_n^2 + \delta_{MN}^2)}$  at every point  $\mathbf{S}(\mathbf{x}_0), \forall \mathbf{x}_0 \in \mathcal{D}$  iii) Lemma 1 is satisfied, i.e., the canal surface  $\mathbf{S} \times \mathbb{S}^{N-M-1}$  has no characteristic points.  $\square$

**Remark:** i) says that  $\mathbf{S}$  must be approximately flat inside a sphere of radius  $\sigma_n$  as  $M, N \rightarrow \infty$  at every point of  $\mathbf{S}$ . That is, the maximal principal curvature  $\kappa_{max}$  must be small enough for the 1st order term in (84) to dominate. ii) and iii) is to avoid anomalous errors. For example, Definition 7 is satisfied for a 1:3 mapping if the right cylinder in Fig. 5 is a valid model locally along the whole curve with high accuracy. To avoid sub-optimal usage of the channel space for a given SNR,  $\rho_{MN}$  should be chosen constant and as small as possible for a given SNR while satisfying Definition 7.

We have the following proposition:

*Proposition 7: Minimum asymptotic distortion for dimension expanding S-K mappings*

Assume that  $f_{\mathbf{x}}(\mathbf{x})$  is Gaussian. Any shape preserving dimension expanding S-K mapping satisfying Definition 7, will in the limit  $M, N \rightarrow \infty$ , for any  $r = N/M \in \mathbb{Q}([1, \infty))$ , have anomalous distortion  $\bar{\varepsilon}_{an}^2 \rightarrow 0$  and potentially obtain weak noise distortion given by

$$\bar{\varepsilon}_{wn_{min}}^2 = \sigma_x^2 \left( 1 + \frac{P_N}{\sigma_n^2} \right)^{-r} \quad (27)$$

*Proof:* See Appendix C-A.  $\square$

For  $\mathcal{S}$  with fixed  $\rho_{MN}$  there is a distinct optimal channel SNR: If  $\sigma_n$  increases beyond this point the system deteriorates due to anomalous errors, while if  $\sigma_n$  decreases there will be unutilized space available to stretch  $\mathcal{S}$  further implying a sub-optimal weak noise distortion. In the latter case the slope of SDR vs SNR will follow that of a linear system according to (84) as the first term dominates.

We summarize the conditions that dimension expanding S-K mappings must satisfy in the limit  $M, N \rightarrow \infty$  to achieve the distortion of Proposition 7:

1. Definitions 2 and 7 must be satisfied. I.e.  $\mathcal{S}$  should be approximately flat within a sphere of radius  $\sigma_n$ . This implies that the larger  $\sigma_n$  is, the smaller the maximal principal curvature  $\kappa_{max}$  should be, so that the 1st order term in (84) dominates.

2. Corollary 1 should be satisfied, i.e.,  $\mathcal{S}$  should be shape preserving (this is a sufficient but not necessary condition).

3. At any point  $\mathbf{S}(\mathbf{x}_0) \in \mathcal{S}$ , the minimum distance  $\Delta_{min}$  between any closest folds of  $\mathcal{S}$  must satisfy  $\Delta_{min} > 2\sqrt{(1 - 1/r)\sigma_n^2}$  to avoid anomalous errors. I.e., the canal surface connected to  $\mathcal{S}$  and  $\sigma_n^2$  should have no characteristic points (Proposition 1 should be satisfied).

4.  $\mathcal{S}$  should fill the channel space as densely as possible while satisfying 1) and 3) for a given power constraint in order to stretch (amplify) the source as much as possible and thereby minimize weak noise distortion. A mapping  $\mathcal{S}$  with  $\rho_{MN} = \Delta_{min} \forall \mathbf{x}_0$  is then sufficient.

What S-K mappings would satisfy all these conditions? Low dimensional equivalents to such mappings are shown for the 1:2 case in Fig 9. The mapping in Fig. 9(a) potentially fulfill all

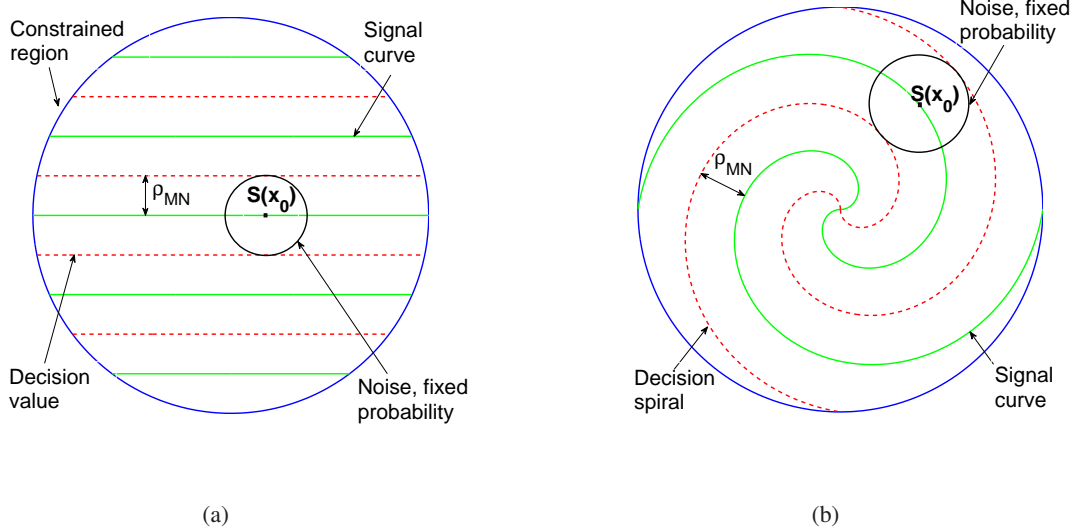


Fig. 9. Structures that potentially satisfies the necessary and sufficient conditions of Proposition 7.  $\rho_{MN}$  should increase with decreasing SNR and decrease with increasing SNR. (a) Piecewise linear (HDA-like) structure (b) Archimedes spiral.

these condition as its uniform,  $\kappa = 0$ , and it simultaneously fills the channel space. The spiral mapping in Fig. 9(b) potentially satisfies 2-4, as well as 1 as long as  $\kappa \ll \sigma_n^2$ . That is, the spiral

must have smaller curvature as the SNR drops (obtained by choosing  $\Delta_{min}$  larger). This is inline with earlier efforts [2]. The question for both these mappings is whether higher dimensional generalizations can be constructed that satisfy the four conditions above. As will be shown in Section V any such mapping would also need to be non-decomposable into lower dimensional sub-mappings (Proposition 9). Since  $\kappa = 0$  for the piecewise linear mapping in Fig. 9(a) this is likely the simplest choice when generalizing S-K mappings to higher dimensional cases.

**Remark:** The equal dimension case  $M = N$  is a special case of Proposition 7, where  $\bar{\varepsilon}_{an}^2 = 0$ . For Gaussian sources and channels,  $\bar{\varepsilon}_{wn}^2$  follows (10) exactly  $\forall M, N$ , and one can set  $g_{ii} = \alpha_i$  (a shape preserving mapping as in Corollary 1) and (27) is achieved even when  $M=N=1$  [5]. For other source distributions than Gaussian, optimality is not necessarily achieved when  $M=N=1$ . One reason may be that a shape preserving mapping is suboptimal, i.e.  $g_{ii}$  must be a function of  $\mathbf{x}$ ,  $\forall i$ , in order to match the source and channel pdf's.

### B. Dimension reducing S-K mappings.

In this section we determine under which conditions dimension reducing S-K mappings may achieve OPTA for  $\forall r \in \mathbb{Q}[0, 1)$  in the limit  $M, N \rightarrow \infty$ . We only treat Gaussian sources.

We consider continuous mappings here to avoid dealing with anomalous errors. We then need to determined the optimal balance between approximation distortion and channel distortion (as in [60]). For the same reason as in Section IV-A, we use a volume approach. The approximation distortion is determined from the way the canal hyper surface of  $\mathcal{S}$  covers the source space, whereas the channel distortion is determined from the *stretching* of  $\mathcal{S}$  necessary to obtain this cover. To obtain the relevant canal surface we need to enclose  $\mathcal{S}$  inside an entity of the same dimension as the source space. For similar reasons as in Section IV-A, the canal surface is  $\mathbf{S} \times \mathbb{S}^{M-N-1}$  which locally can be approximated as  $\mathbb{B}^N \times \mathbb{S}^{M-N-1}$  (now residing in the source space).  $\mathbb{B}^N$  is a ball with radius  $\rho_N$ , while  $\mathbb{S}^{M-N-1}$  is a hyper-sphere with radius  $\rho_{MN}$ .  $\mathbb{B}^N$  is the local representation of the transformed channel space, and will therefore determine the magnitude of the channel distortion.  $\mathbb{S}^{M-N-1}$  corresponds to the decision borders for approximation to a uniform S-K mapping (Definition 6), and will determine the approximation distortion's magnitude, which is then given by (25), approaching equality at high SNR as  $M, N \rightarrow \infty$ . The following definition is needed:

*Definition 8: Local  $\mathbb{B}^N \times \mathbb{S}^{M-N-1}$  regime*

A S-K mapping  $\mathbf{S}$  resides locally at the *center* of  $\mathbb{B}^N \times \mathbb{S}^{M-N-1}$  if: i) Definition 5 is satisfied  
ii) Definition 6 is satisfied with  $\Delta = 2\rho_{MN}$ , where  $\rho_{MN}$  is the radius of  $\mathbb{S}^{M-N-1}$ .  $\square$

Condition i) in Definition 8 states that  $\mathbf{S}$  must be approximately flat inside a sphere of radius  $\alpha\sqrt{b_N}\sigma_n$  at any point  $\mathbf{S}(\mathbf{z}_0)$ , where  $\alpha$  is an amplification factor representing a shape preserving mapping. ii) ensures uniformity (Definition 6). Note that both i) and ii) will be satisfied iff the canal surface  $\mathbf{S} \times \mathbb{S}^{M-N-1}$  has no characteristic points, which limits the maximal principal curvature  $\kappa_{max}$ . Take the 3:1 case: we then have the canal surface in Fig. 5 but where  $\mathbf{n}_{an}$  now corresponds to the approximation error  $\mathbf{x}_0 - \mathbf{p}(\mathbf{x}_0)$  and  $\mathbf{n}_{wn}$  corresponds to the channel error  $\mathbf{S}(\hat{\mathbf{x}}_0) - \mathbf{p}(\mathbf{x}_0)$ .

We have the following Proposition.

*Proposition 8: Minimum asymptotic distortion for dimension reducing S-K mappings*

Assume that  $f_{\mathbf{x}}(\mathbf{x})$  is Gaussian. Any shape preserving and continuous dimension reducing S-K mapping satisfying Definition 8 will in the limit  $M, N \rightarrow \infty$ , for any  $r = N/M \in \mathbb{Q}([0, 1])$ , can potentially obtain the distortion

$$D_{min} = \bar{\varepsilon}_a^2 + \bar{\varepsilon}_{ch}^2 = \sigma_x^2 \left( 1 + \frac{P_N}{\sigma_n^2} \right)^{-r} \quad (28)$$

*Proof:* See Appendix C-B.  $\square$

We summarize the conditions that a dimension reducing S-K mapping should follow in order to satisfy Proposition 8:

1. Definitions 5 and 8 must be satisfied. I.e.  $\mathbf{S}$  should be approximately flat within a sphere of radius  $\alpha\sigma_n$ , implying that larger  $\sigma_n$  necessitates a smaller maximal principal curvature  $\kappa_{max}$ .
2.  $\mathbf{S}$  is uniform (as in Definition 6) and shape preserving (Corollary 2).
3.  $\mathbf{S}$  should be continuous to avoid anomalous errors.
4. For a fixed approximation distortion, the canal surface of  $\mathbf{S}$  should cover the source space with the least possible stretching and curvature of  $\mathbf{S}$  to minimize channel distortion.

As in the expansion case, the mappings would also need to be non-decomposable into lower dimensional sub-mappings (Proposition 9) as proven in Section V.

What  $\mathcal{S}$  satisfies all these conditions? The mapping in Fig 7(a) satisfies 2-4 well in the finite dimensional case. However, as in the expansion case  $\kappa \ll \sigma_n^2$  if point 1) should be satisfied (it may also be hard to find higher dimensional generalizations). A similar mapping to the one shown in Fig. 9(a), now residing in the source space, clearly satisfies 1), 2) and 4) (as the curvature  $\kappa = 0$ ) but now 3) is violated. Recently, it has been shown that generalization of the mapping in Fig. 9(a) to arbitrary dimensionality can achieve the bound as  $\text{SNR} \rightarrow \infty$  [61], [40]. Condition 3 is therefore not necessary, only sufficient. Also, condition 2) is likely sufficient.

**Remark:** One may prove a similar result as Proposition 8 for sources of other distributions than Gaussian. Take for example a Laplacian source: The same conditions may be valid, but now a *diamond* shaped region should be covered by  $\mathcal{S}$  (instead of a spherical) in order to achieve the minimum approximation distortion for a given channel distortion. A shape preserving mapping may not be optimal in the non-Gaussian case, and therefore the general expression in (20) should be addressed. An example on a 2:1 mapping for Laplacian sources is given in [33, pp. 67-75].

## V. MAPPING CONSTRUCTION

Construction of 1: $N$  or  $M$ :1 mappings follow more or less directly from results and conditions derived for curves throughout this paper as exemplified in [2]. However, when it comes to surfaces (and hyper surfaces in general) more constraints have to be imposed in order for the mapping to be well-performing and follow the same slope as the OPTA curve at high SNR. We consider surfaces in  $\mathbb{R}^3$  (if not otherwise stated) in order to obtain more simple and explicit results. These results can be extended to higher dimensional surfaces and spaces more or less directly.

Earlier investigations [35] showed that a diagonal metric tensor with independent components  $g_{ii}(x_i) = \text{constant } \forall i$  is convenient as it avoids nonlinear distortion effects and provides a shape preserving mapping (see Propositions 1 and 2)<sup>13</sup>. Further, for general (source) distributions it may be convenient to choose

$$G(x_1, x_2) = \text{diag}[g_{11}(x_1), g_{22}(x_2)] \quad (29)$$

<sup>13</sup>A diagonal  $G$  arises naturally from (10) and (20) as only the  $g_{ii}$ 's contribute.

where  $g_{ii}(x_i)$  can be “adjusted” to the sources pdf for each coordinate curve on  $\mathcal{S}$  (using for example the method in [47, pp.296-297] for  $1:N$  mappings). However, this constraint is not sufficient. First of all, coordinate curves where  $g_{ii}$  only depends on  $x_i$  are possible only for certain sub-families of surfaces. Also, the metric in (29) is by itself not sufficient to obtain a mapping that has the same slope as the OPTA curve as  $\text{SNR} \rightarrow \infty$ . To further constrain the set of surfaces some more conditions are needed:

*Isometric surfaces* can be mapped onto each other in a length preserving manner [41]:

*Theorem 1:* An allowable mapping of a PoS  $\mathcal{S}$  onto a PoS  $\mathcal{S}^*$  is isometric  $\iff g_{\alpha\beta} = g_{\alpha\beta}^*$  at corresponding points when referred to the same coordinate system on  $\mathcal{S}$  and  $\mathcal{S}^*$ .

*Proof:* See [41, pp.176-177]. □

A subset of surfaces named *developable surfaces* (DS) can be mapped isometrically to the Euclidean plane [41, p.189], and is a special case of a *ruled surface* (RS). A RS is obtained by a set of straight lines, named *generators*  $\mathbf{z}(\ell)$ , interrelated through a space curve  $\mathbf{y}(\ell)$ , named *indicatrix*, as  $\mathbf{S}(\ell, t) = \mathbf{y}(\ell) + t\mathbf{z}(\ell)$ . Here  $\mathbf{z}$  is a unit vector linearly independent of the tangent  $\dot{\mathbf{y}}$  (i.e.,  $\dot{\mathbf{y}} \times \mathbf{z} \neq 0$ ). The indicatrix,  $\mathbf{y}(\ell)$ , acts like the “trajectory” for a straight line through space, and both  $\mathbf{z}$  and  $\mathbf{y}$  are coordinate curves on  $\mathcal{S}$ . Any DS has a G as in (29), where the  $g_{ii}$ ’s can be made constant (and equal to 1)  $\forall x_i$  by arc length parametrization along the indicatrix. An example of a DS is shown in Fig. 10(a) in Section V-A1. Here a straight line,  $\mathbf{z}$ , is moved along Archimedes spiral,  $\mathbf{y}$ .

It is shown in [41, p.182] that an RS is also a DS  $\iff |\dot{\mathbf{y}} \cdot \mathbf{z} \cdot \dot{\mathbf{z}}| = 0$ . It can further be shown that only a DS can be mapped onto a plane without scaling or distorting distances. It may therefore seem like a DS is a good choice of mapping. However, as will be shown below, this is not the case in general. The main reason is the non-optimality of mappings that can be decomposed into sub-mappings: When constructing mappings based on surfaces, one simplifying assumption would be to construct several parallel and independent systems based on curves (i.e.,  $1:N$  or  $M:1$  mappings) and assume that each one represents a coordinate curve on the relevant surface. This approach was taken in [4]. Clearly, any DS will also be a special case of such surfaces. This strategy may seem convenient as will be easier to find mappings between higher dimensional spaces. However, one cannot obtain the optimal slope at high SNR in this way:

Take a surface mapping from  $m+n$  to 2 dimensions in the reduction case and from 2 to  $m+n$  dimensions in the expansion case. Both of these can be realized by two parametric curve-based systems in parallel, the output of each transmitted on separate channels: a  $m:1$  and  $n:1$  scheme when  $M > N$  and a  $1:m$  and  $1:n$  scheme when  $M < N$ . The special case when  $m = 2$ ,  $n = 1$  is illustrated in [42].

We have the Proposition:

*Proposition 9: Splitting of Mappings*

Any  $m+n:2$  or  $2:m+n$  mapping composed of lower dimensional (curve-based) sub-mappings will always have a smaller slope in SDR as a function of SNR than that of the OPTA curve, a slope always corresponding to the system with the smallest exponent.

*Proof:* See Appendix D-1. □

**Remark I:** A statement for general  $M:N$  follow more or less directly from the above proposition by considering several such systems in parallel (using power allocation factors over all systems with water filling etc.).

**Remark II:** As all DS can be seen as a straight line (1:1 system) moved along a curve  $y$  (a  $M:1$  or  $1:N$  system), any DS will diverge from the OPTA bound as SNR grows large, including the suggestion for higher dimensional mappings in [4].

**Remark III:** Although a DS cannot obtain the optimal slope at high SNR, it does provide a simple alternative to implement and generalize to higher dimensions providing quite decent performance in the *small to medium* SNR range, as illustrated in Sections V-A and V-B (RCASD mapping) as well as in [4].

If one consider a uniform dimension reducing mapping, there is yet another condition that has to be satisfied in order for it to have the same slope as OPTA. This condition is deduced directly from the proof of Proposition 8, in Appendix C, Eqn (113):

$$\begin{aligned} D_t &= \bar{\varepsilon}_a^2 + \bar{\varepsilon}_{ch}^2 \\ &= \frac{M-N}{4M(M-N+2)} \Delta^2 + M^{\frac{M}{N}-1} \tilde{B}^{\frac{2}{N}} \left( \frac{\Delta}{2} \right)^{-2\frac{M-N}{N}} \sigma_x^{2\frac{M}{N}} \left( 1 + \frac{P_N}{\sigma_n^2} \right)^{-1}. \end{aligned} \quad (30)$$

As an example take a uniform 3:2 S-K mapping where  $\bar{\varepsilon}_a^2 \sim \Delta^2$  according to Proposition 5. Then we need  $\bar{\varepsilon}_{ch}^2 \sim 1/\Delta$ , in order to obtain  $\text{SDR} \sim \text{SNR}^{2/3}$  as  $\text{SNR} \rightarrow \infty$ .

To avoid the problem of non-optimal slope one have to widen the set of relevant mappings, keeping a similar type of  $G$  as in (29). The most direct generalization are surfaces that can be mapped in an angle preserving way to the Euclidean plane, named *conformal mappings*. The metric between two conformal surfaces  $\mathcal{S}$  and  $\mathcal{S}^*$  are proportional, i.e.  $g_{\alpha\beta}^* = \eta(u^1, u^2)g_{\alpha\beta}$  [41, pp. 193-194]. A subset of surfaces conformal to the Euclidean plane will be shape preserving, i.e., a *Similarity Transform*.

In the rest of this section we valuate and simulate performance for 3:2 and 2:3 S-K mappings in order to illustrate some of the results of this paper. Even for this special case, there are a myriad of possibilities as exemplified in the *Encyclopedia of Analytical Surfaces* [62]. The criteria laid out in this paper will rule out most surfaces as potential candidates for well-performing S-K mappings.

#### A. Examples on 3:2 mappings

We analyze and simulate three 3:2 mappings selected based on intuition obtained through previous sections: 1) A DS-based scheme named *RCASD* which is simple and quite well performing at intermediate SNR values, but which do not follow the optimal exponent at high SNR. 2) The *Snail Surface* which is not decomposable into lower dimensional sub-mappings. 3) A hybrid discrete-analog mapping constructed from scratch that seek to satisfy all requirements needed to obtain the same slope as OPTA at high SNR. To evaluate the performance of the example mappings we compare their performance to OPTA and *Block Pulse Amplitude Modulation* (BPAM) [32]. BPAM is the optimal linear mapping (i.e., a plane in the source- or channel space) for any  $r = N/M \in \mathbb{Q}$ . Obviously, one would like any nonlinear mapping to rise well above BPAM as the SNR increases when  $r \neq 1$ . At the of this section we compare all suggested schemes to other existing superior mappings.

1) *Right Cylinder with Archimedes Spiral Directrix (RCASD)*: Fig. 10(a) depicts the RCASD in the source space. The parametric equation for the RCASD is given by [62, p. 51]

$$\mathbf{S}(\mathbf{x}) = [a\varphi(z_1) \cos(\varphi(z_1)), a\varphi(z_1) \sin(\varphi(z_1)), \alpha_2 z_2], \quad (31)$$

with  $\alpha_2$  some amplification factor and  $a = \Delta/\pi$ .  $\Delta$  is the smallest distance between the two “spiral surfaces” seen in Fig. 10(a). The components of the metric tensor are

$$g_{11} = \left(\frac{\Delta}{\pi}\right)^2 (\varphi'(z_1))^2 (1 + \varphi^2(z_1)), \quad g_{22} = \alpha_2^2, \quad g_{12} = g_{21} = 0, \quad (32)$$

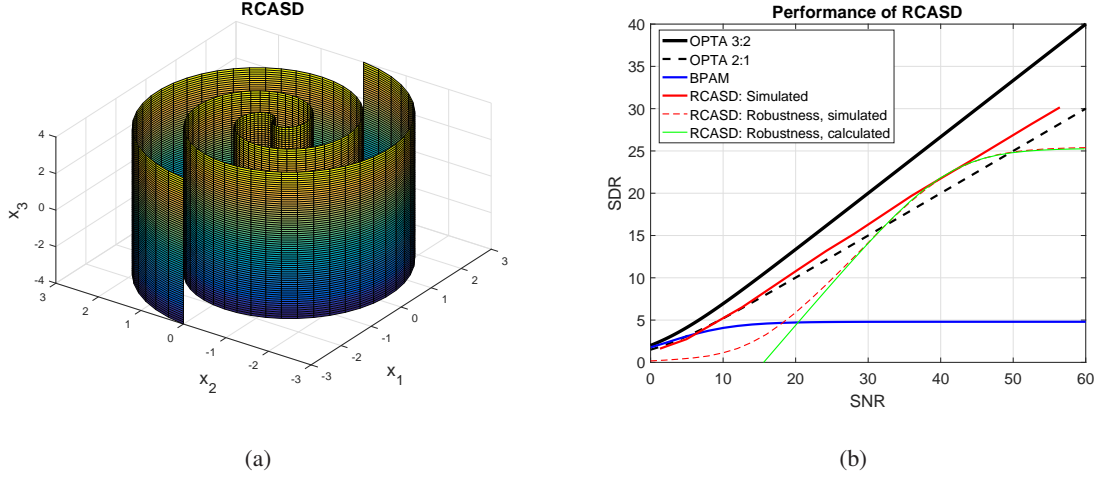


Fig. 10. (a) RCASD in source space with LoC coordinate grid. (b) Performance of RCASD compared to OPTA and BPAM.

and the components of the second fundamental form are

$$b_{11} = -a(\varphi'(z_1))^2 \frac{2 + \varphi^2(z_1)}{\sqrt{1 + \varphi^2(z_1)}}, \quad b_{12} = b_{21} = b_{22} = 0. \quad (33)$$

The components in (32) are computed from  $g_{\alpha\beta} = \mathbf{S}_\alpha \cdot \mathbf{S}_\beta$ , and the components of the SFF are computed from (68) in Appendix A-B. Some of these computations are quite tedious, so we refer to [42] for details. The RCASD is a DS with Archimedes spiral as directrix (a 2:1 sub-mapping), making the RCASD a generalization of the 2:1 mapping in [2]. With (32) and (33) one can from Theorem 3 conclude that the coordinate curves are LoC since  $g_{12} = b_{12} = 0$ . Therefore, Eq. (22) describes the 2nd order behavior of this mapping exactly. The coordinate curves are also geodesics since the directrix is a plane curve as stated in Theorem 50.4 in [41, p.159]. Then, the ML-estimate has the lowest possible distortion for this surface, implying that the choice of coordinates is optimal. The principal curvatures are easily found from the above fundamental forms as we consider LoC

$$\kappa_1 = \frac{b_{11}}{g_{11}} = -\frac{2 + \varphi^2(z_1)}{a(\sqrt{1 + \varphi^2(z_1)})^{3/2}}, \quad \kappa_2 = 0. \quad (34)$$

It can be seen that the curvature is generally not large.

**Optimization of RCASD as 3:2 mapping.** The RCASD's performance is made scalable with SNR through the factor  $a = \Delta/\pi$  with  $\Delta$  adapted to  $\sigma_n^2$ .

*Distortion:* With noise added to the channel signal  $z_i$ , the variable  $\tilde{z}_i = z_i + n_i$  is mapped through (31). We compute the channel distortion according to (20). For this we need the

components of the metric tensor in (32). By choosing

$$\varphi(\alpha_1 z_1) = \pm \sqrt{\frac{\alpha_1 z_1}{\eta \Delta}}, \quad (35)$$

with  $\alpha_1$  some amplification factor depending on the SNR, one will, as shown in [2], obtain arc length parametrization along the spiral in the  $x_1, x_2$  plane of the RCASD. Then  $g_{11} \approx \alpha_1^2, \forall z_1, z_2$ . Similarly, since  $x_3 = \alpha_2 z_2$  is the only dependence on  $z_2$ , therefore  $g_{22} = \alpha_2^2$ . Then we have a diagonal metric tensor with constant components which was one of the criteria sought. The channel distortion then becomes

$$\bar{\varepsilon}_{ch}^2 = \frac{\sigma_n^2}{3} \iint \sum_{i=1}^2 g_{ii}(\mathbf{z}) f_{\mathbf{z}}(\mathbf{z}) d\mathbf{z} = \frac{\sigma_n^2}{3} (\alpha_1^2 + \alpha_2^2) f_{\mathbf{z}}(\mathbf{z}) d\mathbf{z} = \frac{\sigma_n^2 (\alpha_1^2 + \alpha_2^2)}{3}. \quad (36)$$

To compute the approximation distortion one can observe from Fig. 10(a) that we have a (close to) uniform S-K mapping (see Definition 6), implying that Eq. (25) applies as a lower bound with  $N = 2$  and  $M = 3$ :

$$\bar{\varepsilon}_q^2 \geq \frac{\Delta^2}{36}. \quad (37)$$

*Power:* In the  $x_1, x_2$ -plane we have Archimedes spiral which was applied for 2:1 compression in [2]. As shown in [2], under arc length parametrization, we get a Laplace distribution over  $y_1$  with variance  $\sigma_{y_1}^2 = 2(2\eta\sigma_x^2\pi/\Delta)^2$ ,  $\eta = 0.16$ , at high SNR. The channel variable  $y_2$  is a linear mapping of  $x_3$  implying a Gaussian distribution with variance  $\sigma_{y_2}^2 = \sigma_x^2$ .

The channel signal has to be scaled by some factor  $\alpha_i$  to satisfy the power constraint as the SNR changes. That is,  $z_i = y_i/\alpha_i$  and so  $\sigma_{z_i}^2 = \sigma_{y_i}^2/\alpha_i^2$ . The total channel power is then

$$P_t = \frac{1}{2} \left( \frac{\sigma_{y_1}^2}{\alpha_1^2} + \frac{\sigma_{y_2}^2}{\alpha_2^2} \right)^2. \quad (38)$$

*Optimization:* With constraint  $C_t = P_{\max} - P_t(\Delta, \alpha_1, \alpha_2) \geq 0$ , we get the objective function

$$\mathcal{L}(\Delta, \alpha_1, \alpha_2) = \bar{\varepsilon}_q^2(\Delta) + \bar{\varepsilon}_{ch}^2(\alpha_1, \alpha_2) - \lambda C_t(\Delta, \alpha_1, \alpha_2). \quad (39)$$

To determine the optimal parameters we use a similar numerical approach as in [35, pp. 87].

The performance of the optimized RCASD is shown in Fig. 10(b) (red curve). The RCASD clearly improves with SNR, rising well above BPAM as SNR increases. The RCASD is also quite robust to varying SNR as it shows both graceful improvement and reduction for a fixed set of parameters (red dashed curve). One example of calculated performance is also shown (green curve) in order to demonstrate the accuracy of the theoretical analysis introduced in

Section III-B. The distortion contributions discussed in Section III-B can be observed from the robustness graphs: The approximation distortion dominates above the optimal SNR point, whereas below the optimal SNR, channel distortion dominates. The simulated and calculated performance corresponds well indicating that the weak noise regime of Definition 5 is valid for large deviations around the optimal point even for finite SNR. However, the slope at high SNR is lower than that of OPTA, which is what one can expect from Proposition 9 as the RCASD is a developable surface which can be split into a 1:1 and a 2:1 system (a line and a spiral). This is in fact equivalent to the 3:2 scheme proposed in [4]. The slope of RCASD corresponds to that of 2:1 OPTA (black dashed curve) at high SNR, as Proposition 9 states. This is explicitly shown in [42].

2) *Snail Surface*: The *Snail Surface* cannot be decomposed into sub-mappings and covers a spherical subset of the source space properly, avoiding bends with high curvature (i.e. the second order term in (22) should be small). Its parametrization has components [62, p. 280]

$$\begin{aligned} S_1(z_1, z_2) &= a\varphi(z_1) \sin(\varphi(z_1)) \cos(\alpha_2 z_2 + \phi) \\ S_2(z_1, z_2) &= b\varphi(z_1) \cos(\varphi(z_1)) \cos(\alpha_2 z_2 + \phi) \\ S_3(z_1, z_2) &= -c\varphi(z_1) \sin(\alpha_2 z_2 + \phi), \end{aligned} \tag{40}$$

which is valid for  $0 \leq z_1 \leq k\pi$ ,  $-\pi \leq z_2 \leq \pi$ . To include negative values for  $z_1$ , i.e.,  $-k\pi \leq z_1 \leq 0$ , one simply flips the sign of all components in (40), to obtain a *double* snail surface (DSS), which is depicted in Fig. 11(a). By choosing  $\psi = \pi/2$  and  $a = b = c = 2\Delta/\pi$  one obtains a spherical symmetry which further results in a (close to) uniform S-K mapping (Definition 6), and therefore (37) will be a good approximation of the lower bound for the approximation distortion.  $\phi$  will be decided later.

For a general mapping function  $\varphi(z_1)$ , the metric tensor is found by to be [42]

$$\begin{aligned} g_{11} &= (a\varphi'(z_1))^2 (1 + \varphi^2(z_1) \cos^2(\alpha_2 z_2 + \phi)), \\ g_{22} &= a^2 \alpha_2^2 \varphi^2(z_1), \quad g_{12} = g_{21} = 0. \end{aligned} \tag{41}$$

By inserting  $\varphi(z_1) = \alpha_1 z_1$  in (41) one will see that  $g_{ii} \sim z_1^2$ ,  $i = 1, 2$ , implying that the channel distortion increases with  $z_1^2$ . We can compensate this for both  $g_{ii}$ 's at once by choosing  $\varphi \sim \sqrt{z_1}$ . Note also that the RCASD has the same dependence along the directrix when setting  $\varphi(z_1) = \alpha_1 z_1$  (i.e.,  $g_{11} \sim z_1^2$ ). As the Snail Surface scales with  $\Delta$  in the same way as the RCASD, it makes sense to use (35) for the DSS as well (the choice of  $\eta$  is arbitrary).

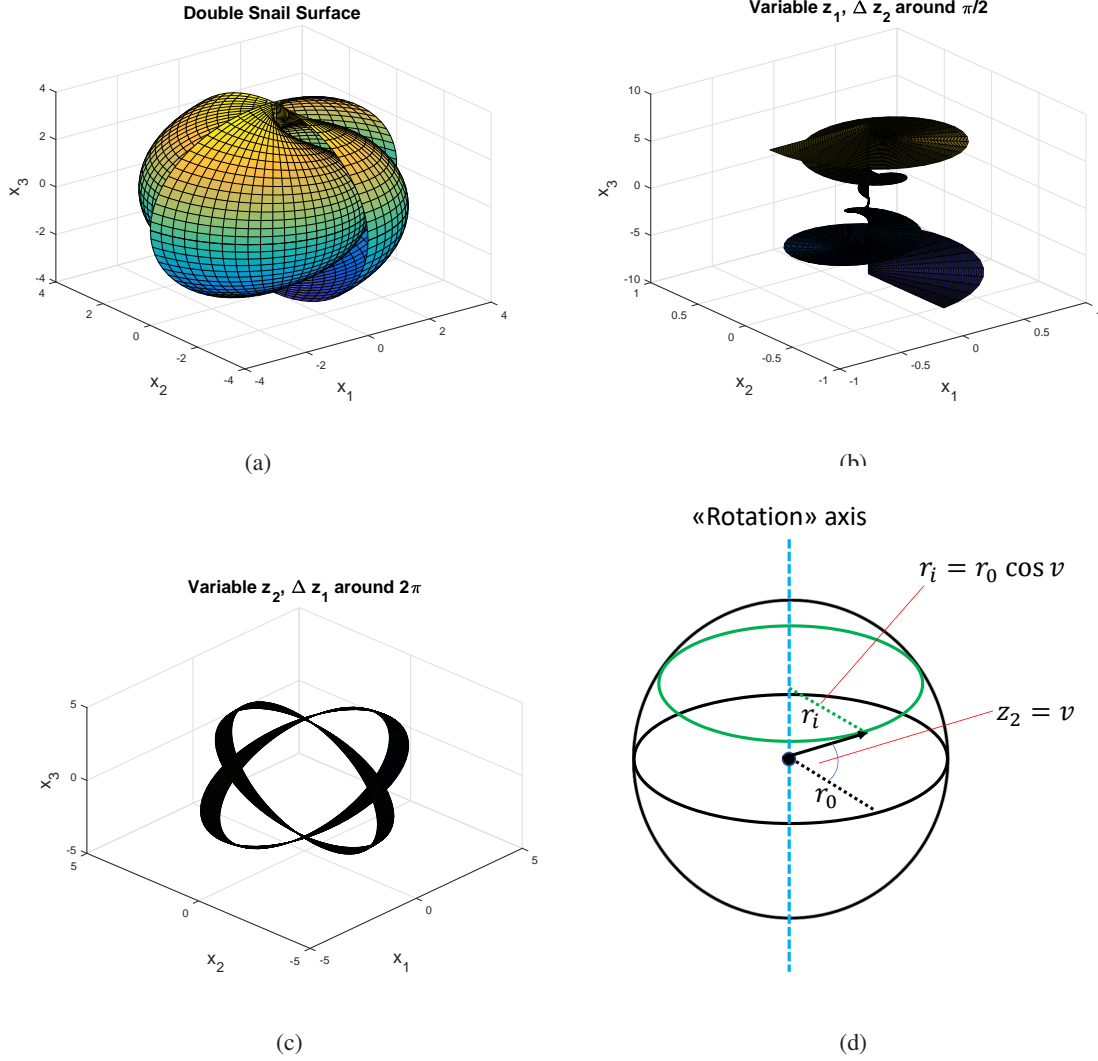


Fig. 11. (a) The DSS ( $a = b = c = 2\Delta/\pi$ ). (b) DSS with  $z_1$  variable and  $z_2 = \pi/2 \pm \epsilon_1$ . (c) DSS with  $z_2$  variable and  $z_1 = 2\pi \pm \epsilon_2$ . (d) Virtual spherical shell applied to compute the channel pdf of  $z_2$ .

### Optimization of DSS as 3:2 mapping.

*Channel Power and Density Function:* To evaluate channel input from DSS its convenient to analyze variation in each channel direction separately, which geometrical configurations are shown in Figs. 11(b) and 11(c) (see [42] for details).

To derive the pdf of  $z_1$  consider Fig. 11(b). By letting  $z_2$  vary slightly ( $\pm\epsilon$ ) around some constant value (here  $\pi/2$ ) with  $z_1$  free, we get a “cork-screw” like structure. In the limit of constant  $z_2$  we get a spiral with torsion  $\tau \neq 0$ , which *rises* from the  $x_1x_2$ -plane at a rate

depending on the value of  $z_2$ : Whenever  $z_2 = \pm(2n+1)\pi/2$ ,  $n \in \mathbb{N}$ ,  $\tau$  is maximal, whereas when  $z_2 = \pm n\pi$ ,  $n \in \mathbb{N}$ ,  $\tau = 0$  and the spiral is plane. This implies that the mapping from the snail surface to  $z_1$  can be approximated as the *radius*,  $\rho = \sqrt{x_1^2 + x_2^2 + x_3^2}$ , that traces out all points inside a sphere as  $z_1$  and  $z_2$  varies over their domains. By assuming that the DSS is dense enough (small  $\Delta$ ), one can approximate the mapping from source space to  $z_1$  as a continuous function  $h : \mathbb{R}^3 \rightarrow \mathbb{R}$  depending on  $\varphi$ . This assumption becomes more accurate as SNR grows as  $\Delta$  should be chosen smaller. By choosing  $\varphi = (\gamma z_1)^n$ ,  $n \in \mathbb{Q}^+$ , then  $z_1 = h(x_1, x_2, x_3) = \pm \gamma a^{-n} (x_1^2 + x_2^2 + x_3^2)^{n/2} = \pm \gamma a^{-n} \rho^n = \ell(\rho)$ . We have

*Lemma 2:* At high SNR, whenever  $\varphi = (\gamma z_1)^n$ , the pdf for  $z_1$  when using DSS as a 3:2 mapping is

$$f_{z_1}(z_1) = \frac{na^3\gamma^3|z_1|^{3n-1}}{\sqrt{2\pi}\sigma_x^3} e^{-\frac{a^2\varphi^2(z_1)}{2\sigma_x^2}}. \quad (42)$$

*Proof:* See Appendix D-2. □

If we now assume that  $\varphi(z_1)$  is as in (35), then  $\gamma = \sqrt{\alpha_1/(\eta\Delta)}$ , and so

$$f_{z_1}(z_1) = \frac{a^3\alpha_1^{3/2}\sqrt{|z_1|}}{2\sqrt{2\pi}\sigma_x^3(\eta\Delta)^{3/2}} e^{-\frac{a^2\alpha_1|z_1|}{2\sigma_x^2\eta\Delta}}. \quad (43)$$

According to [63, p.87,154] a Gamma distribution has the general form  $f_\Gamma(x) = u(x)x^{c-1}e^{-x/b}/(\Gamma(c)b^c)$  with second moment  $E\{x^2\} = c(c+1)b^2$ . Therefore (43) is a *double Gamma distribution* with  $c = 3/2$  and  $b = (2\eta\Delta\sigma_x^2)/(a^2\alpha_1)$ . Since (43) has zero mean, the power of channel 1 becomes

$$P_1 = \text{Var}\{z_1\} = \frac{15(\eta\Delta\sigma_x^2)^2}{a^4\alpha_1^2} = \frac{15(\eta\pi^2\sigma_x^2)^2}{16\alpha_1^2\Delta^2}. \quad (44)$$

To derive the pdf of  $z_2$  consider Fig. 11(c). By letting  $z_1$  vary slightly ( $\pm\epsilon_2$ ) around some constant value (here  $2\pi$ ) while  $z_2$  vary over its domain we get two circles tracing out two Möbius strips. In the limit of constant  $z_1$  ( $\epsilon_2 \rightarrow 0$ ) we get a circle that "rotates" about some axis whose radius increases with the value of  $z_1$  (as  $2\Delta z_1/\pi$ ). Consider  $\phi = 0$  first for simplicity: Then the rotational axis is at  $\pi/2$ . The radius of this rotating circle is insignificant as seen from  $z_2$  (as  $z_2 \in [-\pi, \pi]$ , independent of  $z_1$ ). From the perspective of  $z_2$ , as the joint pdf of  $\mathbf{x}$  is spherically symmetric, we have a uniform mass distribution over a virtual spherical shell of arbitrary radius as depicted in Fig. 11(d). To find the probability mass associated with each value of  $z_2$  consider the sum of all points along circles of intersection of this virtual sphere by planes perpendicular

to the rotation axis. The radius,  $r_i$ , of such a circle is  $r_i = r_0 \cos(v)$ , where  $v = z_2$  is the angle from the equatorial plane, i.e.  $v = \pi/2 - \varrho$ , and  $\varrho$  the polar angle. The circumference as a function of  $z_2$  is then  $O(z_2) = 2\pi r_0 \cos(z_2)$ . Since  $r_0$  is arbitrary, one can set  $r_0 = 1/(2\pi)$  implying that  $f_{z_2}(z_2) \sim |\cos(z_2)|$ ,  $z_2 \in [-\pi, \pi]$ . The resulting pdf will have its minimum at the rotation axis. To avoid high probability for the highest channel amplitude values one can set  $\phi = \pi/2$  to obtain zero probability there<sup>14</sup>. Then we get a *sine distribution*. To normalize, as  $\int_0^\pi \sin(z_2) dz_2 = 2$ , then

$$f_{z_2}(z_2) = \frac{\alpha_2}{4} |\sin(\alpha_2 z_2)|. \quad (45)$$

Since  $f_{z_2}(z_2)$  is proportional to *Gilberts sine distribution*  $f_x(x) = \sin(2x)$ , which according to [64] has variance  $E\{x^2\} = (\pi^2/4 - 1)/2$ , the power for channel 2 becomes

$$P_2 = \text{Var}\{z_2\} = \frac{2}{\alpha_2^2} \left( \frac{\pi^2}{4} - 1 \right). \quad (46)$$

*Weak Channel Distortion:* From (20) we get

$$\bar{\varepsilon}_{ch}^2 = \frac{\sigma_n^2}{3} \iint (g_{11}(\mathbf{z}) + g_{22}(\mathbf{z})) f_{\mathbf{z}}(\mathbf{z}) d\mathbf{z} = \frac{\sigma_n^2 (I_1 + I_2)}{3}. \quad (47)$$

We have, using (41)

$$I_2 = \iint g_{22}(\mathbf{z}) f_{\mathbf{z}}(\mathbf{z}) d\mathbf{z} = 2(a\alpha_2)^2 \frac{\alpha_1}{\eta\Delta} \int_{-\infty}^{\infty} z_1 f_{z_1}(z_1) dz_1 = 3\alpha_2^2 \sigma_x^2. \quad (48)$$

The last equality comes from the fact that  $z_1$  is gamma distributed, therefore the integral in (48) becomes [63, p.154]  $bc/2 = 3\eta\Delta\sigma_x^2/(a^2\alpha_1)$ . Further, we have using (41) (see [42] for details)

$$I_1 = \iint g_{11}(\mathbf{z}) f_{\mathbf{z}}(\mathbf{z}) d\mathbf{z} = \frac{\alpha_1\Delta}{\eta\pi^2} E\{z_1^{-1}\} + \frac{2\alpha_1^2}{3\pi^2\eta^2}, \quad (49)$$

Through power series expansion one can show that (see [42])  $E\{z_1^{-1}\} \approx 4(1 + \text{Var}\{z_1\})$  up to 3rd order. Inserting this into (49), the channel distortion in (47) becomes

$$\bar{\varepsilon}_{ch}^2 \approx \frac{\sigma_n^2}{3} \left( \frac{4\alpha_1\Delta}{\eta\pi^2} \left( 1 + \frac{15(\eta\pi^2\sigma_x^2)^2}{16\alpha_1^2\Delta^2} \right) + \frac{2\alpha_1^2}{3\pi^2\eta^2} + 3\alpha_2^2\sigma_x^2 \right). \quad (50)$$

*Optimization:* With constraint  $C_t = P_{\max} - P_t(\Delta, \alpha_1, \alpha_2) \geq 0$ , we get a similar objective function as in (39) which is found numerically by the same method.

Using the optimized parameters we plot the performance of the optimized DSS in Fig. 13(a). The DSS clearly improves with SNR (green curve), raising well above BPAM (blue curve).

<sup>14</sup>This is in line with the criteria laid out for optimal mapping construction in [52, pp.102-104]

Its also clearly better than the RCASD at high SNR (see Fig. 10(b)) which is expected due to Proposition 9. The DSS is also noise robust (green dashed curve), and the magenta line confirms that the theoretical model derived for DSS above is quite accurate. However, one can see that the gap to OPTA increases somewhat above 40dB. The reason is that  $\bar{\varepsilon}_{ch}^2 \sim 1/\Delta^2$  instead of  $\bar{\varepsilon}_{ch}^2 \sim 1/\Delta$  which is required according to (30). Therefore, the DSS will eventually diverge from OPTA (albeit at a much higher SNR than a decomposable mapping).

3) 3:2 HVQLC: We try to construct a mapping that has the same slope as 3:2 OPTA when  $\text{SNR} \rightarrow \infty$ , a mapping satisfying all criteria laid out at the start of this section. This is most easily obtained by a HDA approach: Consider approximating the sources to planes parallel to  $x_1, x_2$ -plane<sup>15</sup> in  $\mathbb{R}^3$  with distance  $\Delta$  between each of them. One will then have a uniform S-K mapping, i.e.,  $\bar{\varepsilon}_q^2 \sim \Delta^2$ . For each plane we induce a metric  $G = \alpha I$ , with  $\alpha$  some scaling factor. To make sure that this mapping is non-decomposable, one maps the planes onto the channel with their centroids placed on Archimedes spiral, and thereby obtain a *mix* of several sources on each channel. A spiral is chosen to obtain a regular mapping that can easily be scaled with SNR. Other mappings may also do. By choosing  $\varphi$  as in (35), one obtains equal distance  $\Delta$  between the spiral arms as well as between the centroids along each arm, i.e., a uniform VQ structure on a disc is obtained (an illustration is given in [35, p. 90]). One will also obtain the condition  $\bar{\varepsilon}_{ch}^2 \sim 1/\Delta$  as sought from (30), as shown below. The block diagram for the 3:2 HVQLC is depicted in Fig. 12.

A drawback of this mapping is that it introduces anomalous errors when centroids are mis-detected. This event has probability  $Pr\{\|\mathbf{y}_{12} + \mathbf{n}\| \geq \Delta/(2\alpha_3)\}$ , where  $\mathbf{y}_{12} = [x_1 \ x_2]/\alpha$ . The error for this event is upper bounded by  $2b_x\sigma_x$  (with  $b_x$  typically in the order of 4 – 5). The pdf of  $\mathbf{y}_{12} + \mathbf{n}$  is the product of two marginal distributions of the sum  $x_i + n_i$ ,  $i = 1, 2$  each with pdf  $\mathcal{N}(0, \sigma_y^2 + \sigma_n^2)$  [63, pp.181-182]. The variable  $w = \|\mathbf{y}_{12} + \mathbf{n}\|$  is then Rayleigh distributed [63, pp. 202-203],  $f_w(w) = w/(\sigma_y^2 + \sigma_n^2) \exp(-w^2/2(\sigma_y^2 + \sigma_n^2))$ . Then

$$\bar{\varepsilon}_{an}^2 = 4b_x^2\sigma_x^2 Pr\left\{w \geq \frac{\Delta}{2\alpha_3}\right\} = 4b_x^2\sigma_x^2 \int_{\Delta/(2\alpha_3)}^{\infty} f_w(w)dw = 4b_x^2\sigma_x^2 e^{-\frac{\Delta^2}{8\alpha_3^2(\sigma_y^2/\alpha^2 + \sigma_n^2)}}. \quad (51)$$

In order to obtain a mapping where anomalous errors happen with low probability one will either condition  $\Delta/\alpha_3$  to small values or limit  $x_1$  and  $x_2$  at some value (through the green block in

<sup>15</sup>Orientation is arbitrary due to the spherical symmetry of the Gaussian.

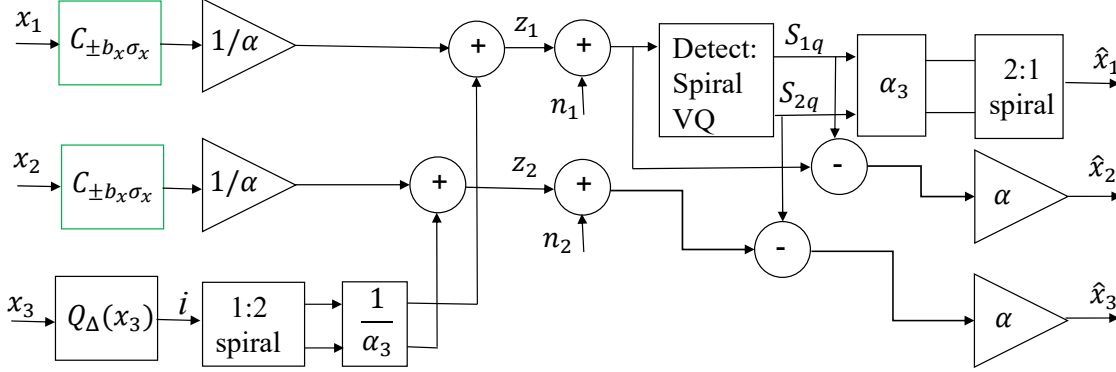


Fig. 12. HVQLC 3:2 block diagram. Green blocks are optional.

Fig. 12). By limiting at  $b_x \sigma_x$ , one introduces a distortion [65]

$$\bar{\varepsilon}_{\kappa}^2 = \frac{4}{3} \int_{b_x \sigma_x}^{\infty} (x_i - b_x \sigma_x)^2 f_x(x_i) dx_i, \quad i = 1 \text{ or } 2. \quad (52)$$

By limiting each source separately, parallel planes in  $\mathbb{R}^3$  are obtained, whereas by limiting  $\sqrt{x_1^2 + x_2^2}$ , parallel discs are obtained.

In order to control the probability of anomalous errors, the distance between each centroid on the spiral has to be properly constrained,

$$\frac{\Delta}{\alpha_3} > \frac{2b_x \sigma_x}{\alpha_1} + 2b_n \sigma_n. \quad (53)$$

The probability for anomalies is then adjusted with the  $b_x$  parameter.  $b_n$  is the same as in Section IV, and is typically in the order 4 – 5 for low delay systems. By choosing  $b_x > 4$  then 99.99% of all source values are still present.

As mentioned above,  $g_{ii} = \alpha^2$  and so the channel distortion (in the absence of anomalies) becomes  $\bar{\varepsilon}_{ch}^2 = 2\sigma_n^2 \alpha^2 / 3$ . As we have a uniform S-K mapping, the total distortion becomes

$$D_t = \frac{\Delta^2}{36} + \frac{2\sigma_n^2 \alpha^2}{3} + 4b_x^2 \sigma_x^2 e^{-\frac{\Delta^2}{8\alpha_3^2(\sigma_x^2/\alpha^2 + \sigma_n^2)}}. \quad (54)$$

Since  $x_1$  and  $x_2$  are scaled Gaussians, the power used on sending them becomes  $P_1 + P_2 = 2\sigma_x^2/\alpha^2$ .  $x_3$  is mapped through a discretized version of the 1:2 mapping in [2]. Therefore, the same power expression can approximately be used<sup>16</sup>,  $P_3 \approx 2\Delta\sigma_x/(\eta\sqrt{2\pi^5}\alpha_3^2)$ , at high SNR

<sup>16</sup>A factor appearing in [2] is removed as we assume  $x_3$  to take on values over  $\mathbb{R}$ . In [2] the source was limited to  $[-1, 1]$ .

where  $\Delta$  should be chosen small. The fact that  $P_3 \sim \Delta/\alpha_3^2$  provides  $\bar{\varepsilon}_{ch}^2 \sim 1/\Delta$  as required by (30). The total power is then

$$P_t = \frac{2\sigma_x^2}{\alpha^2} + \frac{2\Delta\sigma_x}{\eta\sqrt{2\pi^5}\alpha_3^2}. \quad (55)$$

To determine optimal performance we consider the Lagrangian

$$\mathcal{L}(\Delta, \alpha, \alpha_3) = D_t(\Delta, \alpha) - \lambda_1 C_1(\Delta, \alpha, \alpha_3) - \lambda_2 C_2(\Delta, \alpha, \alpha_2), \quad (56)$$

where  $C_1 = P_t - (P_1 + P_2 + P_3)$  and  $C_2(\Delta, \alpha, \alpha_2) = \Delta - 2b_x\sigma_x\alpha_3/\alpha_1 - 2b_n\sigma_n\alpha_3$ . The slight difference from the constraint in (53) is to obtain better stability when solving (56) numerically.

The optimized performance of the HVQLC without any limitation performed is depicted in Fig. 13(b) (magenta curve) in Section V-A4. Note that the HVQLC seem to follow the right slope at high SNR, and that it is noise robust (magenta dashed curve) despite the introduction of anomalous errors.

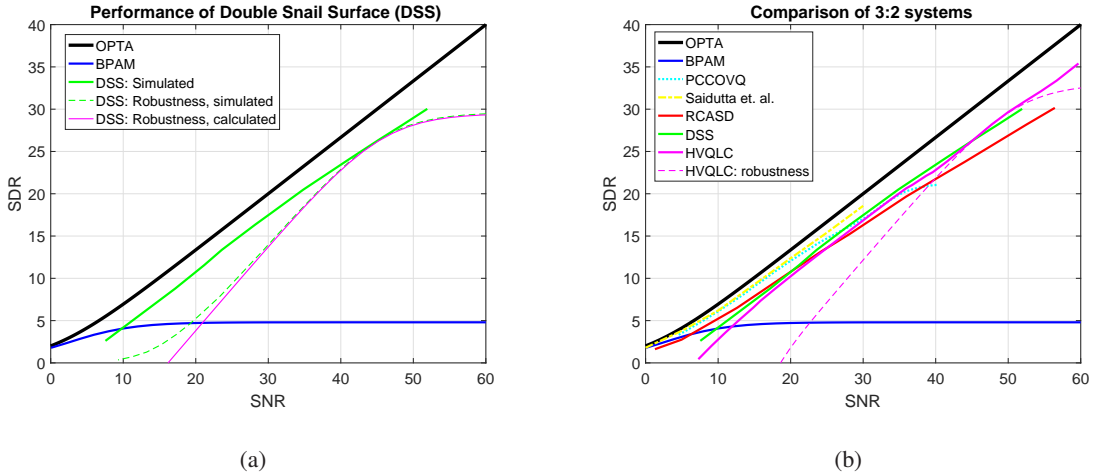


Fig. 13. (a) Performance of Double Snail Surface (DSS) compared to OPTA and BPAM. (b) Performance of all suggested 3:2 mappings as well as other known mappings.

4) *Comparison of different 3:2 schemes:* The performance of all mappings proposed in this section are compared in Fig. 13(b). We also include the performance of Saidutta et. al.'s 3:2 mapping [6] found using Deep Learning (a method named *Variational Auto Encoders* (VAE)) as well as *Power Constrained Channel Optimized Vector Quantizer* (PCCOVQ) [31], [66]. PCCOVQ is a numerically optimized discrete mapping (for any  $r = N/M \in \mathbb{Q}$ ) that often replicate

continuous or piece-wise continuous curves or surfaces when the number of centroids or PAM symbols in the mapping is large. When many centroids or PAM symbols are used, the PCCOVQ is often hard to beat since there is more flexibility in moving points in space rather than being stuck to a given curve or surface. Approaching (or beating) the VAE or PCCOVQ system is a good indication of a well performing mapping.

Not surprisingly, Saidutta’s VAE mapping (yellow dash-dot curve) and PCCOVQ (cyan dotted curve) have the best performance in the SNR range they have been optimized for. These schemes are on par (note that the reason why the PCCOVQ system declines above 22dB is likely that 4096 centroids are used during optimization, which is too small a number for representing a 2D space at higher SNR). All proposed schemes of this section is overall about 1dB inferior to the two reference systems. The RCASD, which is basically equivalent to the 3:2 mapping proposed in [4], is best at low SNR, the DSS has the best performance between 20 and 45 dB, whilst the HVQLC is best from 45dB and above and is the only system that does not diverge from OPTA at high SNR. We do not know if Saidutta’s VAE mapping has the right slope at high SNR, as performance is only displayed up to 30dB, where also the DSS follows the slope of OPTA.

It is quite interesting to see that quite different configurations provide well performing mappings. However, any such configuration will need to comply with the conditions presented in this paper. Although DS-based mappings, like RCASD, diverge from OPTA at high SNR, such decomposable mappings have their *virtue* as they are a low complexity alternative that perform well at low to medium SNR, being easier to generalize to higher dimensions. Other surface-based mappings were compared in [42], the Helicoid from [35], [51] and the MS-CDS which is a generalization of the RCASD. Both of these are inferior to the mappings proposed here as they do not obey several of the criteria laid down throughout this paper (see [42] Section IV.A for details).

Although mappings proposed here perform inferior to some optimized schemes proposed in the literature, their advantage is that they have a single parametric representation, providing one codebook that only needs to be scaled in order to adapt to varying SNR. The losses from optimal mappings are also relatively small, only about 1dB over all.

### B. Examples on 2:3 mappings

We analyze two mappings: i) A hybrid discrete analog scheme, *Hybrid Vector Quantizer Linear Coders* (HVQLC) suggested in [35, pp. 89-93]. ii) The RCASD treated in Section V-A1.

1) *HVQLC*: This mapping is a generalization of the Hybrid Scalar Quantizer Linear Coder (HSQLC) proposed in [17] and is like a *dual* to the 3:2 HVQLC proposed in Section V-A3. The block diagram is depicted in Fig. 14.

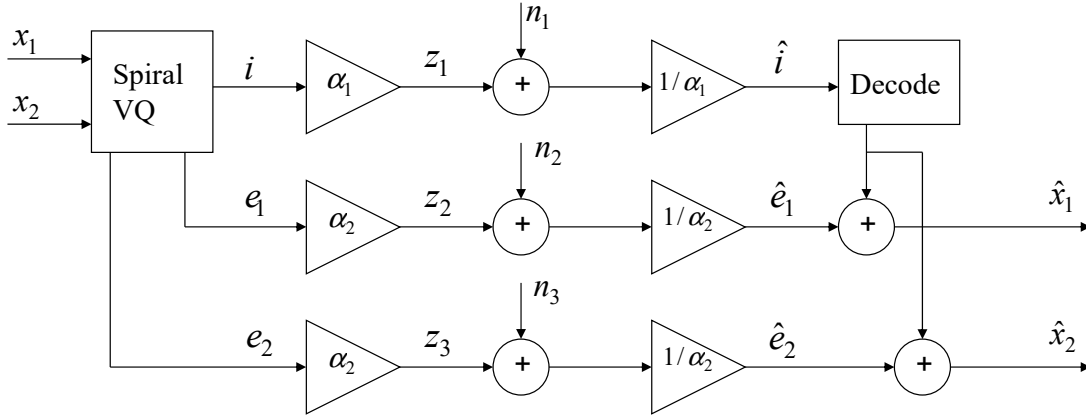


Fig. 14. 2:3 HVQLC block diagram.

The VQ indices are denoted by  $i$ , whereas  $e_1$  and  $e_2$  denotes the two error components from the quantization process.  $\alpha_1$  and  $\alpha_2$  are scaling factors to adjust channel power. To make the VQ code-book adaptable to varying SNR, the centroids are placed on Archimedes' spiral. Arc length parametrization is chosen along the spiral for the same reason as for the 3:2 HVQLC. The VQ indices are scaled by  $\alpha_1$  and transmitted on channel 1, while the two error components are scaled by  $\alpha_2$  and transmitted on channels 2 and 3, leading to a “mix” of both sources on all three channels. Fig. 15(a) shows a scatter plot of the 2:3 HVQLC mapping in the channel space, which is similar to the source space structure of 3:2 HVQLC.

At high SNR an approximate mathematical model can be made based on the theory in section III-A:

*Weak noise distortion*: The weak noise distortion can be found from (11), as the HVQLC is a shape preserving mapping. The only contributions to the weak noise distortion comes from the noise in the two error components, and so  $\bar{\varepsilon}_{wn}^2 = \sigma_n^2 / \alpha_2^2$ .

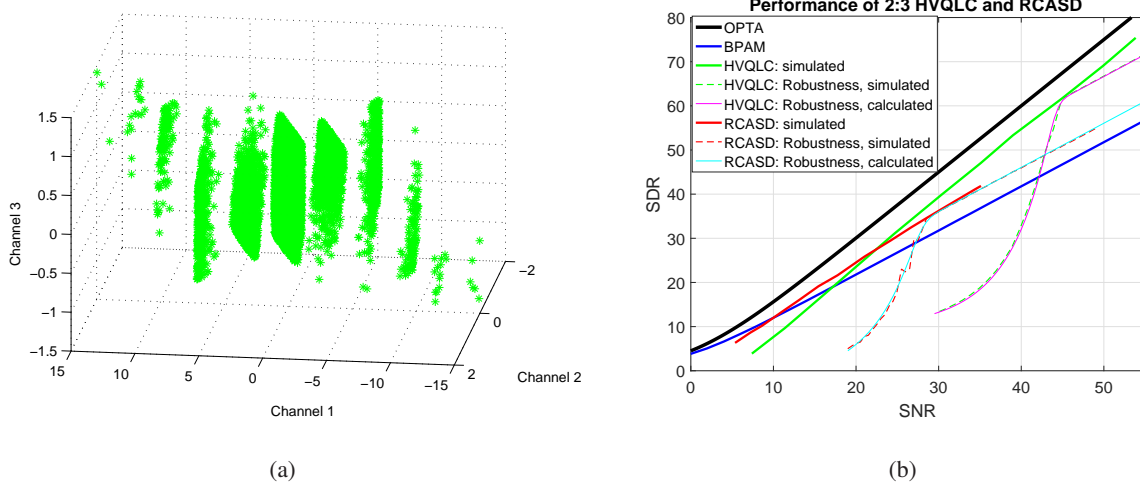


Fig. 15. (a) Scatter plot of 2:3 HVQLC channel symbols with  $\alpha_1 = 1$ . (b) Performance of 2:3 HVQLC and RCASD compared to OPTA and BPAM.

*Anomalous distortion:* The distance between each plane in Fig. 15(a) is  $\alpha_1$  as the VQ indices are scaled by  $\alpha_1$ . Therefore, the probability for anomalous errors is  $p_{th} = \Pr\{n_1 \geq \alpha_1/2\}$ . Since  $n_1$  is Gaussian,  $p_{th} = (1 - \text{erf}(\alpha_1/2\sqrt{2}\sigma_n))$  (see [35, p.90]). The error made when anomalous errors occur is  $\Delta$ , as the distance to the nearest neighbor for any given centroid is  $\Delta$ . The anomalous distortion is then

$$\bar{\varepsilon}_{th}^2 = \frac{\Delta^2}{2} \left( 1 - \text{erf}\left(\frac{\alpha_1}{2\sqrt{2}\sigma_n}\right) \right). \quad (57)$$

*Channel power:* Take channel one: As centroids are placed on Archimedes' spiral in an equidistant manner, the pdf of  $z_1$  will be a discretized version of the pdf for RCASD directrix, i.e., a discretized Laplace pdf. However, for small  $\Delta$ , its variance can be approximated by the variance of a Laplace pdf. After scaling with  $\alpha_1^2$ , the power can be approximated as

$$P_1 = \text{Var}\{z_1\} \approx 2\alpha_1^2 \left( 2\eta \frac{\pi^2}{\Delta^2} \sigma_x^2 \right)^2, \quad (58)$$

(with  $\eta = 0.16$ ). This variance will always be somewhat smaller than the real power, but the higher the SNR (the smaller  $\Delta$  is) the better they coincide. Note especially that  $\sigma_{z_1}^2 \sim 1/\Delta^4$ , different from the 3:2 RCASD directrix where  $\sigma_{z_1}^2 \sim 1/\Delta^2$ . The reason is that indices are sent on the channel, implying that the arc length is independent of  $\Delta$ . This difference in exponent is crucial to make HVQLC obtain the same slope as 2:3 OPTA.

For channels 2 and 3, assuming that the spiral is dense ( $\Delta$  small), each of the error components ( $e_1$  and  $e_2$ ) are nearly uniformly distributed over  $(\Delta/2) \times (\Delta/2)$ . Therefore, the power on channel 2 and 3 can be approximated by (93) substituting  $m = 1$ , and scaled by  $\alpha_2$ :  $P_2 = P_3 = \alpha_2^2 \Delta^2 / 12$ .

The total channel power is then

$$P = \frac{2}{3} \left( \left( 2\alpha_1 \eta \frac{\pi^2}{\Delta^2} \sigma_x^2 \right)^2 + \frac{\alpha_2^2 \Delta^2}{12} \right). \quad (59)$$

*Optimization of the HVQLC:* The optimal performance is found by minimizing distortion over  $\Delta$ ,  $\alpha_1$  and  $\alpha_2$  w.r.t. a channel power constraint. The Lagrangian for this problem is  $\mathcal{L}(\Delta, \alpha_1, \alpha_2, \lambda) = \bar{\varepsilon}_{wn}^2(\alpha_2) + \bar{\varepsilon}_{th}^2(\Delta, \alpha_1) - \lambda c_t(\Delta, \alpha_1, \alpha_2)$ , with constraining function  $c_t(\Delta, \alpha_1, \alpha_2) = P_{max} - P(\Delta, \alpha_1, \alpha_2) \geq 0$ , with  $P(\Delta, \alpha_1, \alpha_2)$  given in (59), and  $P_{max}$  the maximum allowed power per channel. Numerical optimization is applied (see [35, p. 92] for details).

Both calculated and simulated performance of the optimized HVQLC system is shown in Fig. 15(b) (green curve). One can observe that the HVQLC system has quite good performance above 20dB SNR, where it is about 5dB from OPTA, seemingly following the slope of the OPTA curve at high SNR. Both simulated (green dashed curve) and calculated (magenta curve) robustness performance is shown: The distortion contributions discussed in Sections III-A can be seen: Weak noise distortion contributes above the optimal SNR point and behaves like a linear scheme (i.e. it has the same slope as BPAM) which is to be expected from Definition 2 and Proposition 1. Below the optimal SNR, anomalous distortion dominates, and is observed to diverge faster from OPTA than weak noise distortion. Note also that the theoretical model coincides well with simulations at high SNR, indicating that the weak noise regime of Definitions 2 is valid around the optimal SNR also for finite SNR.

*High SNR analysis:* We want to determine the exponent of the HVQLC at high SNR analytically. To simplify analysis, one can eliminate anomalous distortion by assuming sufficiently large distance between the parallel planes in the channel space shown in Fig. 15(a). Since  $\alpha_1$  is the distance between these planes, one can set  $\alpha_1 \geq 2b_n \sigma_n$ . With  $b_n > 4$ , 99.99% of all possible events are included, and the total distortion can be approximated as  $D_t \approx \sigma_n^2 / \alpha_2^2$ . Under this assumption we have the following proposition:

*Proposition 10: 2:3 HVQLC at high SNR:* At high SNR, the SDR and SNR of 2:3 HVQLC

are related as

$$\text{SDR} = \frac{7\sqrt{3}\sigma_x^2}{6\eta\pi^2\sigma_x^2b_n}\text{SNR}^{\frac{3}{2}}. \quad (60)$$

*Proof:* See Appendix D-3. □

From (60) it's clear that HVQLC has the same slope as 2:3 OPTA. With  $\sigma_x = 1$ ,  $b_n = 4$ ,  $\eta = 0.16$ , the loss from OPTA is  $\text{SDR}_{\text{loss}} = -10 \lg(7\sqrt{3}/(6\eta\pi^2b_n)) \approx 4.95\text{dB}$ , which corresponds to the performance gap in Fig. 15(b).

2) 2:3 RCASD: The distortion and power for this mapping is easily derived using results from preceding sections and existing papers.

To compute weak noise distortion we assume arc length parametrization and obtain the same metric  $G$  as for the 3:2 RCASD in Section V-A1. Just as the expression for channel distortion (36) became very simple, so does weak noise distortion in (10) reduce to a simple expression  $\bar{\varepsilon}_{wn}^2 = 0.5\sigma_n^2(\alpha_1^{-2} + 1/\alpha_2^{-2})$ . Further, the anomalous distortion is exactly the same as for the 1:2 mapping in [2], Eqn.(25), scaled by 0.5.

The power on channels 1 and 2 is also the same as for the 1:2 mapping in [2], and is given by  $P_1 + P_2 = 2\Delta\sigma_x\alpha_2/(\eta\sqrt{2\pi})$ . As  $x_3$  is simply scaled with  $\alpha_3$  and sent on channel 3, the power is  $P_3 = \sigma_x^2\alpha_3^2$ . The total power per channel is then  $P_t = (P_1 + P_2 + P_3)/3$ . Following the same procedure for optimization as previous mappings, the optimal parameters are found.

The performance is shown in Fig. 15(b). As expected from Proposition 9, this scheme diverges from OPTA, following the slope of a 1:1 system at high SNR. However, between 10-22 dB SNR, the RCASD outperforms the HVQLC. As for 3:2 case, a DS based approach brings advantages at low to medium SNR. The correspondence between the calculated and simulated robustness curves indicate that the theoretical model fits well with reality at high SNR.

### C. Remarks for both 3:2 and 2:3 mappings:

From the analysis and simulations in Sections V-A and V-B it may appear like fully continuous mappings based on surfaces may suffer from sub-optimality in the sense that they cannot follow the slope of OPTA at high SNR. This is in contrast to when curves are applied, where such divergence is not observed [2], [35], [33]. However, we still have not investigated the optimal choice of coordinate system on  $\mathcal{S}$ . Just as curve-based mappings will diverge from OPTA for

most choices of  $\varphi$ , it may be that the divergence observed for surfaces is due to wrong choice of coordinate system. This may be indicated by [6] where fully continuous mappings results from a Deep Learning approach, a structure quite similar to the DSS proposed in this paper, that seem to follow OPTA at high SNR. However, this is not conclusive as they only show performance up to 30dB, where also the DSS does not appear to divergence from OPTA.

Determining the optimal coordinate system is difficult even for 2D surfaces, and should be followed up in future effort(s). Also, the fact that two mappings look similar (as Saiduttas VAE surface and DSS) does not imply that they perform in the same way. One example is the extension of RCASD analyzed in [42, pp.19-20], named MS-CDS, using a nonlinear 1:1 mapping. Although this mapping seemingly fills the space in a similar (spherically symmetric) way as DSS, and in a more proper way than RCASD, its performance is inferior to the RCASD. Its performance is reduced both because its decomposable (Proposition 9), as well as the ML estimate becoming less accurate due to curvature in the 1:1 part.

## VI. SUMMARY, DISCUSSION AND EXTENSIONS

In this paper a theoretical framework for analyzing and constructing analog mappings used for joint source-channel coding has been proposed. A general set of continuous or piecewise continuous mappings named Shannon-Kotel'nikov (S-K) mappings have been considered for the case of memoryless sources and channels.

S-K mappings are nonlinear or linear direct mappings between source- and channel space. In this paper we focused on spaces of different dimensions. The distortion framework introduced describes S-K mapping behaviour in general, that is without reference to a specific mapping realization. Also, the framework provides guidelines for construction of well performing mappings for both low and arbitrary complexity and delay.

Two propositions (Proposition 7 and 8) indicate under which conditions S-K mappings may achieve the information theoretical bounds (OPTA) for Gaussian sources. Not surprisingly, the dimensionality of a mapping must be infinite to achieve optimality when the source and channel dimension do not match. This is because the optimal “space utilization” with such mappings is obtained only in the limit of infinite dimensionality.

When it comes to construction of mappings it is shown that any mapping which can be decomposed into combinations of lower dimensional sub-mappings cannot obtain the same (optimal)

slope as the information theoretical bounds at high SNR. We also apply the provided theory to construct mappings for 2:3 and 3:2 mappings. These mappings have decent performance, albeit not beating mappings obtained by deep learning and numerical optimization methods (PCCOVQ). However, the loss is small (about 1dB), and the mappings found can easily be adapted to varying channel conditions simply by scaling the given structure, reducing complexity.

The results provided can place constraints to numerical approaches [5], [67]. By imposing the conditions presented throughout this paper, one will likely obtain mappings closer to the global optimum without having to input a pre-determined, close to optimal mapping. The conditions presented may also provide a wider understanding of why certain configurations are favored by Deep Learning (AI) approaches [6].

#### A. Extensions

**1) Low SNR:** Many results in this paper are accurate at high SNR. Further analysis may be necessary in order to deal properly with the low SNR regime. This paper only consider ML decoding, and it is well known that MMSE decoding is needed at low SNR to obtain optimal performance. However, when dealing with MMSE decoding for nonlinear mappings in general it is difficult to find analytical solutions one can analyze further.

**2) Global (Manifold) structure:** Although the main results of this paper gives some clear indications on the global structure of S-K mappings, they do not necessarily provide the exact optimal solution. For low dimensional mappings, several approaches for finding the global structure exists, like the PCCOVQ algorithm [66], [49], approach using variational calculus [68], [67] and machine learning [6]. Since these works all rely on numerical methods, there is no guarantee that the optimal mappings has been found. It is therefore necessary to find, if possible, a way of determining global optimality of a given  $M:N$  mapping. It is likely that by setting initial/border conditions and constraining solutions based on conditions determined throughout this paper may lead to solutions closer to the global optimum.

**3) Correlated sources:** Some of the results here can be extended to include correlated sources. If the two variables in Fig. 7(a) were correlated, the curve would only need to fill an elliptical subset of this spherical region (see [31] and [39]). Since a smaller volume then needs to be covered, one can, for a given approximation distortion, cover the relevant source with a “smaller”  $\mathcal{S}$  leading to a smaller channel distortion. The performance will then improve when correlation

increases. The special case  $M = N = 2$  was treated in [39] where it was shown that a special case of a RS (a *principal normal surface*) can utilize correlation to obtain significant gains.

**4) Multiple Access networks:** The theory presented may be extended to S-K like mappings for small networks. Some attempts have already been made for correlated Gaussian sources communicated on a Gaussian multiple access channel with both orthogonal and simultaneous transmission [39], [65], [40].

## APPENDIX A

### CONCEPTS FROM DIFFERENTIAL GEOMETRY

#### A. Arc length parametrization, Formula of Frenet.

Let  $\mathbf{S} : x \in [a, b] \subseteq \mathbb{R} \rightarrow \mathbf{S}(x) \in \mathbb{R}^N$  with  $\mathbf{S}(x) \in C^1$  be a parametrization for the curve  $\mathcal{C}$  w.r.t.  $\ell(x)$ . Let  $\ell(x)$  denote the arc length of  $\mathbf{S}$

$$\ell(x) = \int_a^x \|\mathbf{s}'(q)\| dq, \quad (61)$$

and  $\varphi$  denote its inverse.

*Theorem 2:* Let  $\mathbf{y}(\ell)$  be a parametrization of  $\mathcal{C}$ . Then  $\mathbf{y}(\ell)$  and  $\mathbf{s}(\varphi(x))$  will have the same image, and  $\|\mathbf{y}'(\ell)\| = \|\mathbf{s}'(\varphi(\ell))\| \equiv 1, \quad \forall \ell.$  □

*Proof 1:* See[69, pp. 115-116]. □

*Definition 9: Formula of Frenet(FoF)* [41, p. 41] relates the derivatives  $\dot{\mathbf{t}}$ ,  $\dot{\mathbf{p}}$  and  $\dot{\mathbf{b}}$  to linear combinations of  $\mathbf{t}$ ,  $\mathbf{p}$ , and  $\mathbf{b}$  defined in Section II-C as follows:

$$\dot{\mathbf{t}} = \kappa \mathbf{p}, \quad \dot{\mathbf{p}} = -\kappa \mathbf{t} + \tau \mathbf{b}, \quad \dot{\mathbf{b}} = -\tau \mathbf{p}, \quad (62)$$

where  $\kappa$  is the curves curvature and  $\tau$  its torsion. □

#### B. Einstein Summation Convention, Fundamental Forms and Curvature

*1) Summation Convention:* To efficiently express multiple sum-operations resulting when analyzing surfaces, *Einstein summation convention* is convenient [41, p.84]:

**If in a product a letter figures twice, once a superscript and once a subscript, summation should be carried out from 1 to  $N$  w.r.t. this letter.**

For example, for simple and double sums we have

$$\sum_{\alpha=1}^N a^\alpha b_\alpha = a^\alpha b_\alpha, \quad \sum_{\alpha=1}^N \sum_{\beta=1}^N a_{\alpha\beta} u^\alpha u^\beta = a_{\alpha\beta} u^\alpha u^\beta. \quad (63)$$

2) *Fundamental Forms: First Fundamental Form (FFF)*: Consider a hyper surface  $\mathcal{S}$  realized by (2) or (3). In order to measure lengths, angles and areas on  $\mathcal{S}$ , a metric is needed. A length differential of a curve  $C \in \mathcal{S}$  is given by [41, p.82]<sup>17</sup>:

$$d\ell^2 = (\mathbf{S}_1 du^1 + \mathbf{S}_2 du^2) \cdot (\mathbf{S}_1 du^1 + \mathbf{S}_2 du^2) = \mathbf{S}_1 \cdot \mathbf{S}_1 (du^1)^2 + 2\mathbf{S}_1 \cdot \mathbf{S}_2 du^1 du^2 + \mathbf{S}_2 \cdot \mathbf{S}_2 (du^2)^2. \quad (64)$$

The quantities  $g_{\alpha\beta} = \mathbf{S}_\alpha \cdot \mathbf{S}_\beta$  are the components of a *2nd order covariant tensor* (see [41, pp.88-105] or [42] for definition of covariant and contravariant tensor) named *metric tensor*. By the summation convention,  $d\ell^2 = g_{\alpha\beta} du^\alpha du^\beta$ , named *First Fundamental Form (FFF)*. For a smooth embedding  $\mathbf{S}$  in  $\mathbb{R}^N$  ( $M \leq N$ ) the metric tensor can be seen as a symmetric, positive definite  $M \times M$  matrix  $G = J^T J$  [50, pp.301-343], with  $J$  the *Jacobian* [70, p.47] of  $\mathcal{S}$ , a  $N \times M$  matrix with entries  $J_{ij} = \partial \mathbf{S}_i / \partial u_j$ ,  $i \in 1, \dots, N$ ,  $j \in 1, \dots, M$ . Then  $g_{ii}$  is the squared norm of the tangent vector along the  $i$ 'th coordinate curve of  $\mathbf{S}$ . All *cross terms*  $g_{ij}$ , are inner products of tangent vectors along the  $i$ 'th and  $j$ 'th coordinate curve of  $\mathbf{S}$ .

The *contravariant metric tensor* is a tensor with components  $g^{\alpha\beta}$  satisfying  $g_{\alpha\beta} g^{\alpha\beta} = \delta_\alpha^\beta$ . Let  $g = \det(G)$ . For a 2D  $\mathcal{S}$ , the covariant and contravariant tensors are related as

$$g^{11} = \frac{g_{22}}{g}, \quad g^{12} = g^{21} = -\frac{g_{12}}{g}, \quad g^{22} = \frac{g_{11}}{g}. \quad (65)$$

**Second Fundamental Form (SFF)**: Assume that curve  $\mathcal{C} \in \mathcal{S}$  is represented by arc length parametrization  $u^1(\ell), u^2(\ell)$ . Let  $\gamma$  be the angle between the normal of  $\mathcal{S}$ ,  $\mathbf{n}$ , and the principal normal of  $\mathcal{C}$ ,  $\mathbf{p}$ . Since these are unit vectors, we have  $\cos \gamma = \mathbf{p} \cdot \mathbf{n}$ , which will generally vary along  $\mathcal{C}$ . From the formula of Frenet (62) we have  $\mathbf{p} = \ddot{\mathbf{S}}/\kappa$  and so  $\kappa \cos \gamma = \ddot{\mathbf{S}} \cdot \mathbf{n}$ . From the product rule we have

$$\dot{\mathbf{S}} = \frac{\partial \mathbf{S}}{\partial u^1} \frac{du^1}{d\ell} + \frac{\partial \mathbf{S}}{\partial u^2} \frac{du^2}{d\ell} = \mathbf{S}_\alpha \dot{u}^\alpha. \quad (66)$$

<sup>17</sup>We look at a 2D surface here for better readability. The general case is straight forward to determine.

Differentiating w.r.t.  $\ell$  again, we get  $\ddot{\mathbf{S}} = \mathbf{S}_{\alpha\beta}\dot{u}^\alpha\dot{u}^\beta + \mathbf{S}_\alpha\ddot{u}^\alpha$ . Since  $\mathbf{S}_\alpha \cdot \mathbf{n} = 0$ , then  $\kappa \cos \gamma = (\mathbf{S}_{\alpha\beta} \cdot \mathbf{n})\dot{u}^\alpha\dot{u}^\beta$ . The term in the parentheses is an important quantity,

$$b_{\alpha\beta} = \mathbf{S}_{\alpha\beta} \cdot \mathbf{n}, \quad \alpha, \beta = 1, \dots, N. \quad (67)$$

The scalar products  $b_{\alpha\beta}$  depend on  $\mathcal{S}$  only (independent of choice of curve  $\mathcal{C}$ ) and are symmetric due to the symmetry of  $\mathbf{S}_{\alpha\beta}$ . The quadratic form  $b_{\alpha\beta}du^\alpha du^\beta$ , is named *second fundamental form* (SFF), and is invariant w.r.t allowable coordinate transformations which preserves the sign of  $\mathbf{n}$ .  $b_{\alpha\beta}$  are therefore the components of a 2nd order covariant tensor (like  $g_{\alpha\beta}$ ).

To compute  $b_{\alpha\beta}$ , the following relation is convenient,

$$b_{\alpha\beta} = \mathbf{S}_{\alpha\beta} \cdot \mathbf{n} = \mathbf{S}_{\alpha\beta} \cdot \left( \frac{\mathbf{S}_1 \times \mathbf{S}_2}{\sqrt{g}} \right) = \frac{1}{\sqrt{g}} |\mathbf{S}_1 \ \mathbf{S}_2 \ \mathbf{S}_{\alpha\beta}|. \quad (68)$$

3) *Normal Curvature, Principal Curvature, Lines of Curvature*: Let  $t$  be any allowable parameter for the curve  $\mathcal{C}$ . Then  $\dot{u}^\alpha = (du^\alpha/dt)(dt/d\ell) = u^{\alpha'}/\ell'$ . and therefore

$$\kappa \cos \gamma = b_{\alpha\beta}\dot{u}^\alpha\dot{u}^\beta = \frac{b_{\alpha\beta}u^{\alpha'}u^{\beta'}}{\ell'^2} = \frac{b_{\alpha\beta}u^{\alpha'}u^{\beta'}}{g_{\alpha\beta}u^{\alpha'}u^{\beta'}} = \frac{b_{\alpha\beta}du^\alpha du^\beta}{g_{\alpha\beta}du^\alpha du^\beta}. \quad (69)$$

It is shown in [41, pp. 121-124] that  $\kappa_n = \kappa \cos \gamma$  is the curvature at point  $P \in \mathcal{S}$  of the *normal section*  $\mathcal{C} \in \mathcal{S}$ , and is therefore named *normal curvature* at  $P$ . Further, the *Theorem of Meusnier* [41, p.122] states that one can restrict the consideration of curvature at any point  $P \in \mathcal{S}$  to that of normal sections without loss of generality.

The directions where  $\kappa_n$  has extremal values can be determined except when  $b_{\alpha\beta} \sim g_{\alpha\beta}$  (named *umbilic point*): Eq. (69) can be rewritten as  $(b_{\alpha\beta} - \kappa_n g_{\alpha\beta})du^\alpha du^\beta = 0$ . By differentiating w.r.t.  $du^\gamma$ , treating  $\kappa_n$  as a constant, one obtains [41, pp.128-129],

$$(b_{\alpha\gamma} - \kappa_n g_{\alpha\gamma})du^\alpha = 0, \quad \gamma = 1, 2. \quad (70)$$

The roots of (70) are directions for which  $\kappa_n$  is extreme, named *principal directions of normal curvature* at  $P$ . The corresponding curvatures,  $\kappa_1$  and  $\kappa_2$ , are the *principal normal curvatures* of  $\mathcal{S}$ , corresponding the maximal and minimal curvature of  $\mathcal{S}$  at  $P$ , respectively.

It is proven in [41, p.129] that the roots of (70) are real, and at every point (not an umbilic), the principal directions are orthogonal. Further, a curve on  $\mathcal{S}$  whose direction at every point is a principal direction is a *line of curvature* (LoC) of  $\mathcal{S}$ . It is proven in [41, p.130] that LoC on any surface  $\mathcal{S} \in C^r$ ,  $r \geq 3$ , are real curves, and if  $\mathcal{S}$  has no umbilics, the LoC form an orthogonal net everywhere on  $\mathcal{S}$ . One may always choose coordinates  $u^1, u^2$  on  $\mathcal{S}$  so that the

LoC are allowable coordinates at any point of  $\mathcal{S}$  (not umbilics). Then [41, p.130]:

*Theorem 3:* The coordinate curves of any allowable coordinate system on  $\mathcal{S}$  coincide with the LoC  $\Leftrightarrow g_{12} = 0$  and  $b_{12} = 0$ , at any point where those coordinates are allowable.

*Proof:* See [41, p.130].  $\square$

Using (70) one can show that  $\kappa_n^2 - b_{\alpha\beta}g^{\alpha\beta}\kappa_n + b/g = 0$ . The principal curvatures  $\kappa_1$  and  $\kappa_2$ , are the roots of this equation. When the coordinate curves are LoC, (70) holds with  $\kappa_n = \kappa_1$ ,  $du^2 = 0$  and again with  $\kappa_n = \kappa_2$ ,  $du^1 = 0$ . Therefore  $\kappa_1 = b_1^1$ ,  $b_1^2 = 0$ ,  $\kappa_2 = b_2^2$ ,  $b_2^1 = 0$ . For this special one obtains  $\kappa_i = b_{ii}/g_{ii}$ .

## APPENDIX B

### PROOFS FOR SECTION III

#### A. Proofs for Section III-A

1) *Proof, Proposition 1:* Assume that  $S_i \in C^1(\mathbb{R}^M)$ ,  $i = 1, \dots, N$ . The tangent space at  $\mathbf{x}_0$  is given by (9). Applying ML detection, then  $\mathbf{S}(\mathbf{x}_{ML}) = \mathbf{S}(\mathbf{x}_0) + P_{proj}\mathbf{n}$  (see Fig. 3(a)), where  $P_{proj}$  is a projection matrix given by [71, p.158]

$$P_{proj} = J(\mathbf{x}_0)(J(\mathbf{x}_0)^T J(\mathbf{x}_0))^{-1} J(\mathbf{x}_0)^T = J(\mathbf{x}_0)G(\mathbf{x}_0)^{-1} J(\mathbf{x}_0)^T, \quad (71)$$

Setting  $\mathbf{S}_{lin}(\mathbf{x}) = \mathbf{S}(\mathbf{x}_{ML})$ , with  $\mathbf{S}_{lin}$  as in (9) and from (71), we get

$$J(\mathbf{x}_0)(\mathbf{x}_{ML} - \mathbf{x}_0) = J(\mathbf{x}_0)G(\mathbf{x}_0)^{-1} J(\mathbf{x}_0)^T \mathbf{n}. \quad (72)$$

Multiplying both sides from the left with  $J^T$ , using the fact that  $G$  is invertible, then  $(\mathbf{x}_{ML} - \mathbf{x}_0) = G(\mathbf{x}_0)^{-1} J(\mathbf{x}_0)^T \mathbf{n}$ . The MSE given that  $\mathbf{x}_0$  was transmitted is then

$$\varepsilon_{wn}^2 = \frac{1}{M} E\{(\mathbf{x}_{ML} - \mathbf{x}_0)^T (\mathbf{x}_{ML} - \mathbf{x}_0)\}. \quad (73)$$

*Lemma 3:* With ML detection, the minimum MSE in (73) is achieved with a diagonal  $G$

$$\varepsilon_{wn}^2 = \frac{\sigma_n^2}{M} \sum_{i=1}^M \frac{1}{g_{ii}}, \quad (74)$$

where  $g_{ii}$  are the diagonal components of  $G$  at  $\mathbf{x}_0$ .  $\square$

Lemma 3 implies that the smallest possible weak noise MSE is obtained with orthogonal coordinate curves. Expectation over  $\mathcal{D}$  gives the wanted result.  $\square$

*Proof, Lemma 3:* Consider the MSE in (73). To avoid matrix multiplication, the  $N$ -dimensional noise vector  $\mathbf{n}$  is, without loss of generality, replaced by its  $M$  dimensional projection  $\mathbf{n}_P$ , which is also Gaussian since  $P_{proj}$  is a linear transformation [71, p.117]. Let  $J = J(\mathbf{x}_0)$ . Assume that a hypothetical inverse  $\mathbf{B} = J^{-1}$  exists (analysis is then restricted to the  $M$  dimensional tangent space). Let  $\mathbf{S}_t$  denote the tangent space of  $\mathbf{S}$  at  $\mathbf{x}_0$ . Under Def. 2 the linear approximation to  $\mathbf{S}^{-1}$  can be applied, and so  $\hat{\mathbf{x}} = \mathbf{S}^{-1}(\mathbf{S}_t(\mathbf{x}_0) + \mathbf{n}_P) \approx \mathbf{S}^{-1}(\mathbf{S}_t(\mathbf{x}_0)) + \mathbf{B}\mathbf{n}_P = \mathbf{x}_0 + \mathbf{B}\mathbf{n}_P$ . Therefore the MSE in (73), using Einstein summation convention, becomes  $\varepsilon_{wn}^2 = E\{\mathbf{n}_P^T \mathbf{B}^T \mathbf{B} \mathbf{n}_P\}/M = \mathbf{b}_i^T \mathbf{b}_j E\{n^i n^j\}/M$ , with  $\mathbf{b}_i$  column vector no.  $i$  of  $\mathbf{B}$ . With i.i.d. noise,  $E\{n_i n_j\} = \sigma_n^2 \delta_{ij}$ , then

$$\varepsilon_{wn}^2 = \frac{1}{M} E\{\mathbf{n}_P^T \mathbf{B}^T \mathbf{B} \mathbf{n}_P\} = \frac{\sigma_n^2}{M} \sum_{i=1}^M \mathbf{b}_i^T \mathbf{b}_i = \frac{\sigma_n^2}{M} \sum_{i=1}^M \|\mathbf{b}_i\|^2. \quad (75)$$

Since  $\mathbf{B} = J^{-1}$ , and since an orthogonal matrix has an inverse, the above result implies that the basis of the tangent space of  $\mathcal{S}$  can be chosen orthogonal without any loss. An orthogonal  $J$  results in a diagonal  $G$  (see Appendix A-B2). Therefore  $G^{-1}$  as well as  $G^{-1})^n$ , are also diagonal with elements  $1/g_{ii}$ . With  $G^{-2}$  diagonal,  $E\{n_i n_j\} = \sigma_n^2 \delta_{ij}$ , and with (75) in mind, (73) leads to

$$\varepsilon_{wn}^2 = \frac{1}{M} E\{(G^{-1} J^T \mathbf{n})^T (G^{-1} J^T \mathbf{n})\} = \frac{1}{M} E\{(J^T \mathbf{n})^T G^{-2} (J^T \mathbf{n})\} = \frac{\sigma_n^2}{M} \sum_{i=1}^M \frac{1}{g_{ii}^2} \|J_i\|^2, \quad (76)$$

where  $J_i$  is column vector no.  $i$  of  $J$  and  $\|J_i\|^2 \equiv g_{ii}$ .  $\square$

2) *Proof, Proposition 2:* Using the 2nd order approximation when maximizing the likelihood function, a 3rd degree polynomial with no simple solution results. We therefore consider a different approach: Using the concept of the osculating circle in Section II-C we can apply the higher order analysis of distortion for *pulse position modulation* (PPM) in [57, pp. 703-704] to obtain a result valid for any 1: $N$  mapping locally. PPM is geometrically described by a curve on a hyper sphere where the arc between any two coordinate axes is like a circle segment as depicted in Fig. 16. The fact that the curvature of any curve can be described locally by the osculation circle implies that the analysis done for PPM is also valid locally for any 1: $N$  mapping

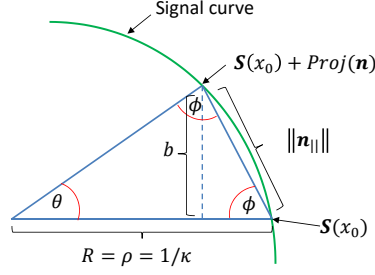


Fig. 16. Circle approximation for calculation of error up to 2nd order.

under (scaled) arc length parametrization. In the following, the signal curve segment in Fig. 16 is named *circle approximation*.

We divide the noise into the components  $\text{Proj}(\mathbf{n}) = \mathbf{n}_{||}$ , i.e., the projection onto the closest point on the circle in Fig. 16, and its normal,  $\mathbf{n}_{\perp}$ . For the circle approximation  $R(x) = \rho(x) = 1/\kappa(x) = 1/\|\ddot{\mathbf{S}}_0\|$  iff  $\mathbf{t} = \|\dot{\mathbf{S}}_0\| = 1$  (i.e., under arc length parametrization). In polar coordinates, a signal curve can be written  $\mathbf{S}(x) \approx [R(x), \theta(x)] = [\rho, \theta]$ . Then  $R(x) = R = \rho, \forall x$  and we have  $\mathbf{S} = [R \cos(\theta(x)), R \sin(\theta(x))]$  exactly. Then

$$\frac{d\mathbf{S}}{dx} = \left[ R \sin(\theta(x)) \frac{d\theta(x)}{dx}, -R \cos(\theta(x)) \frac{d\theta(x)}{dx} \right]. \quad (77)$$

By taking the norm we find that  $\|d\mathbf{S}/dx\|^2 = R^2(d\theta(x)/dx)^2$ . From this we get

$$\frac{d\theta(x)}{dx} = \frac{1}{R} \left\| \frac{d\mathbf{S}}{dx} \right\| = \frac{\|\mathbf{S}'_0\|}{\rho} = \alpha \kappa = \alpha \|\ddot{\mathbf{S}}_0\|. \quad (78)$$

That is,  $d\theta(x)/dx \sim \kappa$ . The two last equalities in (78) are valid only for scaled arc length parametrization. To determine the ML estimate for the circle approximation we rewrite (78) as  $dx = d\theta(x)/(\|\mathbf{s}'_0\| \|\mathbf{s}''_0\|) = d\theta(x) \rho(x_0)/\|\mathbf{s}'_0\|$ . Then

$$x_0 - \hat{x}_{ML} = \frac{\rho(x_0)}{\|\mathbf{s}'_0\|} \theta = \frac{\theta}{\kappa(x_0) \|\mathbf{s}'_0\|}. \quad (79)$$

We need to express  $\theta$  in terms of the noise and  $\rho$  (or  $\kappa$ ). In Fig. 16 we have a right-legged triangle where  $\theta + 2\phi = \pi \Rightarrow \phi = (\pi - \theta)/2$ . Further,  $b = \rho \sin(\theta)$  is the right normal of this triangle. Therefore  $\sin(\phi) = b/\|\mathbf{n}_{||}\| \Rightarrow \|\mathbf{n}_{||}\| = b/\sin(\phi) = \rho \sin(\theta)/\sin(\phi)$ . Furthermore,  $\sin(\phi) = \sin(\pi/2 - \theta/2) = \cos(\theta/2)$ . Since  $\sin 2y = 2 \sin y \cos y$ , with  $y = \theta/2$ , then  $\sin(\theta) = 2 \sin(\theta/2) \cos(\theta/2)$ , implying that  $\|\mathbf{n}_{||}\| = 2\rho \sin(\theta/2)$ . Therefore  $\theta = 2 \sin^{-1}(\|\mathbf{n}_{||}\|/(2\rho(x_0)))$ .

By the expansion [72, p. 117]  $\sin^{-1}(x) = x + x^3/(2 \cdot 3) + x^5 \cdot 1 \cdot 3/2 \cdot 4 \cdot 5 + \dots$ , we get  $\theta$  up to 2nd order as

$$\theta \approx \frac{\|\mathbf{n}_{||}\|}{\rho(x_0)} \left( 1 + \frac{\|\mathbf{n}_{||}\|^2}{24\rho^2(x_0)} \right). \quad (80)$$

One can then compute the error up to second order from (79) and (80)

$$\begin{aligned} \varepsilon_{wn}^2 &= E\{(x - \hat{x}_{ML})^2 | x = x_0\} = E\left\{ \left( \frac{\rho(x_0)}{\|\mathbf{s}'_0\|} \theta \right) \right\} = \frac{\rho^2(x_0)}{\|\mathbf{s}'_0\|^2} E\left\{ \left( \frac{\|\mathbf{n}_{||}\|}{\rho(x_0)} \left( 1 + \frac{\|\mathbf{n}_{||}\|^2}{24\rho^2(x_0)} \right) \right)^2 \right\} \\ &= \frac{1}{\|\mathbf{s}'_0\|^2} E\left\{ \|\mathbf{n}_{||}\|^2 + \frac{2\|\mathbf{n}_{||}\|^4}{24\rho^2(x_0)} + \frac{\|\mathbf{n}_{||}\|^6}{24^2\rho^4(x_0)} \right\}. \end{aligned} \quad (81)$$

Since  $E\{n^a\} = 1 \cdot 3 \cdots (a-1)\sigma_n^a$ ,  $a$  even, and zero otherwise [63, p.148], we get

$$\varepsilon_{wn}^2 = \frac{\sigma_n^2}{\|\mathbf{s}'_0\|^2} \left( 1 + \frac{\sigma_n^2}{4\rho^2(x_0)} + \frac{5\sigma_n^4}{48\rho^4(x_0)} \right) = \frac{\sigma_n^2}{\|\mathbf{s}'_0\|^2} \left( 1 + \frac{1}{4}\sigma_n^2\kappa^2(x_0) + \frac{5}{48}\sigma_n^4\kappa^4(x_0) \right) \quad (82)$$

The relation  $\kappa(x_0) = \|\ddot{\mathbf{s}}(x_0)\|$  is valid only under arc length parametrization. In general, the curvature is given by (5). Since we most often consider scaled arc length parametrization, that is  $\|\mathbf{S}'(x_0)\| = \alpha\|\dot{\mathbf{S}}(x_0)\| = \alpha$ ,  $\forall x_0$ , then (5) reduces to  $\kappa(x_0) = \|\mathbf{S}''_0(x_0)\|/\|\mathbf{S}'_0\|^2$  (since  $\mathbf{S}'_0 \perp \mathbf{S}''_0$  still). Then we can express the error in terms of the signal curve's derivatives as

$$\varepsilon_{wn}^2 = \frac{\sigma_n^2}{\|\mathbf{S}'_0\|^2} \left( 1 + \frac{1}{4}\sigma_n^2 \frac{\|\mathbf{S}''_0\|^2}{\|\mathbf{S}'_0\|^4} + \frac{5}{48}\sigma_n^4 \frac{\|\mathbf{S}''_0\|^4}{\|\mathbf{S}'_0\|^8} \right). \quad (83)$$

As will be shown in Lemma 1, one should let  $\sigma_n^2 \ll \rho^2(x_0)$  to avoid larger errors (at least at high SNR). At high SNR ( $\sigma_n^2 \ll 1$ ) one can then make the approximation

$$\varepsilon_{wn}^2 \approx \frac{\sigma_n^2}{\|\mathbf{S}'_0\|^2} \left( 1 + \frac{1}{4}\sigma_n^2\kappa^2(x_0) \right) = \frac{\sigma_n^2}{\|\mathbf{S}'_0\|^2} \left( 1 + \frac{1}{4}\sigma_n^2 \frac{\|\mathbf{S}''_0\|^2}{\|\mathbf{S}'_0\|^4} \right) \quad (84)$$

At high SNR the curve can be significantly stretched, that is  $\|\mathbf{S}'_0\| = \alpha \gg 1$ . The second term in (84) will then diminish, making the 1st order term more and more dominant with increasing SNR. As will be shown in the proof of Proposition 4, higher order terms will contribute even less, and therefore the circle approximation above will do.

To see that the circle approximation above will be valid locally for any signal curve  $\mathbf{S}$ , take Fig. 1: For a general curve in polar coordinates, the product rule gives

$$\frac{d\mathbf{S}}{dx} = \left[ R'(x) \cos(\theta(x)) + R(x) \sin(\theta(x)), R'(x) \sin(\theta(x)) - R(x) \cos(\theta(x)) \right]. \quad (85)$$

Locally,  $R'(x)$  is small if the curvature of  $\mathbf{S}$  changes slowly with  $x$ . Therefore, the smaller the derivative  $\kappa'(x)$ , the more accurate the circle approximation is. As will be seen in Lemma 1, it is not convenient to use a curve (or surface in general) with a rapidly changing curvature.

For generalization to surfaces, consider first  $2:N$  mappings. Assume that  $x_1$  and  $x_2$  are the parameters in a LoC coordinate representation. Then, according to Theorem 3 in Section A-B3,  $g_{12} = b_{12} = 0$ , therefore the curvature is given solely in terms of  $g_{\alpha\alpha}$  and  $b_{\alpha\alpha}$  as  $\kappa_i(\mathbf{x}_0) = b_{ii}(\mathbf{x}_0)/g_{ii}(\mathbf{x}_0)$ , with  $b_{ii}$  computed in a similar way as (68). Since  $x_1, x_2, n_1$  and  $n_2$  are independent and i.i.d., and we have two orthogonal coordinate curves, we get

$$\varepsilon_{wn}^2(\mathbf{x}_0) \approx \frac{\sigma_n^2}{2} \sum_{i=1}^2 \left\{ \frac{1}{g_{ii}(\mathbf{x}_0)} \left( 1 + \frac{\sigma_n^2}{4} \kappa_i^2(\mathbf{x}_0) \right) \right\} = \frac{\sigma_n^2}{2} \sum_{i=1}^2 \left\{ \frac{1}{g_{ii}(\mathbf{x}_0)} \left( 1 + \frac{\sigma_n^2}{4} \frac{b_{ii}^2(\mathbf{x}_0)}{g_{ii}^2(\mathbf{x}_0)} \right) \right\}, \quad (86)$$

which is a straight forward generalization of the result for  $1:N$  mappings.

For  $M:N$  mappings, the generalization follows directly as we have  $M$  orthogonal curves forming a coordinate grid, and the result is obtained by letting the sum in (86) run from 1 to  $M$ .

□

3) *Proof, Lemma 1*:: Condition i) is obvious, and can be seen directly from Fig. 4(b).

Condition ii): We begin with  $1:N$  mappings (see [41, pp.266-267]): The spheres  $\mathbb{S}^{N-2} \in F$  can be represented as  $S_c(z_i, x) = (\mathbf{z} - \mathbf{S}(x)) \cdot (\mathbf{z} - \mathbf{S}(x)) - r^2 = 0$ ,  $i = 1, \dots, N$ . Further,  $\partial S_c / \partial x = -2\dot{\mathbf{S}} \cdot (\mathbf{z} - \mathbf{S}) = 0$ ,  $\dot{\mathbf{S}} = \partial \mathbf{S} / \partial x$ , implying that  $(\mathbf{z} - \mathbf{S}) \perp \dot{\mathbf{S}}$  and

$$\frac{\partial^2 S_c}{\partial x^2} = -2\ddot{\mathbf{S}} \cdot (\mathbf{z} - \mathbf{S}) + 2 = -2\kappa_s \mathbf{p} \cdot (\mathbf{z} - \mathbf{S}) + 2 = 0. \quad (87)$$

The last equality is due to the formula of Frenet (62). With  $\rho_s = 1/\kappa_s$  we get  $\mathbf{p} \cdot (\mathbf{z} - \mathbf{S}) - \rho_s = 0$ .

$\Rightarrow$ : The condition follows directly from (87).  $\Leftarrow$ : Since  $\|\mathbf{p} \cdot (\mathbf{z} - \mathbf{S})\| = \|\mathbf{z} - \mathbf{S}\| = r$ , one can see that if  $\rho_s > r \forall x$ , then the last equation in (87) does not have any real solution. I.e., no real characteristic points exists.

With the definition of principal curvatures it is straight forward to extend the proof to  $M:N$  mappings (canal hyper surfaces): The result follows directly from  $1:N$  case by letting a curve  $\mathcal{C}$  be the LoC with maximal principal curvature for all points of  $\mathcal{S}$ . That is,  $\mathcal{C}$  is always in the direction of the maximal curvature on  $\mathcal{S}$ . □

## B. Proofs Section III-B

1) *Proposition 3*:: Under Def. 5, the received signal  $\hat{\mathbf{x}} = \mathbf{S}(\hat{\mathbf{z}})$  can be approximated by (19), where the term  $J(\mathbf{z}_0)\mathbf{n}$  contributes to the distortion. The MSE per source component given that

$\mathbf{z}_0$  was transmitted is then

$$\begin{aligned}\varepsilon_{ch}^2 &= \frac{1}{M} E\{ (J(\mathbf{z}_0)\mathbf{n})^T (J(\mathbf{z}_0)\mathbf{n}) \} \\ &= \frac{1}{M} E\left\{ \left( \frac{\partial S_1}{\partial z_1} n_1 + \cdots + \frac{\partial S_1}{\partial z_N} n_N \right)^2 + \cdots + \left( \frac{\partial S_M}{\partial z_1} n_1 + \cdots + \frac{\partial S_M}{\partial z_N} n_N \right)^2 \right\}.\end{aligned}\quad (88)$$

Since noise on each sub-channel is independent,  $E\{n_i n_j\} = \sigma_n^2 \delta_{ij}$ . After some rearrangement,

$$\begin{aligned}\varepsilon_{ch}^2 &= \frac{\sigma_n^2}{M} \left( \left[ \left( \frac{\partial S_1}{\partial z_1} \right)^2 + \cdots + \left( \frac{\partial S_M}{\partial z_1} \right)^2 \right] + \cdots + \left[ \left( \frac{\partial S_1}{\partial z_N} \right)^2 + \cdots + \left( \frac{\partial S_M}{\partial z_N} \right)^2 \right] \right) \\ &= \frac{\sigma_n^2}{M} (g_{11} + g_{22} + \cdots + g_{NN}) = \frac{\sigma_n^2}{M} \sum_{i=1}^N g_{ii}.\end{aligned}\quad (89)$$

Expectation w.r.t.  $\mathbf{z}$  gives the wanted result.  $\square$

2) *Proof, Proposition 4:* With  $z_0$  transmitted, and noise  $n$ , we have:

$$\mathbf{S}(z_0 + n) \approx \mathbf{S}(z_0) + n\mathbf{S}'(z_0) + \frac{n^2}{2}\mathbf{S}''(z_0) + \frac{n^3}{3!}\mathbf{S}'''(z_0), \quad (90)$$

from the 3rd order Taylor expansion. From this we can derive the *channel distortion* as

$$\varepsilon_{ch}^2(z_0) = E\left\{ \left\| n\mathbf{S}'(z_0) + \frac{n^2}{2}\mathbf{S}''(z_0) + \frac{n^3}{3!}\mathbf{S}'''(z_0) \right\|^2 \right\}. \quad (91)$$

To expand this expression and take the expectation, it is advantageous to use arc length as parameter (see Appendix A-A). Then the first, second and third derivatives at each point of the curve makes out a vector space of mutually orthogonal vectors as explained in Section II-C (or [41, pp. 36-37]). That is,  $\dot{\mathbf{S}} \cdot \dot{\mathbf{S}} = 0$ ,  $\dot{\mathbf{S}} \cdot \ddot{\mathbf{S}} = 0$  and  $\ddot{\mathbf{S}} \cdot \ddot{\mathbf{S}} = 0$ . With this in mind, using the fact that  $E\{n^a\} = 1 \cdot 3 \cdots (a-1)\sigma_n^a$ ,  $a$  even, and zero otherwise [63, p.148], when  $n$  is Gaussian, the expectation in (91) can be found from straight forward calculations

$$\varepsilon_{ch}^2(z_0) = \sigma_n^2 \|\dot{\mathbf{S}}(z_0)\|^2 + \frac{3\sigma_n^4}{4} \|\ddot{\mathbf{S}}(z_0)\|^2 + \frac{5\sigma_n^6}{12} \|\ddot{\mathbf{S}}(z_0)\|^2, \quad (92)$$

where  $\|\dot{\mathbf{S}}(x_0)\| = 1$  according to Theorem 2 in Appendix A-A. The first term in (92) dominates when  $\sigma_n$  is small if the curvature  $\kappa$  and torsion  $\tau$  are sufficiently small (see Eq. (24)).

Consider now scaled arc length parametrization. We then have  $\|\mathbf{S}'(z_0)\| = \alpha \|\dot{\mathbf{S}}(z_0)\| = \alpha$ ,  $\forall z_0$ . Then (5) reduces to  $\kappa(z_0) = \|\mathbf{S}''_0(z_0)\|/\|\mathbf{S}'_0\|^2$  (since  $\mathbf{S}'_0 \perp \mathbf{S}''_0$ , still). Therefore we can express the channel error up to 2nd order in terms of the signal curves derivatives as in (22).

For general hyper surfaces the Taylor expansion for vector valued functions leads to a complicated expression, making it hard (if at all possible) to draw conclusions. Therefore it is more convenient to consider LoC: By choosing LoC as coordinates on a  $M:2$  mapping  $\mathcal{S}$ , then, as for

the  $M < N$  case, the most direct and simple generalization of the  $M:1$  case results. Assume that  $z_1$  and  $z_2$  are along the LoC. Then, according to Theorem 3,  $g_{12} = b_{12} = 0$ . Therefore the curvature is given solely in terms of  $g_{\alpha\alpha}$  and  $b_{\alpha\alpha}$ , i.e.,  $\kappa_i(\mathbf{z}_0) = b_{ii}(\mathbf{z}_0)/g_{ii}(\mathbf{z}_0)$  with  $g_{ii}$  and  $b_{ii}$  as defined before, but now evaluated w.r.t. the channel variables  $z_i$  (instead of the source variables  $x_i$ ). The result in (23) then follows.  $\square$

3) *Proof, Proposition 5:* Consider an  $m$ -dimensional vector quantizer (VQ) with equal the distance among each neighboring centroids,  $\Delta$ , named *uniform* VQ. The distortion for a uniform VQ is lower bounded by assuming that Voronoi regions are  $m - 1$ -spheres [54], [55], i.e., a sphere bound. Let the radius of these be  $\rho_m$ . We have

*Lemma 4:* For a uniform VQ of dimension  $m$  with centroids  $\mathbf{q}(\mathbf{x})$ , the distortion is lower bounded by<sup>18</sup>

$$\bar{\varepsilon}_a^2 \geq E\{\|\mathbf{x} - \mathbf{q}(\mathbf{x})\|^2\} = \frac{m}{4(m+2)}\Delta^2. \quad (93)$$

$\square$

Since the decision borders of a uniform VQ become spherical as  $m \rightarrow \infty$  [54], [55], [73], equality is obtained in (93) as  $m \rightarrow \infty$  when  $\Delta$  is sufficiently small.

Eqn. (93) must be modified to encompass S-K mappings. Assuming uniform S-K mapping (Def. 6), then for each point  $\mathbf{S}_0 \in \mathbf{S}$  the decision borders for approximating values in  $\mathbb{R}^M$  to this point is an  $M - N - 1$ -sphere,  $\mathbb{S}^{M-N-1}$  (the family of such sphere  $\forall \mathbf{S}_0 \in \mathbf{S}$  is a canal surface). The  $N - M$  dimensional space where this sphere lies, is orthogonal to  $\mathbf{S}$  at  $\mathbf{S}_0$ , implying that the approximation to an  $N$ -dimensional uniform S-K mapping results in the same distortion as that of an  $M - N$  dimensional VQ. By substituting  $m = M - N$  in (93) and dividing by  $M$  the wanted result is obtained.  $\square$

*Proof, Lemma 4:* Consider first the special case of high dimensional VQ with spherical Voronoi regions of unit radius  $\rho_m = 1$  with one centroid at the origin. If the source variance  $\sigma_x \gg \rho_m$ , then the pdf of  $\|\mathbf{x} - \mathbf{q}(\mathbf{x})\|$ ,  $f_q$ , will be approximately uniform [54]. In this case one may

<sup>18</sup>Note that (93) differs from the bound derived in [54], since that bound is invariant with respect to size of the quantizer cells. Here we need the distortion to scale with the cell size so it can depend on the SNR.

consider any one of the centroids to quantify distortion  $\bar{\varepsilon}_a^2$ . Choose  $\mathbf{q}(\mathbf{x}) = 0$  for simplicity. Let  $B_m$  denote the volume contained within the relevant Voronoi region (see (97) for analytical expression). Then  $f_{\mathbf{q}} = 1/B_m, q \in [0, \rho_m]$ , and 0 otherwise. Then

$$\bar{\varepsilon}_a^2 = \int \cdots \int_{B_m} \|\mathbf{x}\|^2 f_{\mathbf{q}} d\mathbf{x} = \frac{1}{B_m} \int \cdots \int_{B_m} \|\mathbf{x}\|^2 d\mathbf{x}. \quad (94)$$

From [54, p. 375], we have that the moment of inertia

$$\int \cdots \int_{B_m} \|\mathbf{x}\|^2 d\mathbf{x} = \frac{m}{m+1} B_m. \quad (95)$$

Therefore  $\bar{\varepsilon}_a^2 = m/(m+1)$ . As the quantization error scales with the radius of the Voronoi regions,  $\rho_m$ , the distortion  $\bar{\varepsilon}_a^2$ , will scale with  $\rho_m = \Delta^2/4$ .  $\square$

## APPENDIX C

### PROOFS FOR SECTION IV

#### A. Proof, Proposition 7:

Assume that the channel signal and the noise are normalized with the channel dimension  $N$ . Considering a power constrained Gaussian channel, the normalized received vector will lie within an  $N-1$  sphere of radius

$$\rho_N = \sqrt{P_N + b_N \sigma_n^2}, \quad (96)$$

with high probability.  $P_N$  is the channel signal power per dimension, and  $\sigma_n^2$  the noise variance per dimension. By multiplying with  $b_N$  one takes into consideration that  $\rho_N$  exceeds  $\sqrt{P_N + \sigma_n^2}$  for finite  $N$ , so  $b_N \rightarrow 1$  as  $N \rightarrow \infty$ .

Let  $B_n$  denote the volume contained within an  $(n-1)$ - sphere of unit radius [74]

$$B_n = \frac{\pi^{\frac{n}{2}}}{\Gamma(\frac{n}{2} + 1)}, \quad (97)$$

where  $\Gamma(\cdot)$  is the Gamma function [59]. The volume of the canal surface,  $\mathbf{S}^M \times \mathbb{S}^{N-M-1}$ , must at most be smaller than or equal to the channel space volume in order to satisfy the channel power constraint. If  $\mathbf{S}^M \times \mathbb{S}^{N-M-1}$  has no characteristic points, then locally we have  $\mathbb{B}^M \times \mathbb{S}^{N-M-1}$ , for all points on  $\mathbf{S}$ . Then

$$B_M \rho_M^M B_{N-M} \rho_{MN}^{N-M} \leq B_N \rho_N^N, \quad (98)$$

where  $\rho_{MN}$  is the canal hyper surface radius and  $\rho_M$  is the radius of the source space.

Further assume that the noise vectors at each point of  $\mathcal{S}$  is decomposed into two statistically independent contributions (as in Fig. 5):  $M$  components tangential to  $\mathcal{S}$ ,  $\mathbf{n}_{wn}$ , and  $N - M$  components normal  $\mathcal{S}$ ,  $\mathbf{n}_{an}$ . To avoid anomalous errors, Proposition 6 states that  $\rho_{MN} \geq \|\mathbf{n}_{an}\| = \sqrt{((N - M)/N)b_{NM}\sigma_n^2}$ , where  $b_{NM} \rightarrow 1$  as  $M, N \rightarrow \infty$ . When  $M, N$  is large enough, (98) becomes (we assume  $b_N = b_{NM} = 1$  here for simplicity as their contribution disappear when  $M, N \rightarrow \infty$ )

$$B_M \rho_M^M B_{N-M} \left( \frac{N-M}{N} \sigma_n^2 \right)^{\frac{N-M}{2}} \leq B_N (P_N + \sigma_n^2)^{\frac{N}{2}}. \quad (99)$$

With a shape preserving mapping, the weak noise distortion is determined by  $\rho_M$ . Solving (99) with respect to  $\rho_M$ , we get

$$\rho_M \leq \sqrt[M]{\tilde{B}} \sigma_n \left( \frac{1}{1 - M/N} \right)^{\frac{N-M}{2M}} \left( 1 + \frac{P_N}{\sigma_n^2} \right)^{\frac{N}{2M}}, \quad (100)$$

where from (97)

$$\tilde{B} = \frac{B_N}{B_M B_{N-M}} = \frac{\Gamma\left(\frac{N-M}{2} + 1\right) \Gamma\left(\frac{M}{2} + 1\right)}{\Gamma\left(\frac{N}{2} + 1\right)}. \quad (101)$$

Eqn. (101) can be expressed by the *Beta function* using [59, p. 9]

$$\mathcal{B}(\varrho, \varsigma) = \int_0^1 t^{\varrho-1} (1-t)^{\varsigma-1} dt = \frac{\Gamma(\varrho) \Gamma(\varsigma)}{\Gamma(\varrho + \varsigma)}, \quad (102)$$

and the *Functional relation*  $\Gamma(a+1) = a\Gamma(a)$  [59, p. 3]. Letting  $\varrho = (N - M)/2 + 1$  and  $\varsigma = M/2 + 1$ , and using the above relations, we obtain

$$\tilde{B} = \left( \frac{N}{2} + 1 \right) \mathcal{B}\left( \frac{N-M}{2} + 1, \frac{M}{2} + 1 \right) = \left( \frac{N}{2} + 1 \right) \mathcal{B}_{(N,M)}. \quad (103)$$

Since  $M$  of  $N$  noise components ( $\mathbf{n}_{wn}$ ) contribute to weak noise distortion, we get

$$\bar{\varepsilon}_{wn}^2 = \frac{E\{\|\mathbf{n}_{wn}\|^2\}}{\rho_M^2} = \frac{M\sigma_n^2}{N\rho_M^2}, \quad (104)$$

using (11). With  $\rho_{MN} > \|\mathbf{n}_{an}\|$ ,  $\bar{\varepsilon}_{wn} = 0$  according to Proposition 6, and  $\bar{\varepsilon}_{wn}$  can be considered as the total distortion  $D_t$ . Assume a fixed dimension expansion  $r = N/M$ . Substituting  $M = N/r$  and inserting (100) into (104) then

$$D_t = \frac{1}{r} \left( 1 - \frac{1}{r} \right)^{r-1} \left( \frac{N}{2} + 1 \right)^{-\frac{2r}{N}} \mathcal{B}_{(N,r)}^{-\frac{2r}{N}} \left( 1 + \frac{P_N}{\sigma_n^2} \right)^{-r}, \quad (105)$$

where

$$\mathcal{B}_{(N,r)} = \int_0^1 t^{\frac{N}{2r}(r-1)} (1-t)^{\frac{N}{2r}} dt. \quad (106)$$

What is left to show is then

$$\lim_{N \rightarrow \infty} \left( \frac{N}{2} + 1 \right)^{-\frac{2r}{N}} \mathcal{B}_{(N,r)}^{-\frac{2r}{N}} = r \left( 1 - \frac{1}{r} \right)^{1-r}. \quad (107)$$

Using the product rule for limits [75, p.68], the first term on the left in (107) is eliminated since its limit equals 1. Further, using Hölders inequality [76, p. 135-136], we get

$$\mathcal{B}_{(N,r)} \leq \left\| t^{\frac{N}{2r}(r-1)} (1-t)^{\frac{N}{2r}} \right\|_{\infty}, \quad (108)$$

with equality in the limit  $N \rightarrow \infty$ . By differentiation one find that  $t_{max} = 1 - 1/r$  maximizes the norm in (108), and so

$$\mathcal{B}_{(N,r)} = \left( 1 - \frac{1}{r} \right)^{\frac{N}{2r}(r-1)} \left( \frac{1}{r} \right)^{\frac{N}{2r}}, \quad (109)$$

as  $N \rightarrow \infty$ . Raising both sides of (109) to the power  $-2r/N$  gives the wanted result<sup>19</sup>.  $\square$

**Comments on finite dimensionality:** For finite  $M, N$  anomalous errors will always have a probability of occurrence because  $\|\tilde{\mathbf{n}}\|$  has a nonzero variance. To make the above analysis valid for finite  $M, N$ ,  $b_N$  and  $b_{NM}$  must be included to account for the nonzero variance around the mean length of the source- and channel vectors. For a certain probability for anomalous errors,  $b_{MN}$  can be found from (26) by substituting  $N - M$  for  $N$ . Some further elaboration on finite dimensionality was given in [56].

### B. Proof, Proposition 8:

To make the approximation distortion small,  $\mathbf{S} \times \mathbb{S}^{M-N-1}$  should *cover* the source space that is, the following inequality should be satisfied

$$B_N \rho_N^N B_{M-N} \rho_{MN}^{M-N} \geq B_M \rho_M^M. \quad (110)$$

$\rho_M = \|\mathbf{x}\| = \sqrt{M b_M \sigma_x^2}$  is the radius of the source-space,  $\rho_N = \alpha \sqrt{N(P_N + b_N \sigma_n^2)}$  is the radius of the channel space (these are not normalized in this proof), where  $\alpha$  is an amplification factor, and  $\rho_{MN} = \Delta/2$  is the tube radius and  $b_M, b_N \rightarrow 1$  as  $M, N \rightarrow \infty$ . As in Appendix C-A these

<sup>19</sup>The above result does not contain  $\sigma_x$ , but can easily be included by setting  $\rho_M = \alpha \sigma_x$ , solving (100) with respect to  $\alpha$ , and substituting  $\alpha$  for  $\rho_M$  in (104)

are set to one in the rest of the proof. Inserting the above in (110) and solving with respect to  $\alpha$ , we obtain

$$\alpha \geq \sqrt{\frac{M^{\frac{M}{N}}}{N}} \tilde{B}^{\frac{1}{N}} \left(\frac{\Delta}{2}\right)^{-\frac{M-N}{N}} \sigma_x^{\frac{M}{N}} \sigma_n^{-1} \left(1 + \frac{P_N}{\sigma_n^2}\right)^{-\frac{1}{2}}, \quad (111)$$

where

$$\tilde{B} = \left(\frac{M}{2} + 1\right) \mathcal{B}\left(\frac{M-N}{2} + 1, \frac{N}{2} + 1\right) = \left(\frac{M}{2} + 1\right) \mathcal{B}_{(M,N)}, \quad (112)$$

derived in a similar way as in Appendix C-A. Assuming a shape preserving mapping and inserting (111) into (21), an expression for the weak channel distortion is found. Furthermore, the approximation distortion and the channel distortion can be considered independent under Definition 8 as they are perpendicular, thus

$$D_t = \bar{\varepsilon}_a^2 + \bar{\varepsilon}_{chw}^2 = \frac{M-N}{4M(M-N+2)} \Delta^2 + M^{\frac{M}{N}-1} \tilde{B}^{\frac{2}{N}} \left(\frac{\Delta}{2}\right)^{-2\frac{M-N}{N}} \sigma_x^{\frac{2M}{N}} \left(1 + \frac{P_N}{\sigma_n^2}\right)^{-1}. \quad (113)$$

Differentiating (113) with respect to  $\Delta$ , equating to zero and solving for  $\Delta$ , we obtain

$$\Delta_{opt} = M^{\frac{M-N}{2M}} \left(\frac{4M(M-N+2)}{M-N}\right)^{\frac{N}{2M}} \left(\frac{M-N}{N}\right)^{\frac{N}{2M}} 2^{1-\frac{N}{M}} \tilde{B}^{\frac{1}{M}} \sigma_x \left(1 + \frac{P_N}{\sigma_n^2}\right)^{-\frac{N}{2M}}. \quad (114)$$

Inserting (114) and (112) into (113) and using the relation  $N = Mr$ , with  $r \in \mathbb{Q}[0, 1]$ , we get

$$D_t = \left(1 + \frac{r}{1-r}\right) \left(\frac{1-r}{1-r+2/M}\right)^{1-r} \left(\frac{1-r}{r}\right)^r \left(\frac{M}{2} + 1\right)^{\frac{2}{M}} \mathcal{B}_{(M,r)}^{\frac{2}{M}} \sigma_x^2 \left(1 + \frac{P_N}{\sigma_n^2}\right)^{-r}. \quad (115)$$

where

$$\mathcal{B}_{(M,r)} = \int_0^1 t^{\frac{M}{2}(1-r)} (1-t)^{\frac{Mr}{2}} dt. \quad (116)$$

We get rid of two terms since

$$\lim_{M \rightarrow \infty} \left[ \left(\frac{M}{2} + 1\right)^{\frac{2}{M}}, \left(\frac{1-r}{1-r+2/M}\right)^{1-r} \right] = [1, 1], \quad (117)$$

further using the product rule for limits [75, p.68]. From Hölders inequality [76, p. 135-136]

$$\mathcal{B}_{(M,r)} \leq (1-r)^{\frac{M}{2}(1-r)} r^{\frac{Mr}{2}}, \quad (118)$$

with equality when  $M \rightarrow \infty$ , and so

$$\lim_{M \rightarrow \infty} \left(1 + \frac{r}{1-r}\right) \left(\frac{1-r}{r}\right)^r \mathcal{B}_{(M,r)}^{\frac{2}{M}} = \left(1 + \frac{r}{1-r}\right) \left(\frac{1-r}{r}\right)^r (1-r)^{(1-r)} r^r = 1 \quad (119)$$

□

## APPENDIX D

## PROOFS FOR SECTION V

1) *Proof, Proposition 9:* Consider OPTA for  $M:N$  mappings:

$$\text{SDR}_{M:N} = \frac{\sigma_x^2}{D_{M:N}} = \left(1 + \frac{P_{M:N}}{\sigma_n^2}\right)^{\frac{N}{M}}. \quad (120)$$

Take the dimension reduction case: The minimal distortion for a  $n:1$  system is found by solving (120) w.r.t.  $D_t$  for  $N = 1, M = n$ ,

$$D_{n:1} = \left(\frac{\sigma_x^2}{1 + \frac{P_{n:1}}{\sigma_n^2}}\right)^{\frac{1}{n}}. \quad (121)$$

Similarly, for an  $m:1$  system, we obtain the same formula by exchanging  $n$  with  $m$ . With  $P_t$ , the total power of the  $(m+n):2$  system, one can allocate power to the two sub-systems through a factor  $\kappa \in [0, 1]$  so that  $P_{n:1} = \kappa P_t$ . Let  $\text{SNR} = P_t/\sigma_n^2$  and use the fact that  $1 + x \approx x$  as  $x$  becomes large, then the total distortion in the limit of large SNR becomes,

$$\begin{aligned} \lim_{\text{SNR} \rightarrow \infty} D_{t(m+n:2)} &= \lim_{\text{SNR} \rightarrow \infty} \frac{\sigma_x^2}{m+n} \left[ \left(1 + \kappa \text{SNR}\right)^{\frac{1}{n}} + \left(1 + (1-\kappa) \text{SNR}\right)^{\frac{1}{m}} \right] \\ &= \frac{\sigma_x^2}{m+n} \lim_{\text{SNR} \rightarrow \infty} \left[ \frac{1}{\kappa^{1/n} \text{SNR}^{1/n}} + \frac{1}{(1-\kappa)^{1/m} \text{SNR}^{1/m}} \right], \end{aligned} \quad (122)$$

According to the laws of limits  $\lim_{x \rightarrow \infty} \kappa x = \kappa \lim_{x \rightarrow \infty} x$ , and so the power allocation factor(s) can be moved outside the limit. Then, for  $m > n$  since  $\text{SNR}^{1/m}$  grows more slowly than  $\text{SNR}^{1/n}$ ,  $D_{t(m+n:2)}$  will be dominated by the second term in (122) as  $\text{SNR} \rightarrow \infty$ .

In the expansion case, a similar derivation leads to

$$\lim_{\text{SNR} \rightarrow \infty} D_{t(2:m+n)} = \frac{\sigma_x^2}{m+n} \lim_{\text{SNR} \rightarrow \infty} \left[ \frac{1}{\kappa \text{SNR}^n} + \frac{1}{(1-\kappa) \text{SNR}^m} \right]. \quad (123)$$

If now  $m > n$ , the first term in (123) will dominate as  $\text{SNR} \rightarrow \infty$ .  $\square$

2) *Proof, Lemma 2:* The cumulative distribution is given by (a straight forward generalization of the  $h : \mathbb{R}^2 \rightarrow \mathbb{R}$  case in [63, pp. 180-181])

$$\begin{aligned} F_{z_1}(z_1) &= p_r\{Z_1 \leq z_1\} = p_r\{(x_1, x_2, x_3) \in \mathcal{D}_{Z_1}^+ \cup \mathcal{D}_{Z_1}^-\} \\ &= \iiint_{\mathcal{D}_{Z_1}^+ \cup \mathcal{D}_{Z_1}^-} f_{X_1 X_2 X_3}(x_1, x_2, x_3) dx_1 dx_2 dx_3, \end{aligned} \quad (124)$$

where  $f_{X_1 X_2 X_3}(x_1, x_2, x_3)$  is the joint Gaussian distribution and

$$\begin{aligned}\mathcal{D}_{Z_1}^+ &= \left\{ (x_1, x_2, x_3) \mid (x_1^2 + x_2^2 + x_3^2)^{\frac{n}{2}} \leq \rho^n, z_1 \geq 0 \right\}, \\ \mathcal{D}_{Z_1}^- &= \left\{ (x_1, x_2, x_3) \mid (x_1^2 + x_2^2 + x_3^2)^{\frac{n}{2}} \geq -\rho^n, z_1 < 0 \right\}.\end{aligned}\quad (125)$$

The pdf is found by differentiating (124) with respect to  $z_1$ . To simplify, one can consider only the  $\mathcal{D}_{Z_1}^+$  in (125) then use the fact that the channel pdf will be symmetric about the origin with the chosen  $\mathcal{S}$ . Further, since the domain in (125) is spherical, it is convenient to do the integration in spherical coordinates [77]

$$f_{z_1}(z_1) = \frac{1}{2} \frac{d}{dz_1} \int_0^{2\pi} \int_0^\pi \int_0^{a\varphi(z_1)} f_\rho(\rho) \rho^2 \sin(\theta) d\rho d\theta d\phi, \quad (126)$$

where  $f_\rho(\rho) = \exp(-\rho^2/(2\sigma_x^2))/((2\pi)^{3/2}\sigma_x^3)$ . The integrals over  $\theta, \phi$  become  $I_{(\theta, \phi)} = \pi$ . The integral over  $\rho$  remains,

$$\frac{d}{dz_1} \int_0^{a\varphi(z_1)} f_\rho(\rho) \rho^2 d\rho = \frac{1}{(2\pi)^{3/2}\sigma_x^3} \frac{d}{dz_1} \int_0^{a\varphi(z_1)} e^{-\frac{\rho^2}{2\sigma_x^2}} \rho^2 d\rho = \frac{na^3\gamma^3 z_1^{3n-1}}{(2\pi)^{3/2}\sigma_x^3} e^{-\frac{a^2\varphi^2(z_1)}{2\sigma_x^2}}. \quad (127)$$

By multiplying with  $\pi$  and further using absolute value (to make the pdf symmetric around the origin) we get the wanted result.  $\square$

3) *Proof, Proposition 10:* The Lagrangian for the problem is now

$$\mathcal{L}(\Delta, \alpha_2, \lambda) = \frac{\sigma_n^2}{\alpha_2^2} + \lambda_1 \left( \frac{\kappa^2 \alpha_1^2}{\Delta^4} + \frac{\alpha_2^2 \Delta^2}{12} - P_t \right) + \lambda_2 (2b_n \sigma_n - \alpha_1), \quad (128)$$

where  $\kappa = 2\eta\pi^2\sigma_x^2$ . Equality constraints are assumed, i.e.,  $P_t = 0.5(P_1 + P_2)$  and  $\alpha_1 = 2b_n\sigma_n$ , since we want to use all the available power, and the HVQLC should fill the channel space as properly as possible under the given constraints. By solving (59) w.r.t.  $\alpha_2$  we get  $\alpha_2 = 12(3P_t/2 - \kappa^2\alpha_1^2/\Delta^4)/\Delta^2$ . Then, since we avoid anomalous errors,

$$\text{SDR} = \frac{\sigma_x^2}{D_t} = \frac{\sigma_x^2 \alpha_2^2}{\sigma_n^2} = \frac{12\sigma_x^2}{\sigma_n^2 \Delta^2} \left( \frac{3P_t}{2} - \frac{\kappa^2 \alpha_1^2}{\Delta^4} \right) \quad (129)$$

We have now converted the constrained problem over  $\Delta, \alpha_1, \alpha_2$  to an unconstrained problem over  $\Delta$ . By solving  $\partial \text{SDR} / \partial \Delta = 0$  we get  $\Delta^* = \sqrt[4]{12\kappa^2 b_n^2 / \text{SNR}}$ , with  $\text{SNR} = P_t / \sigma_n^2$ . By inserting this into (129), we get the wanted result.  $\square$

## REFERENCES

- [1] M. Skoglund, N. Phamdo, and F. Alajaji, “Hybrid digital-analog source-channel coding for bandwidth compression/expansion,” *IEEE Trans. Information Theory*, vol. 52, no. 8, pp. 3757–3763, Aug. 2006.
- [2] F. Hekland, P. A. Floor, and T. A. Ramstad, “Shannon-Kotel’nikov mappings in joint source-channel coding,” *IEEE Trans. Commun.*, vol. 57, no. 1, pp. 94–105, Jan. 2009.
- [3] E. Akyol, K. Rose, and T. A. Ramstad, “Optimal mappings for joint source channel coding,” in *Proc. Information Theory Workshop (ITW)*. Dublin, Ireland: IEEE, Aug. 30th - Sept. 3rd 2010.
- [4] Y. Hu, J. Garcia-Frias, and M. Lamarca, “Analog joint source-channel coding using non-linear curves and mmse decoding,” *IEEE Trans. Commun.*, vol. 59, no. 11, pp. 3016–3026, Nov. 2011.
- [5] E. Akyol, K. B. Viswanatha, K. Rose, and T. A. Ramstad, “On zero-delay source-channel coding,” *IEEE Trans. Information Theory*, vol. 60, no. 12, pp. 7473–7489, Dec. 2014.
- [6] Y. M. Saidutta, A. Abdi, and F. Fekri, “Joint source-channel coding over additive noise analog channels using mixture of variational autoencoders,” *IEEE Journal on Selected Areas in Communications*, vol. Early Access, May 2021.
- [7] R. E. Blahut, *Principles and practice of information theory*, first (reprint) ed. Addison-Wesley, 1991.
- [8] J. Gobble, T., “Theoretical limitations on the transmission of data from analog sources,” *IEEE Trans. Information Theory*, vol. 11, no. 4, pp. 558–567, Oct. 1965.
- [9] T. Berger and D. W. Tufts, “Optimum pulse amplitude modulation part I: Transmitter-receiver design and bounds from information theory,” *IEEE Trans. Information Theory*, vol. IT-13, no. 2, pp. 196–208, Apr. 1967.
- [10] T. A. Ramstad, “On joint source-channel coding for the non-white Gaussian case,” in *7th Workshop on Signal Processing Advances in Wireless Communications*. Cannes, France: IEEE, Jul. 2006.
- [11] J. Schalkwijk and L. Bluestein, “Transmission of analog waveforms through channels with feedback,” *IEEE Trans. Information Theory*, vol. 13, pp. 617–619, 1967.
- [12] M. Gastpar, B. Rimoldi, and M. Vetterli, “To code, or not to code: Lossy source-channel communication revisited,” *IEEE Trans. Information Theory*, vol. 49, no. 5, pp. 1147–1158, May 2003.
- [13] V. Kostina and S. Verdú, “Lossy joint source-channel coding in the finite blocklength regime,” in *International Symposium on Information Theory (ISIT)*. IEEE, Jul. 2012.
- [14] —, “To code or not to code: Revisited,” in *Information Theory Workshop (ITW)*. IEEE, Sept. 2012.
- [15] Y. Kochman and R. Zamir, “Analog matching of colored sources to colored channels,” *IEEE Trans. Information Theory*, vol. 57, no. 6, pp. 3180–3195, Jun. 2011.
- [16] D. McRae, “Performance evaluation of a new modulation technique,” *IEEE Trans. Information Theory*, vol. 19, no. 4, pp. 431–445, Aug. 1971.
- [17] H. Coward and T. A. Ramstad, “Quantizer optimization in hybrid digital-analog transmission of analog source signals,” in *Proc. IEEE Int. Conf. on Acoustics, Speech, and Signal Proc. (ICASSP)*, vol. 5. Istanbul, Turkey: IEEE, Jun. 2000, pp. 2637–2640.
- [18] U. Mittal and N. Phamdo, “Hybrid digital-analog (HDA) joint source-channel codes for broadcasting and robust communications,” *IEEE Trans. Information Theory*, vol. 48, no. 5, pp. 1082–1102, May 2002.
- [19] M. Kleiner and B. Rimoldi, “Asymptotical optimal joint source-channel coding with minimal delay,” in *Globecom Communication Theory Symposium*. Honolulu, HI: IEEE, Dec. 2009.
- [20] V. M. Prabhakaran, R. Puri, and K. Ramchandran, “Hybrid digital-analog strategies for source-channel broadcast,” in *Annual Allerton Conference on Communication, Control and Computing*. IEEE, 2005.

- [21] S.-Y. Chung, “On the construction of some capacity-approaching coding schemes,” Ph.D. dissertation, Massachusetts Institute of Technology, Sep. 2000. [Online]. Available: <http://wicl.kaist.ac.kr/pdf/sychung%20phd%20thesis.pdf>
- [22] T. A. Ramstad, “Shannon mappings for robust communication,” *Teletronikk*, vol. 98, no. 1, pp. 114–128, 2002. [Online]. Available: [http://www.telenor.com/teletronikk/volumes/pdf/1.2002/Page\\_114-128.pdf](http://www.telenor.com/teletronikk/volumes/pdf/1.2002/Page_114-128.pdf)
- [23] C. Thomas, C. May, and G. Welti, “Hybrid amplitude-and-phase modulation for analog data transmission,” *IEEE Trans. Commun.*, vol. 23, no. 6, pp. 634–645, Jun. 1975.
- [24] C. E. Shannon, “Communication in the presence of noise,” *Proc. IRE*, vol. 37, pp. 10–21, Jan. 1949.
- [25] V. A. Kotel’nikov, *The Theory of Optimum Noise Immunity*. New York: McGraw-Hill Book Company, Inc, 1959.
- [26] V. A. Vaishampayan, “Combined source-channel coding for bandlimited waveform channels,” Ph.D. dissertation, University of Maryland, 1989.
- [27] V. A. Vaishampayan and S. I. R. Costa, “Curves on a sphere, shift-map dynamics, and error control for continuous alphabet sources,” *IEEE Trans. Information Theory*, vol. 49, no. 7, pp. 1658–1672, Jul. 2003.
- [28] N. Merhav, “Threshold effects in parameter estimation as phase transitions in statistical mechanics.” arXiv:1005.3620v1 [cs.IT], 2010.
- [29] —, “Weak-noise modulation-estimation of vector parameters,” *IEEE Transactions on Information Theory*, vol. 66, no. 5, pp. 3268–3276, May 2020.
- [30] J. M. Lervik, A. Fuldseth, and T. A. Ramstad, “Combined image subband coding and multilevel modulation for communication over power- and bandwidth limited channels,” in *Proc. Workshop on Visual Signal Processing and Communications*. New Brunswick, NJ, USA: IEEE, Sep. 1994, pp. 173–178.
- [31] A. Fuldseth and T. A. Ramstad, “Bandwidth compression for continuous amplitude channels based on vector approximation to a continuous subset of the source signal space,” in *Proc. IEEE Int. Conf. on Acoustics, Speech, and Signal Proc. (ICASSP)*, 1997.
- [32] K.-H. Lee and D. P. Petersen, “Optimal linear coding for vector channels,” *IEEE Trans. Commun.*, vol. COM-24, no. 12, pp. 1283–1290, Dec. 1976.
- [33] F. Hekland, “On the design and analysis of Shannon-Kotel’nikov mappings for joint source-channel coding,” Ph.D. dissertation, Norwegian University of Science and Engineering (NTNU), 2007.
- [34] X. Cai and J. W. Modestino., “Bandwidth expansion shannon mapping for analog error-control coding,” in *40th Annual Conference on Information Sciences and Systems*. IEEE, Mar. 2006.
- [35] P. A. Floor, “On the theory of Shannon-Kotel’nikov mappings in joint source-channel coding,” Ph.D. dissertation, Norwegian University of Science and Engineering (NTNU), 2008.
- [36] Y. Hu, J. Garcia-Frias, and M. Lamarca, “Analog joint source-channel coding using non-linear mappings and MMSE decoding,” *IEEE Trans. Commun.*, vol. 59, no. 11, Nov 2011.
- [37] B. Chen and G. W. Wornell, “Analog error-correcting codes based on chaotic dynamical systems,” *IEEE Trans. Commun.*, vol. 46, no. 7, pp. 881–890, Jul. 1998.
- [38] T. J. Goblick, “Theoretical limitations on the transmission of data from analog sources,” *IEEE Trans. Information Theory*, vol. 11, no. 10, pp. 558–567, Oct. 1965.
- [39] P. A. Floor, A. N. Kim, T. Ramstad, and I. Balasingham, “Zero delay joint source channel coding for multivariate Gaussian sources over orthogonal Gaussian channels,” *Entropy*, vol. 15, no. 6, pp. 2129–2161, Jun. 2013.
- [40] P. A. Floor, A. N. Kim, T. A. Ramstad, I. Balasingham, N. Wernersson, and M. Skoglund, “On joint source-channel coding

- for a multivariate gaussian on a gaussian mac,” *IEEE Transactions on Communications*, vol. 63, no. 5, pp. 1824–1836, May 2015.
- [41] E. Kreyszig, *Differential Geometry*. Dover Publications, Inc., 1991.
  - [42] P. A. Floor and T. A. Ramsted, “Tools for analysis of shannon-kotel’nikov mappings,” 2021, arXiv:2107.08526 [cs.IT]. [Online]. Available: <https://arxiv.org/abs/2107.08526>
  - [43] J. L. Troutman, *Variational Calculus and Optimal Control*. Springer-Verlag, 1996.
  - [44] P. A. Floor and T. A. Ramstad, “Noise analysis for dimension expanding mappings in source-channel coding,” in *7th Workshop on Signal Processing Advances in Wireless Communications*. Cannes, France: IEEE, Jul. 2006.
  - [45] C. Therrien, *Discrete Random Signals and Statistical Signal Processing*. Prentice Hall, 1992.
  - [46] N. Merhav, “Threshold effects in parameter estimation as phase transitions in statistical mechanics,” *IEEE Trans. Information Theory*, vol. 57, no. 10, pp. 7000–7010, Oct. 2011.
  - [47] D. J. Sakrison, *Communication Theory: Transmission of Waveforms and Digital Information*. New York: John Wiley & Sons, Inc, 1968.
  - [48] E. Akyol and K. Rose, “On linear transforms in zero-delay Gaussian source-channel coding,” in *Proc. International Symposium on Information Theory (ISIT)*. IEEE, 2012.
  - [49] P. A. Floor, T. A. Ramstad, and N. Wernersson, “Power constrained channel optimized vector quantizers used for bandwidth expansion,” in *International Symposium on Wireless Communication Systems*. Trondheim, Norway: IEEE, Oct. 2007.
  - [50] M. Spivak, *A Comprehensive Introduction to Differential Geometry*, 3rd ed. Publish or Perish, Houston Texas, Inc, 1999.
  - [51] P. A. Floor and T. A. Ramstad, “Dimension reducing mappings in joint source-channel coding,” in *Nordic Signal Processing Symposium*. Reykjavik, Iceland: IEEE, Jun. 2006.
  - [52] J. M. Lervik, “Subband image communication over digital transparent and analog waveform channels,” Ph.D. dissertation, NTNU, 1996.
  - [53] N. S. Jayant and P. Noll, *Digital Coding of Waveforms*. Prentice-Hall Inc. Englewood Cliffs, 1984.
  - [54] A. Gersho, “Asymptotically optimal block quantization,” *IEEE Trans. Information Theory*, vol. 25, no. 4, pp. 373–380, Jul. 1979.
  - [55] J. H. Conway and N. J. A. Sloane, *Sphere Packings, Lattices and Groups*. Springer Verlag, 1999.
  - [56] P. A. Floor and T. A. Ramstad, “Optimality of dimension expanding Shannon-Kotel’nikov mappings,” in *Information Theory Workshop*. Tahoe City, CA, USA: IEEE, Sep. 2007.
  - [57] J. M. Wozencraft and I. M. Jacobs, *Principles of Communication Engineering*. New York: John Wiley & Sons, Inc, 1965.
  - [58] H. Cramér, *Mathematical Methods of Statistics*, first (reprint) ed. Princeton University Press, 1951.
  - [59] H. Bateman, *Higher Transcendental Functions*, F. O. Arthur Erdélyi, Wilhelm Magnus and F. G. Tricomi, Eds. McGraw-Hill book company, Inc, 1953, vol. One.
  - [60] F. Hekland, G. E. Øien, and T. A. Ramstad, “Using 2:1 Shannon mapping for joint source-channel coding,” in *Proc. Data Compression Conference*, IEEE. Snowbird, Utah: IEEE Computer Society Press, Mar. 2005, pp. 223–232.
  - [61] P. A. Floor, A. N. Kim, T. A. Ramstad, and I. Balasingham, “On transmission of multiple Gaussian sources over a Gaussian MAC using a VQLC mapping,” in *Information Theory Workshop (ITW)*. Lausanne, Switzerland: IEEE, Sept. 3rd-7th 2012.
  - [62] S. N. Krivoshapko and V. N. Ivanov, *Encyclopedia of Analytical Surfaces*. Springer International Publishing Switzerland, 2015.

- [63] A. Papoulis and S. U. Pillai, *Probability, Random Variables and Stochastic Processes*, 4th ed. New York: McGraw-Hill higher education, Inc, 2002.
- [64] A. Edwards, “Gilberts sine distribution,” *Teaching Statistics*, vol. 22, no. 3, pp. 70–71, 2000.
- [65] P. A. Floor, A. N. Kim, N. Wernersson, T. Ramstad, M. Skoglund, and I. Balasingham, “Zero-delay joint source-channel coding for a bivariate Gaussian on a Gaussian MAC,” *IEEE Trans. Commun.*, vol. 60, no. 10, Oct. 2012.
- [66] A. Fuldseth, “Robust subband video compression for noisy channels with multilevel signaling,” Ph.D. dissertation, Norwegian University of Science and Engineering (NTNU), 1997.
- [67] M. S. Mehmetoglu, E. Akyol, and K. Rose, “Deterministic annealing-based optimization for zero-delay source-channel coding in networks,” *IEEE Transactions on Communications*, vol. 63, no. 12, pp. 5089–5100, Dec. 2015.
- [68] E. Akyol, K. Rose, and T. A. Ramstad, “Optimized analog mappings for distributed source-channel coding,” in *Proc. Data Compression Conference*, IEEE. Snowbird, Utah: IEEE Computer Society Press, Mar. 2010.
- [69] J. J. Callahan, *The Geometry of Spacetime: An Introduction to Special and General Relativity*, S. Axler, F. W. Gehring, and K. A. Ribet, Eds. New York: Springer-Verlag, Inc, 2000.
- [70] J. R. Munkres, *Analysis on Manifolds*. Westview Press, 1991.
- [71] G. Strang, *Linear Algebra and its Applications*, 3rd ed. Thomson Learning, Inc, 1986.
- [72] K. Rottmann, *Mathematische Formelsammlung*. Bibliographisches Institut & F. A. Brockhaus, 1991.
- [73] R. Zamir and M. Feder, “On lattice quantization noise,” *IEEE Trans. Information Theory*, vol. 42, no. 4, pp. 1152–1159, Jul. 1996.
- [74] Wikipedia contributors, “m-sphere— Wikipedia, the free encyclopedia,” [Online; accessed 26-December-2020]. [Online]. Available: [https://en.wikipedia.org/wiki/N-sphere#Closed\\_forms](https://en.wikipedia.org/wiki/N-sphere#Closed_forms)
- [75] C. H. Edwards and D. E. Penney, *Calculus with analytic geometry*. Prentice-Hall, Inc., 1998.
- [76] C. Gasquet and P. Witomski, *Fourier Analysis and Applications*, 1st ed., M. G. J.E. Marsden, L. Sirovich and W. Jäger, Eds. Springer-Verlag New York, Inc, 1999.
- [77] W. D. Richter, “Generalized spherical and simplicial coordinates,” *Journal of Mathematical Analysis and Applications*, vol. 336, pp. 1187–1202, 2007.